

The Nottingham Trent University
Library & Information Services
SHORT LOAN COLLECTION

Date	Time	Date	Time
31 MAR 2009	Ref.		

Please return this item to the Issuing Library.
Fines are payable for late return.

THIS ITEM MAY NOT BE RENEWED

Short Loan Coll May 1996

ProQuest Number: 10290166

All rights reserved

INFORMATION TO ALL USERS

The quality of this reproduction is dependent upon the quality of the copy submitted.

In the unlikely event that the author did not send a complete manuscript and there are missing pages, these will be noted. Also, if material had to be removed, a note will indicate the deletion.



ProQuest 10290166

Published by ProQuest LLC (2017). Copyright of the Dissertation is held by the Author.

All rights reserved.

This work is protected against unauthorized copying under Title 17, United States Code
Microform Edition © ProQuest LLC.

ProQuest LLC.
789 East Eisenhower Parkway
P.O. Box 1346
Ann Arbor, MI 48106 – 1346

111-111

THE DEVELOPMENT AND ANALYSIS
OF FABRICATED CONVEYOR PULLEYS

by

STEPHEN BAUGH

MASTER OF PHILOSOPHY

This thesis is submitted as partial fulfilment of the requirements for the degree of Master of Philosophy under the CNAA regulations

SPONSORING ESTABLISHMENT :- NOTTINGHAM POLYTECHNIC
BURTON STREET,
NOTTINGHAM,
NOTTINGHAMSHIRE.

COLLABORATING ESTABLISHMENT:- JENKINS OF RETFORD LTD.
RETFORD,
NOTTINGHAMSHIRE.

SUBMISSION DATE :- JUNE 1990

40 0690197 2



THE DEVELOPMENT AND ANALYSIS
OF FABRICATED CONVEYOR PULLEYS

by

STEPHEN BAUGH

ABSTRACT

This work has developed a series of theoretical techniques to establish the stress behaviour within a fabricated conveyor pulley. The distribution of the bending moments between the pulley and the through shaft are confirmed. The Rayleigh-Ritz energy method is adapted to develop a theoretical technique to analyse any variable thickness disc which is represented by cubic spline functions. This technique is verified on analysis of constant discs using a traditional well proven method. Extensive strain gauge experiments are used for further verification. The belt traction distribution between the belt and pulley is modelled. The analysis of the shell is developed using double Fourier series to represent the symmetrical and anti-symmetrical loading conditions produced by the belt traction. The variation in stress distribution absorbed by the shell for various belt wrap angles is illustrated. An account of the shell end effects is also developed. A complete strain gauged pulley assembly is subjected to a static belt pull, to verify theoretical predictions with respect to component stiffnesses and boundary conditions. A Finite Element Analysis is also presented as further comparison.

INDEX

Abstract	i
List of Symbols	iv
Index of Tables	vii
Index of Figures	viii

CHAPTER 1 INTRODUCTION

1.1	Review	1
1.2	Historial background	2
1.3	Literature review	6
1.4	Purpose of this investigation	7

CHAPTER 2 GENERAL THEORY

2.1	Applied belt pull	16
2.2	Determination of shaft size	17
2.3	Shaft stiffness	18

CHAPTER 3 END DISC ANALYSIS

3.1	Overall moment distribution and boundary conditions	24
3.2	Method of analysis	28
3.3	Analysis of a disc with constant thickness (bending only)	33
3.4	Analysis of a disc with variable thickness (bending only)	38
3.5	Analysis of a disc (in-plane loading only)	40
3.6	Experimental verification (bending only)	40
3.7	Experimental verification (in-plane only)	43

CHAPTER 4 SHELL ANALYSIS	
4.1	Method of Analysis (Belt loading only) 75
4.2	Method of Analysis (Shell end effects only) 90
4.3	Shell stiffness 95
CHAPTER 5 STATIC BELT PULL SUBJECTED TO A PULLEY ASSEMBLY	
5.1	Pulley assembly 111
5.2	Experimental frame 112
5.3	Results 113
CHAPTER 6 FINITE ELEMENT ANALYSIS OF A PULLEY ASSEMBLY	
6.1	Method of Analysis 127
6.2	Results 129
CHAPTER 7 DESIGN PROCEDURE	
7.1	Design Procedure 139
CHAPTER 8 CONCLUSION	
8.1	Summary of work 148
8.2	Future work 150
8.3	Acknowledgement 151
	References 152

LIST OF SYMBOLS

b	outside radius of end disc
B	belt width
$d_s, d_1; d_2$	shaft diameters
D_p	pulley diameter
D	plate bending stiffness
$D_o; D(\rho)$	plate bending stiffness, constant and variable thickness respectively
E	modulus of elasticity (Young's modulus)
$f_d; f_k$	dynamic load factors
G	modulus of elasticity in shear
$h; h_d$	disc thickness
$h_o; h(\rho)$	disc thickness, constant and variable thickness respectively
h_c	centre diaphragm thickness
$I_{s1}; I_{s2}$	moment of inertia, various shaft cross-section
I_{sh}	moment of inertia, shell
$k_p, k_s, k_d, k_f, k_h, k_{sh}$	stiffnesses, pulley, shaft, disc, fastener, hub, shell respectively
K	plate membrane stiffness
$K_b; K_t$	fatigue factors
L	distance between bearing support and end disc
L_{10}	bearing life
M_t	total bending moment

$M_p, M_s; M_d$	bending moment carried by pulley, shaft; disc respectively
$M_r, M_\theta; M_{r\theta}$	internal disc moment
$M_x, M_\phi, M_{x\phi}, M_{\phi x}$	internal shell moment
$N_x, N_\phi, N_{x\phi}, N_{\phi x}$	internal shear forces
P_b	modulus of rigidity, belt
P	resultant belt pull
$P(,); P'(,)$	normal and tangential components of belt traction respectively
$Q_r; Q_\theta$	shearing forces
Q	force
r	radius
t	shell thickness
$T_p; T_s$	tight and slack side belt tension respectively
T_c	belt tension at the transition between the arc's of stick and slip
u	shell deflection in x direction
U	strain energy
v	shell deflection in y direction
V	total potential energy
w	shell deflection in z direction
W	distance between end disc centres
X	distance between bearing supports
$X(,), Y(,); Z(,)$	external force components in the x,y,z directions
β	ratio between disc's inside and outside diameters
$\epsilon_r; \epsilon_\theta$	strain, disc
$\epsilon_x; \epsilon_\phi$	strain, shell

$\gamma_{r\theta}$	shear strain in $r\theta$ plane
θ	angular co-ordinate
θ_l	angle as the belt enters the pulley
θ_s	angle as the belt exits the pulley
θ_p	angle, resultant belt pull
θ_w	belt wrap / 2
θ_c	transition angle between the arc's of stick and slip
$\chi_{x\phi}$	shear strain
$\lambda(\rho)$	normalised disc thickness
μ	frictional coefficient
ν	poisson's ratio
ρ	non-dimensional radial co-ordinate
σ_b	permissible bending stress
σ_r, σ_θ	radial and tangential stress respectively
σ_x, σ_ϕ	axial and tangential stress respectively
σ_x	normal stress perpendicular to x axes
τ	permissible shear stress
$\tau_{r\theta}, \tau_{rz}, \tau_{\theta z}, \tau_{x\phi}$	shear stresses
ϕ	angular co-ordinate
ϕ_s	angle of twist of shaft
ϕ_{sh}	angle of twist at end disc to shell connection
ω	transverse displacement
Ω	potential energy

TABLE INDEX

- 2.1 Some important shaft calculations
- 3.1 Various kinematic boundary conditions for the analysis of constant thickness discs
- 3.2 Transverse displacement w (constant thickness disc)
- 3.3 Disc stiffness k_d (constant thickness disc)
- 3.4 Important stresses σ_r , σ_θ ; $\tau_{r\theta}$ for constant thickness disc
- 3.5 Some important variables for $\theta = 0$ showing the behaviour of a constant thickness disc, with clamped outer boundary
- 3.6 Transverse displacement w derived using Ragleigh-Ritz method for various boundary conditions
- 3.7 Important stresses σ_r , σ_θ ; $\tau_{r\theta}$ derived using Ragleigh-Ritz method (constant thickness disc)
- 3.8 Important stresses σ_r , σ_θ ; $\tau_{r\theta}$ derived using Ragleigh-Ritz method (variable thickness disc)
- 4.1 Important stresses in the shell due to shell end effects
- 7.1 Input data and calculation for worked example to illustrate design procedure

FIGURE INDEX

- 1.1 Schematic diagram of a typical belt conveyor
- 1.2 Cast iron conveyor pulley
- 1.3 Early fabricated conveyor pulley
- 1.4 Fabricated conveyor pulley with reinforcing ribs
- 1.5 Single compressive shaft fastener
- 1.6 Double compressive shaft fastener without centering
- 1.7 Double compressive shaft fastener with centering
- 2.1 Schematic diagram showing magnitude & direction of belt pull
- 2.2 Schematic diagram of a conveyor pulley
- 2.3 Diagram showing variable section shaft
- 3.1 Schematic diagram of a conveyor pulley with bending moment diagram
- 3.2 Diagram showing stiffness within a conveyor pulley
- 3.3 End disc twist (Schematic)
- 3.4 End disc twist (Schematic)
- 3.5 3D element - Disc (Force)
- 3.6 3D element - Disc (Moment)
- 3.7 Variation in stress σ_r for various ratios of β
- 3.8 Variation in stress σ_θ for various ratios of β
- 3.9 Variation in stress $\tau_{r\theta}$ for various ratios of β
- 3.10 Examples of various types of variable thickness discs
- 3.11 Disc profile illustrating collocation points
- 3.12 Coordinates system for collocation points in spline function

- 3.13 Photograph illustrating experimental frame
- 3.14 Schematics diagram of an experimental frame with parallel discs
- 3.15 Schematics diagram of an experimental frame with profiled discs
- 3.16 Details of experimental profile discs
- 3.17 Displacement w comparisons for constant thickness steel disc
- 3.18 Stress comparisons for constant thickness steel disc ($\beta = 0.3$)
- 3.19 Stress comparisons for constant thickness steel disc ($\beta = 0.5$)
- 3.20 Stress comparisons for variable thickness steel disc ($\beta = 0.3$)
- 3.21 Stress comparisons for variable thickness steel disc ($\beta = 0.5$)
- 3.22 Schematic diagram of a experimental frame with parallel discs for in-plane loading
- 4.1 Important regions of belt contact around a drive pulley
- 4.2 Important regions of belt contact around a idler pulley
- 4.3 Distribution of belt tension across the pulley face
- 4.4 3D element - Shell (Force)
- 4.5 3D element - Shell (Moment)
- 4.6 Co-ordinate system for shell analysis
- 4.7 Stress comparisons for the shell at $x = W/2$ for 120deg. belt wrap
- 4.8 Stress comparisons for the shell at $x = W/2$ for 180deg. belt wrap

- 4.9 Stress comparisons for the shell at $x = W/2$ for 240deg. belt wrap
- 4.10 Stress comparisons along the shell at $\theta = 65$ and 115 degrees
- 4.11 Stress comparisons for the shell at $x = W/2$ (Drive pulley)
- 4.12 Shell end effects
- 4.13 Variation of stress along the shell due to end effects
- 5.1 Photograph illustrating experimental frame (static belt pull)
- 5.2 Schematics diagram of experimental frame (static belt pull)
- 5.3 Stress comparisons at various radii on the disc ($\theta = 0\text{deg.}$)
- 5.4 Variation in stress σ_r at various positions on the disc
- 5.5 Variation in stress σ_θ at various positions on the disc
- 5.6 Stress σ_x comparisons for the shell at $x = W/2$
- 5.7 Stress σ_θ comparisons for the shell at $x = W/2$
- 5.8 Stress σ_x comparisons for the shell at $\theta = 60\text{deg}$
- 5.9 Stress σ_θ comparisons for the shell at $\theta = 60\text{deg}$
- 6.1 Finite Element Model
- 6.2 Stress comparisons at various radii on the disc ($\theta = 30\text{deg.}$)
- 6.3 Variation in stress σ_r at various positions on the disc
- 6.4 Variation in stress σ_θ at various positions on the disc
- 6.5 Stress σ_x comparisons for the shell at $x = W/2$
- 6.6 Stress σ_θ comparisons for the shell at $x = W/2$
- 6.7 Stress σ_x comparisons for the shell at $\theta = 60\text{deg.}$
- 6.8 Stress σ_θ comparisons for the shell at $\theta = 60\text{deg.}$

- 7.1 Flowchart illustrating design procedure
- 7.2 Stress variation within the shell
- 7.3 Variation in stress for a profiled disc

Figures are found at the end of each appropriate chapter.

CHAPTER 1

INTRODUCTION

1.1 REVIEW

The inland movement of bulk solid materials is usually performed by a combination of two modes of transport. For material transport over distances greater than 1-2km the load is generally carried in units of up to 200 tonnes in road or rail containers. This mode is used for national distribution of materials such as solid fossil fuel, ores and some unprocessed chemicals. For distances up to 2km the material, is for at least part of the journey, transported by some form of conveyor; whether underground or overland. The advantage of using a conveyor in this type of material recovery is that it supplies a relatively controlled constant flow of material to a transfer point or processing plant; the plant then need not be rated for peak material delivery rates.

Of the different types of conveyor that are used for bulk material transport the troughed belt conveyor is probably the most popular (a typical schematic layout and cross-section of a troughed conveyor is shown in figure 1.1). A material transportation rate of 10000 tonnes per hour over a distance of 1.5km can be found on some of the larger conveyor installations in Britain; in some countries (e.g. Germany, South Africa and Australia) a more typical maximum is 30000 tonnes per hour.

To achieve these high overall ratings the conveyors are operated 24 hours per day at belt speeds of up to 6 metres

per second on belts up to 3 metres wide. High reliability of the conveyor is essential and a design life of 25 years for the conveyor elements is not uncommon.

There are several ways of automatically monitoring belt conditions and it is easy to assess whether a belt need be replaced or repaired at the next major overhaul. Likewise, the idlers are easily accessible and even if one or two idler sets should fail in service, they are sufficiently closely spaced and the belt has adequate stiffness that the operation of the conveyor is not impaired.

The pulleys, however, and particularly drive pulleys, are usually guarded for safety, or are enclosed behind the sides for a material delivery chute. Hence they are completely inaccessible for inspection and maintenance and failure of the conveyor system is only discovered when the pulley has collapsed.

A pulley failure on a large conveyor system carrying say 5000 tonnes per hour of run-of-mine coal will cost 1000 pounds sterling per minute of lost production. The capital cost of installing a conveyor in parallel would be prohibitive; it is essential therefore, that the highest standards of design manufacturing are implemented in pulley production.

1.2 HISTORICAL BACKGROUND

Early design of conveyor pulleys was performed principally by empirical or rule-of-thumb methods. Conventional conveyor pulleys of forty years ago were made from cast iron (figure 1.2), with either a single or double row of spokes or discs, with integral bosses bored to fit on a central through-shaft.

Generally, the only calculations performed for these pulleys were to determine bending and torsional strength of the shaft, which, once sized, fixed the dimensions of the bosses to which the spokes or discs were attached. The dimensions of the drum shell were fixed to allow proper metal flow during the casting process and shaped to prevent contraction, deformation and cracking during manufacture. Several reasons for their success can be established, but the principal reason was that relatively low belt tensions induced low stresses in a component that was manufactured to minimise stress raising features by virtue of the casting process. Increasing belt tensions began to be subjected to the lower-strength belt carcasses of the time, resulting in the need for larger pulley diameters, which rendered the bulky cast iron pulley design uneconomical. Improvements in welding techniques caused the general introduction of fabricated steel pulleys which could be made larger and more economically.

The fabricated drums originally were straight substitutions for the shapes of the original cast pulleys, manufactured by structural steel fabricators, with a simple rolled steel shell and shell plate diaphragms, welded to bosses and fitted to shafts (figure 1.3). At the same time engineers considered that the stresses within the pulleys did not warrant the dimensions needed for castings and accordingly substituted thinner plates for shells and end discs. Most of these pulleys operated satisfactorily, but problems became more frequent with further increases in belt tensions; some pulleys failed in the shell, others cracked in the end discs

and others broke at the disc-to-hoss welded connection. The earliest specialised manufacturer (in the 1950's) began to construct pulleys based on the primitive theoretical work of Jackson [14] and William [29]. This enabled the size of the shell and discs to be determined. However, this placed greater emphasis on the quality of manufacture than the previous conservative designs and invariably resulted in pulley failure. Attempts were made to cater for the inadequacies of the earlier design methods and poor manufacturing techniques by increasing the strength of the end diaphragms by attaching ribs between the end discs and shell and by strengthening the shaft (figure 1.4). An additional problem, which had existed for many years, was the tendency of pulleys to "walk" off their shafts; this occurred more frequently with wider belts and fabricated pulleys. Key or shrink fitting of the hubs onto the shaft was popular in early designs, attempting to both prevent walking and to integrate the discs with the shaft for strength. Keyed hubs had limited load carrying capacity and usually were used in addition shrink fitting. The shrinking method of shaft attachment was costly and made shaft replacement difficult, in the event of damage prompting the introduction of various clamping devices. These clamping mechanisms usually featured a form of wedging action, which gave high pressure between the shaft and hub. The wedges were forced into position by screws which could be released to allow shafts to be withdrawn from the drum for replacement. Assembly of these earlier taper attachments (figure 1.5) involved unwieldy procedures for alignment. If

alignment after welding was not carefully maintained then inefficient, eccentric clamping was produced and unnecessary bending moments were introduced into the boss and discs, leading to disc failures. These earlier single taper attachments moved laterally along the shaft during the clamping process, again causing unnecessary forces to be applied to the disc. Early double wedge type attachments (figure 1.6) overcame the problem of lateral movement, but still required accurate alignment. These devices offered reliable torque transmission, which eliminated the need for keyways as the secondary means of support. Later, a self-aligning double-wedge-type attachment (figure 1.7) was developed, which maintained the same reliable torque transmission features but, at lower surface pressures and required only simple machining techniques.

Initial pulley constructions used a boss bored to suit the single or double type taper-lock attachments, with a disc diaphragm welded to the boss and shell. With higher belt tensions there was an increasing number of failures of disc to boss welds. To overcome these problems engineers developed what became known as the 'turbine blade' shaped pulley end disc. This style dispensed with the disc-to-boss joint and the equivalent of a boss was used to house and restrain the shaft clamping unit. The disc thickness reduced smoothly from inner to outer diameter to allow proper metal flow during the casting process.

This design proved successful for many installations. However, failures of pulleys continued, where still further increases of both belt tensions and belt widths had occurred.

Further innovations of the types of end disc shape are presented in chapter 3.

Early shell designs were adopted from pressure vessel stress analysis. Failures of satisfactory shell welds on low wrap (30 degrees) pulleys, where 180 degree pulleys with the same belt tension worked successfully, highlighted the need to reappraise the shell analysis to account for various wrap angles; this analysis is presented in chapter 4.

1.3 LITERATURE REVIEW

Literature associated directly with the analysis of conveyor pulleys is rare, usually illustrating only simple theoretical formulae to determine disc stresses and shaft deflections.

Jackson [14] considered the interactive influence between pulley elements in an integral assembly, making the first important distinction between 'thick' and 'thin' end-disc designs.

Lange [17] derived some interesting results concerning the distribution of stresses across the pulley face, and presented a basic analysis of variable thickness end discs. The shell analysis was limited to one belt wrap angle and ignored the end effects normal to closed end shells.

Schmoltzi [25] studied the effects of transverse bending moments applied through a double-wedge-type attachment from the shaft to disc.

Theoretical work on the analysis of the end disc and shell was also scarce. Conway ([3], [4], [5]) presented basic analyses of constant and variable thickness discs. Mansfield [19] and Olsson [20] illustrated more complex theoretical models

of variable thickness discs. However the disc profiles were very simple. Flugge [10] analysed various shell loading conditions.

1.4 PURPOSE OF THIS INVESTIGATION

Whilst the most sophisticated non-destructive testing methods can be applied to the pulley during its manufacture little detailed information exists for the designer to be able to assess the levels of stress that a pulley experiences during service. The aim of the present investigation is to provide a comprehensive method of determining the stresses and displacements in a conveyor pulley under practical conditions. The individual objectives are to provide stress and deformation information for the pulley shell, end discs and shaft and to reinforce the proposed methods of analysis with experimental data. Further, a procedure for obtaining a minimum weight design of end disc is proposed, again verified by experimental data.

The text of this thesis is presented as follows:

Chapter 2 presents an overview of shaft design methods.

Chapter 3 presents the theoretical model for bending stresses induced in constant and variable thickness discs.

Experimental verification is also provided.

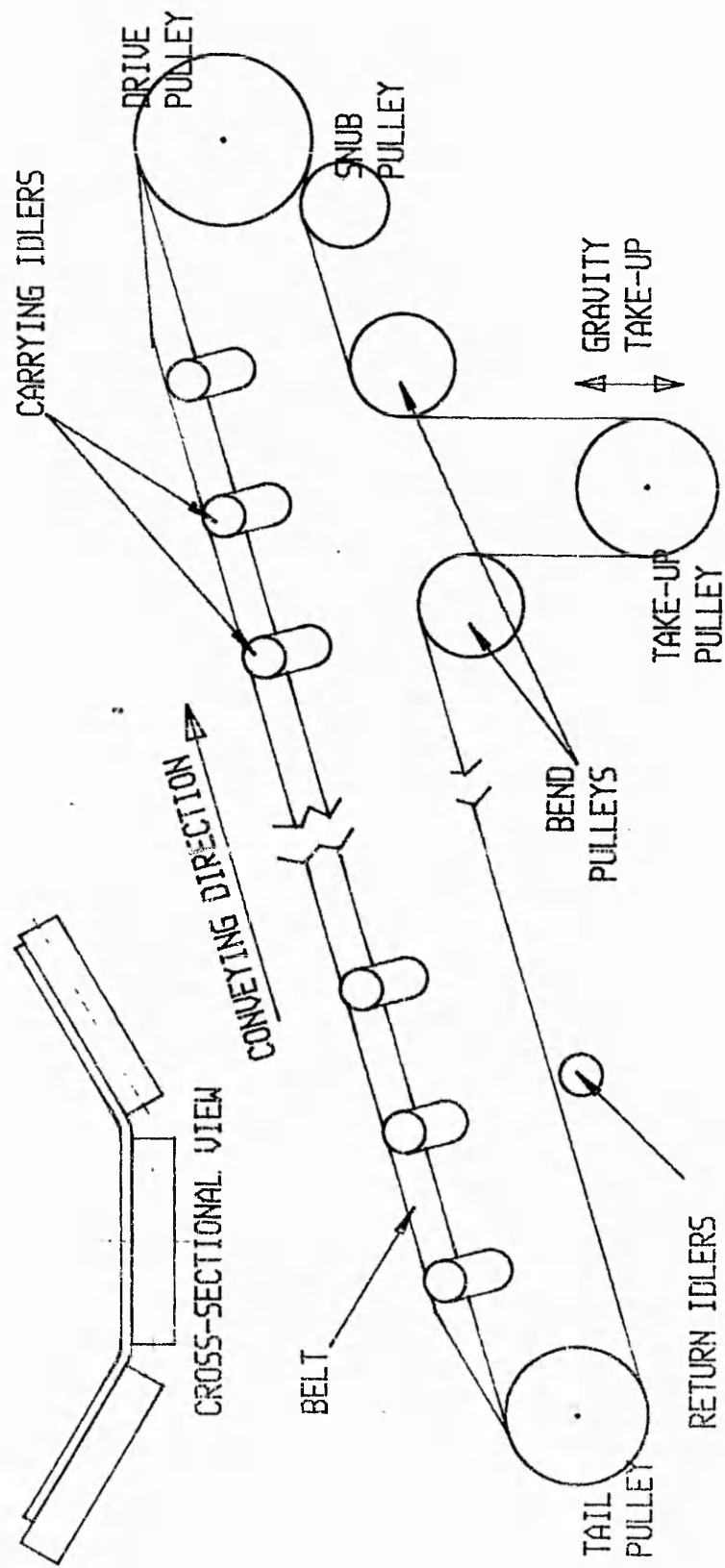
Chapter 4 presents a detailed consideration of the belt loading characteristics and theoretical model for shell stresses and deflections.

Chapter 5 presents experimental verification for both end disc and shell theoretical models.

Chapter 6 presents a finite element analysis, which is provided for purposes of comparing various theoretical methods and experimental results.

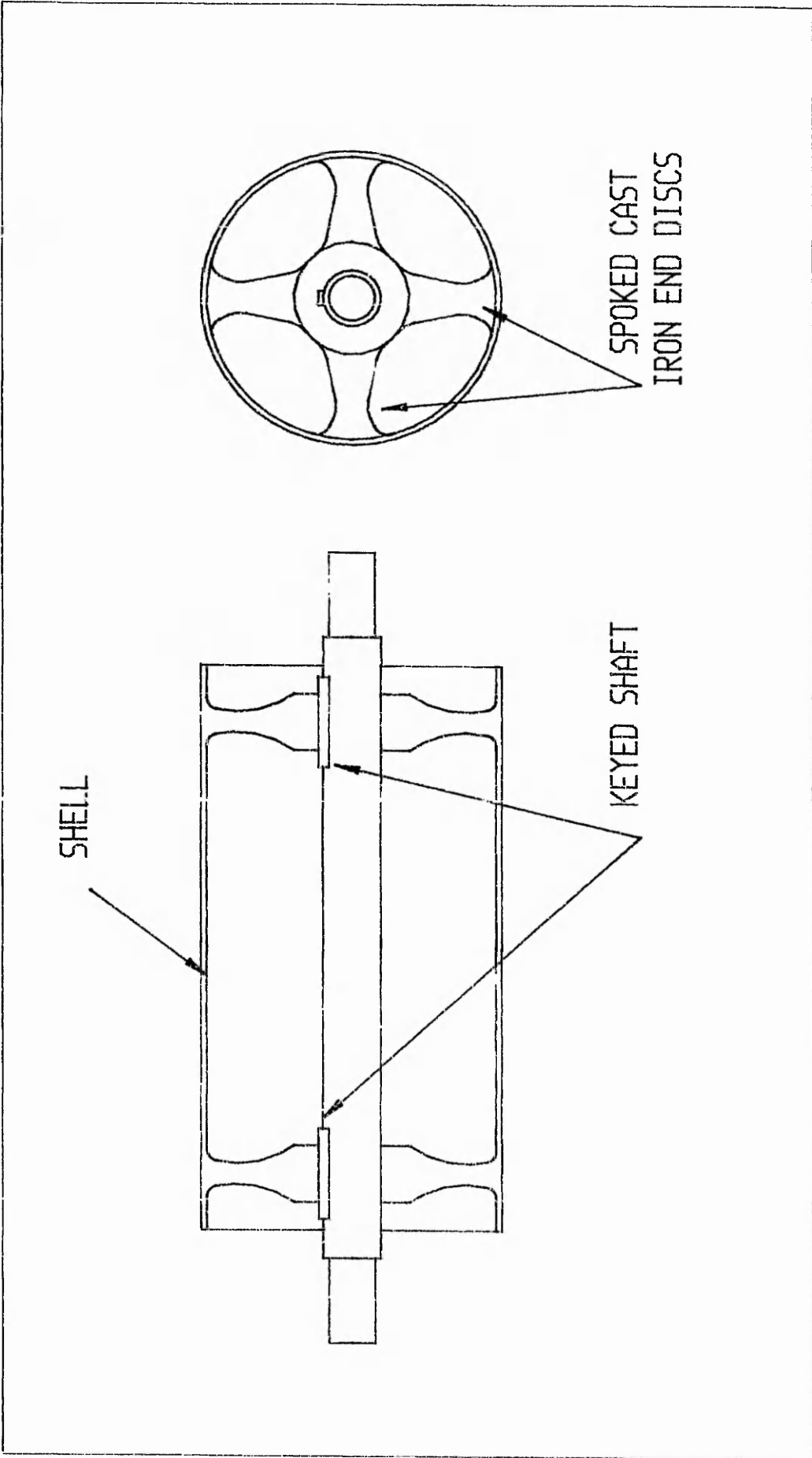
Chapter 7 presents a complete design procedure for conveyor pulleys.

Chapter 8 finally draws conclusions from the above discussion and presents ideas for further work which could be carried out to enhance the theoretical models considered.



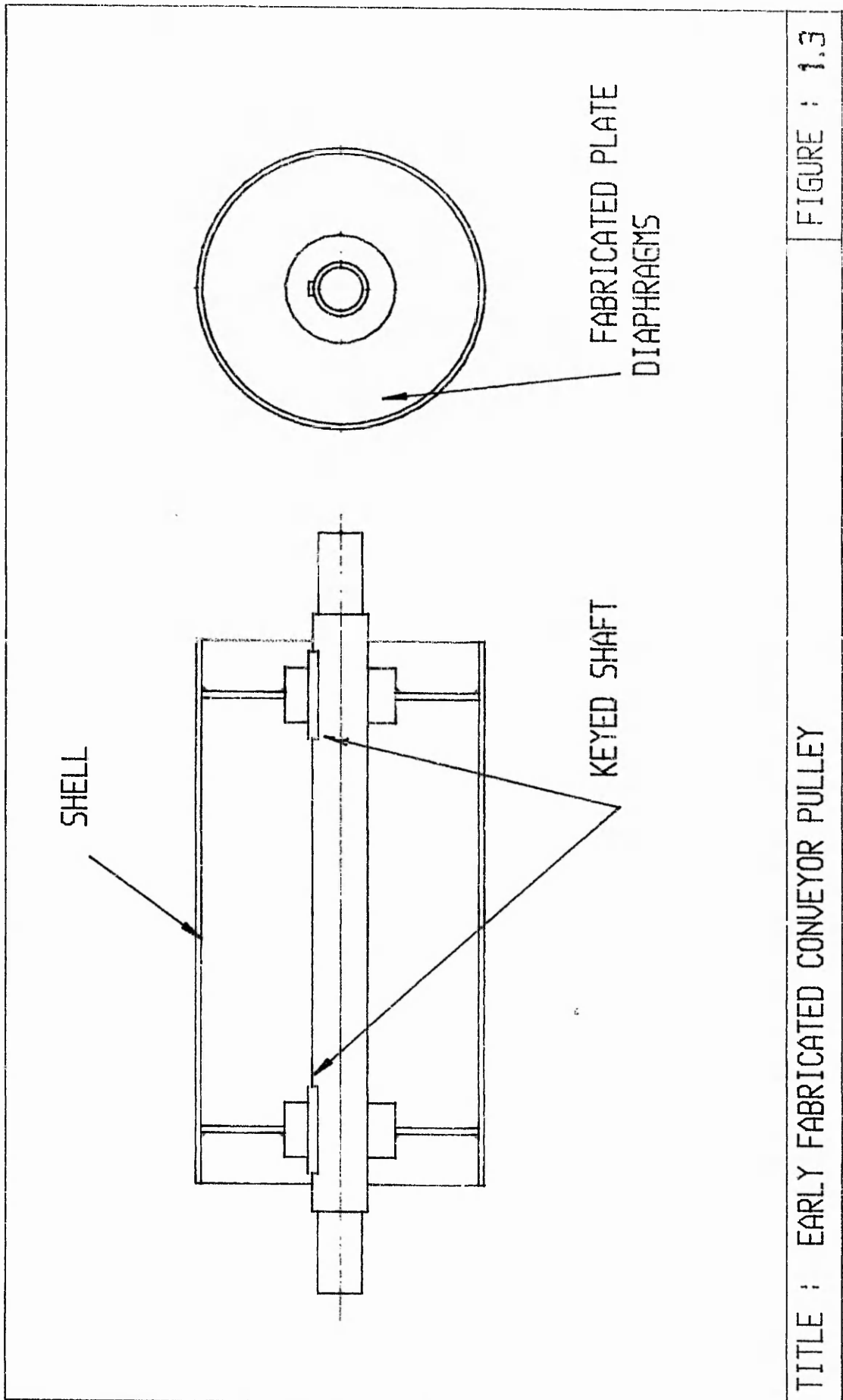
TITLE : SCHEMATIC DIAGRAM OF A TYPICAL BELT CONVEYOR

FIGURE : 1.1



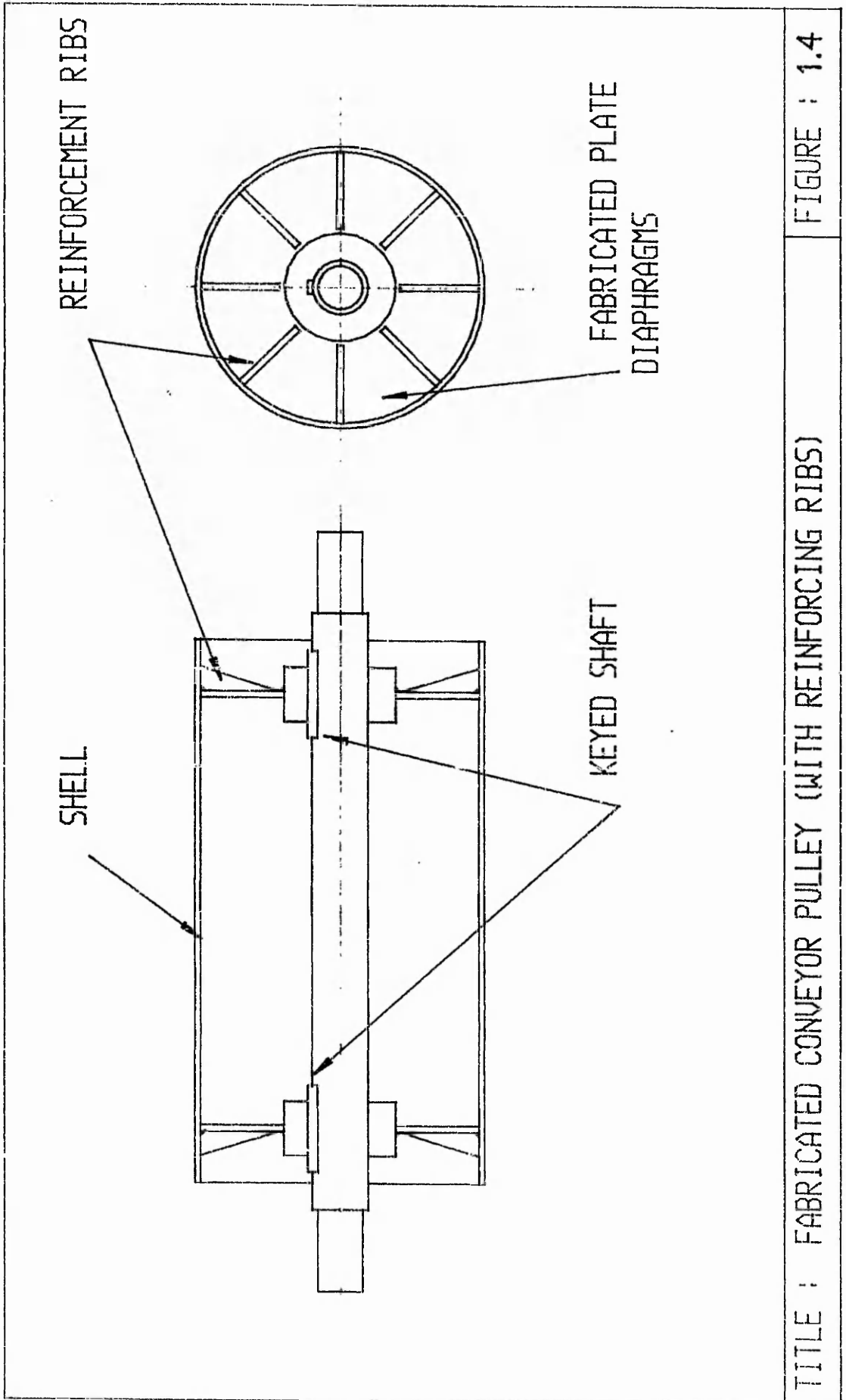
TITLE : CAST IRON CONVEYOR PULLEY

FIGURE : 1.2



TITLE : EARLY FABRICATED CONVEYOR PULLEY

FIGURE : 1.3



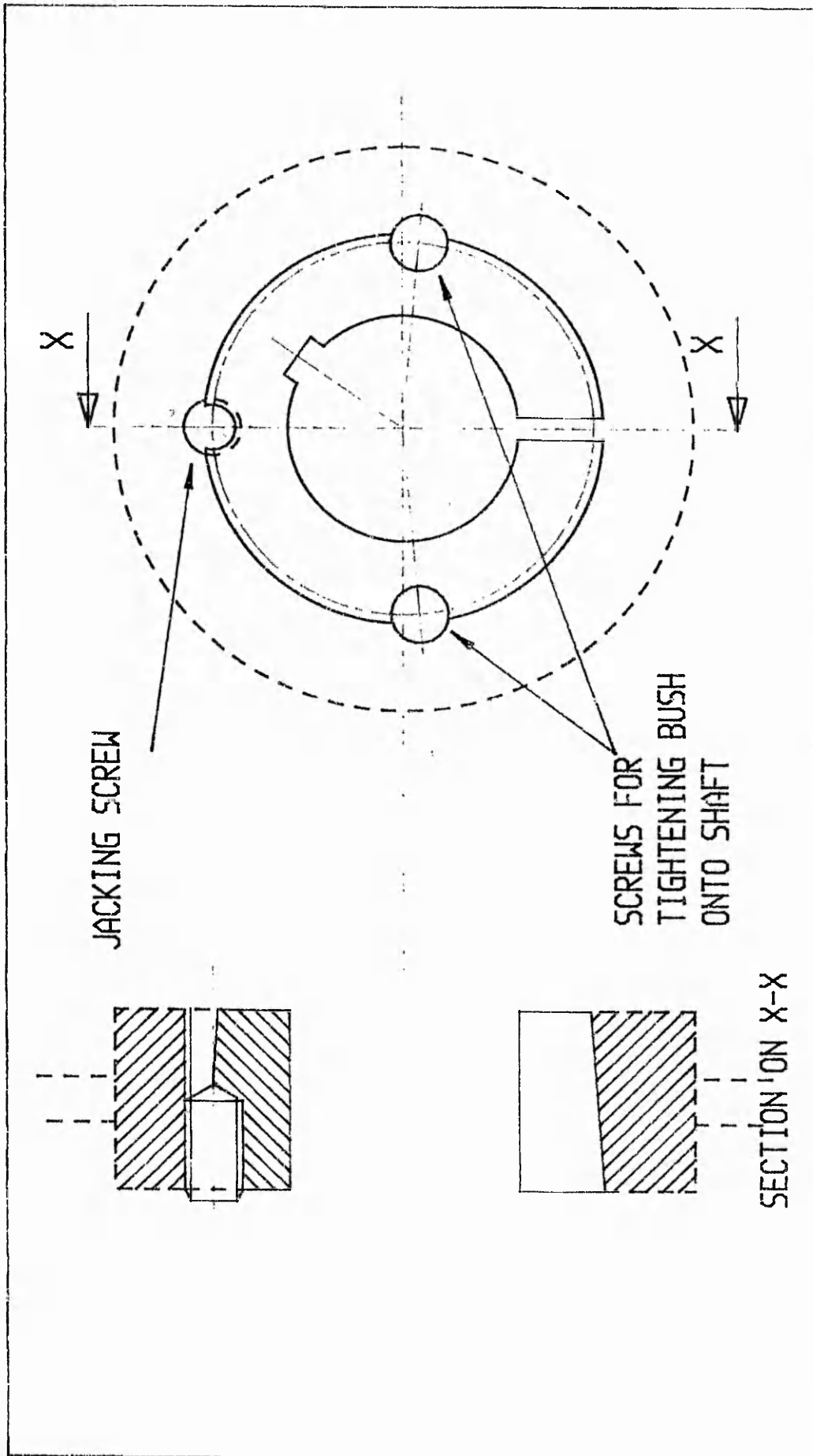
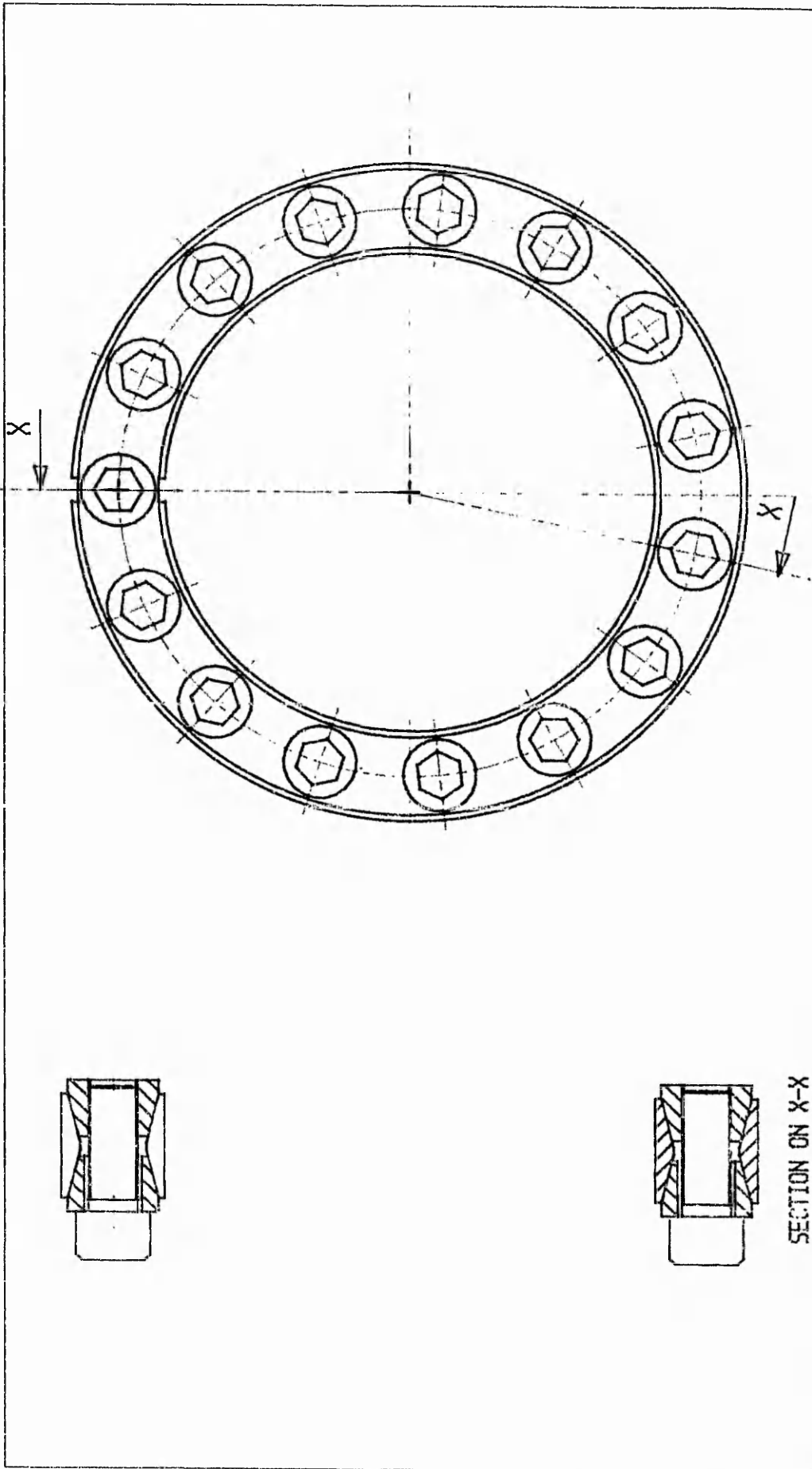


FIGURE : 1.5

TITLE : SINGLE WEDGE COMPRESSIVE SHAFT FASTENER



TITLE : DOUBLE WEDGE COMPRESSIVE SHAFT FASTENER (WITHOUT CENTERING) FIGURE : 1.6

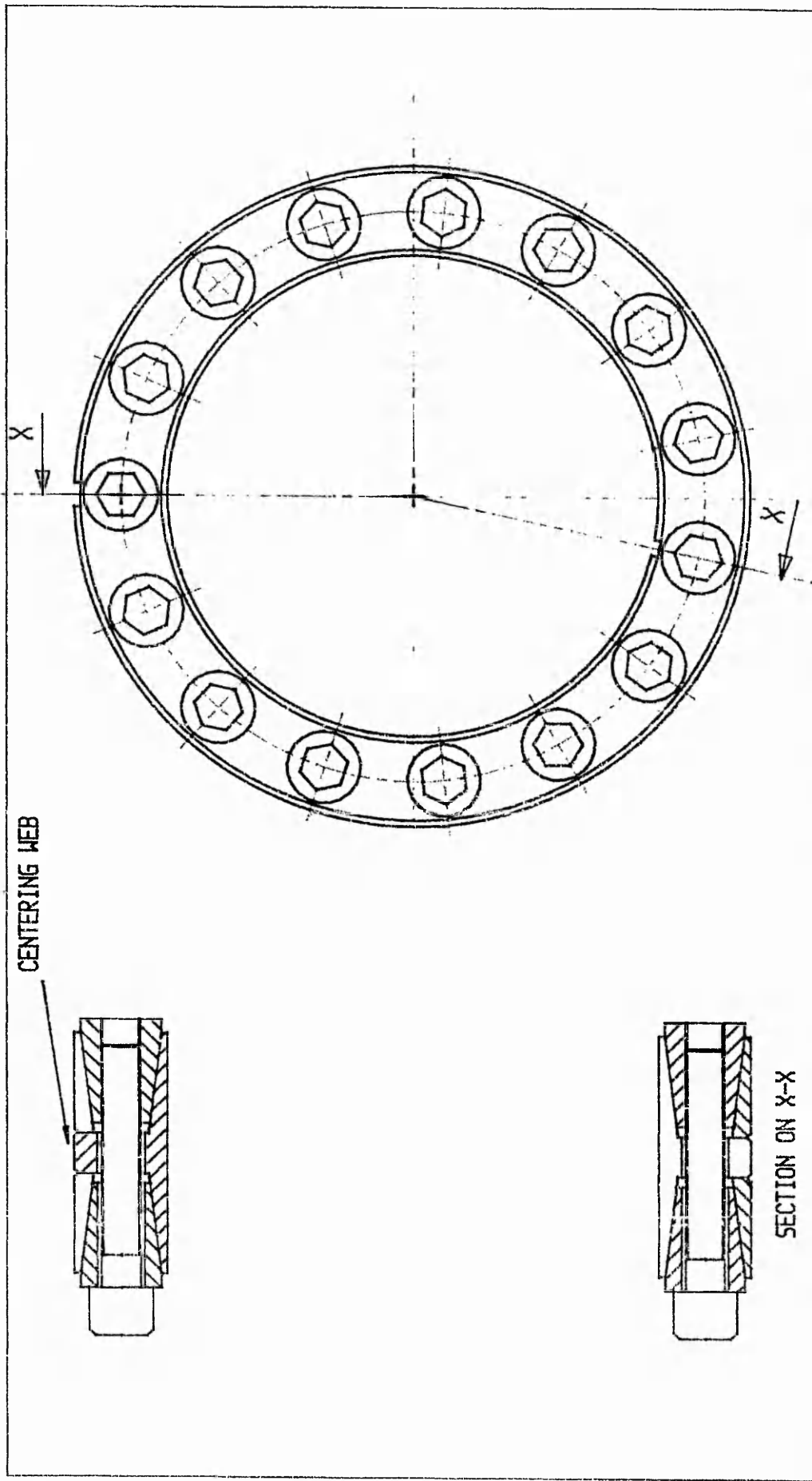


FIGURE : 1.7

TITLE : DOUBLE WEDGE COMPRESSIVE SHAFT FASTENER (WITH CENTERING)

GENERAL THEORY

The theoretical analysis carried out in the thesis will be based on loads induced during normal operation. The overall moment distribution within the pulley assembly will be presented in the chapter, with formulas to determine resultant forces, pulley and shaft sizes.

The complex stresses induced within a pulley are due to reaction loads resulting from the belt pull and the statically indeterminate moments induced by the deflection of the pulley assembly may be determined independently and summed in the final analysis.

2.1 APPLIED BELT PULL

To determine the magnitude and direction of the resultant belt pull P (figure 2.1), consider a pulley to be subjected to a tight side belt tension T_t and a slack side belt tension T_s (figure 2.1). The angle of the belt as it enters the pulley and exits the pulley are θ_s and θ_t respectively. The weight of the pulley is generally small in relation to the belt tensions, and therefore is ignored. The resultant belt pull is determined by resolving the tensions, which gives

(2.1)

$$P = \left[T_t^2 + T_s^2 + 2.T_t.T_s.\cos(\theta_t - \theta_s) \right]^{0.5}$$

$$\text{where } \theta_p = \tan^{-1} \left[\frac{T_t.\sin(\theta_t) + T_s.\sin(\theta_s)}{T_t.\cos(\theta_t) + T_s.\cos(\theta_s)} \right]$$

The minimum outside diameter of the pulley is normally

specified by the belt manufacturer, who has carried out exhaustive tests to establish the minimum diameter of his belt to wrap around a pulley. A simple formula is still used for guidance which takes into account the belts stiffness, the angle of wrap and belt width.

(2.2)

$$\text{Pulley outside diameter } D_p = 2.b = \frac{360.P}{\pi.B.p_b.(2.\theta_w)}$$

where p_b is effective modulus of rigidity of the belt, $2 \times \theta_w$ represents the total wrap of the belt and B is the belt width.

2.2 DETERMINATION OF SHAFT SIZE

The shaft is sized to accommodate the stresses and deflections corresponding to a beam supported at its ends and loaded at two symmetrically positioned forces which coincide with the end disc centres.

Often, the minimum shaft diameter is already established by the size of the bearings which are determined on the basis of the bearing load and the required life in hours (table 2.1, equation A). The value 3/10 is the factor for roller bearings which are normally used with conveyor pulleys.

The size of the shaft fastener is the next consideration in determining the shaft size, established by limiting the slope of the shaft at fastener centreline (table 2.1, equation B). Equation B, table 2.1 assumes that the shaft diameter between the end discs is the same as the diameter determined for the fastener. The manufacturers recommended maximum allowable slope varies for different fastener types between 3 and 8

minutes. These limits should be related to the fastener's ability to absorb the bending moments carried by the pulley. This limit is set to prevent the surface pressures within the fastener (various types discussed in chapter 1) from becoming either too high causing plastic deformation or too low causing joint movement.

Finally, the shaft size is confirmed by checking the ability to absorb simultaneously stresses induced by the driving torque T on drive shafts (table 2.1, equation C) and the bending moment which reaches a maximum for the shaft just outside the end discs (table 2.1, equation D). The bending (K_b) and torsional (K_t) fatigue factors used in equations C and D are typically set to 1.5 and 1.0 respectively. The value for bending fatigue factor is typical for the design of a rotating shaft with variable amplitude bending load.

Similarly the value for torsional fatigue factor is typical as the driving torque is reasonably constant. It will only vary during the starting and stopping of the conveyor, which normally only occurs in an emergency.

Consideration was not given to shear deformation, however with $L(\text{min.}) = 300\text{mm}$ and the ratio $d_s/\chi(\text{max.}) \leq 0.2$ the effect of shear deformations is to increase the maximum deflection found at the centre of the shaft by less than 5%, thus its influence can be safely ignored.

2.3 SHAFT STIFFNESS

The shaft stiffness is easily obtained from elementary beam theory. However, it is custom and practice by many pulley manufacturers to increase the effective diameter from that

used for the fastener. Again using beam theory for variable-section shafts (figure 2.3) the effective stiffness of the shaft is written as

$$k_s = \frac{M_s}{\phi_s} \quad (2.3)$$

where M_s and ϕ_s are bending moment carried by the shaft and shaft rotation at the end disc centreline respectively. Using simple beam theory the shaft rotation ϕ_s is defined by

$$\phi_s = \frac{M_s}{E} \left[\int_0^{(W-L_s)/2} \frac{1}{I_{s2}} dx + \int_{(W-L_s)/2}^{W/2} \frac{1}{I_{s1}} dx \right] \quad (2.4)$$

where $I_{s1} = \frac{\pi \cdot d_1^4}{64}$ and $I_{s2} = \frac{\pi \cdot d_2^4}{64}$

Substituting the integral 2.4 into equation 2.3

$$k_s = \frac{2 \cdot E}{\left[\frac{W - L_s}{I_{s2}} + \frac{L_s}{I_{s1}} \right]} \quad (2.5)$$

The end disc and shell stiffnesses will be determined in chapter 3 and 4 respectively. Chapter 6 will conclude these discussions by illustrating the design principles instigated in this chapter.

TABLE 2.1

Some important shaft calculations.

Ref. Description & Equation

A d_s (min) obtained from a bearing manufacturers data sheets for the following rating C.

$$C = \frac{P \cdot f_d \cdot f_k}{2} \left[\frac{1.8S \cdot L_{10}}{\pi} \right]^{3/10}$$

f_d ; f_k dynamic load factors

B d_s (min) is determined from limiting the slope ϕ_s at the centreline of the end disc.

$$d_s = \left[\frac{M_s \cdot W}{\phi_s} \left[\frac{32}{\pi \cdot E} \right] \right]^{1/4}$$

C d_s (min) is determined from limiting the stress τ (permissible shear), subject to drives only

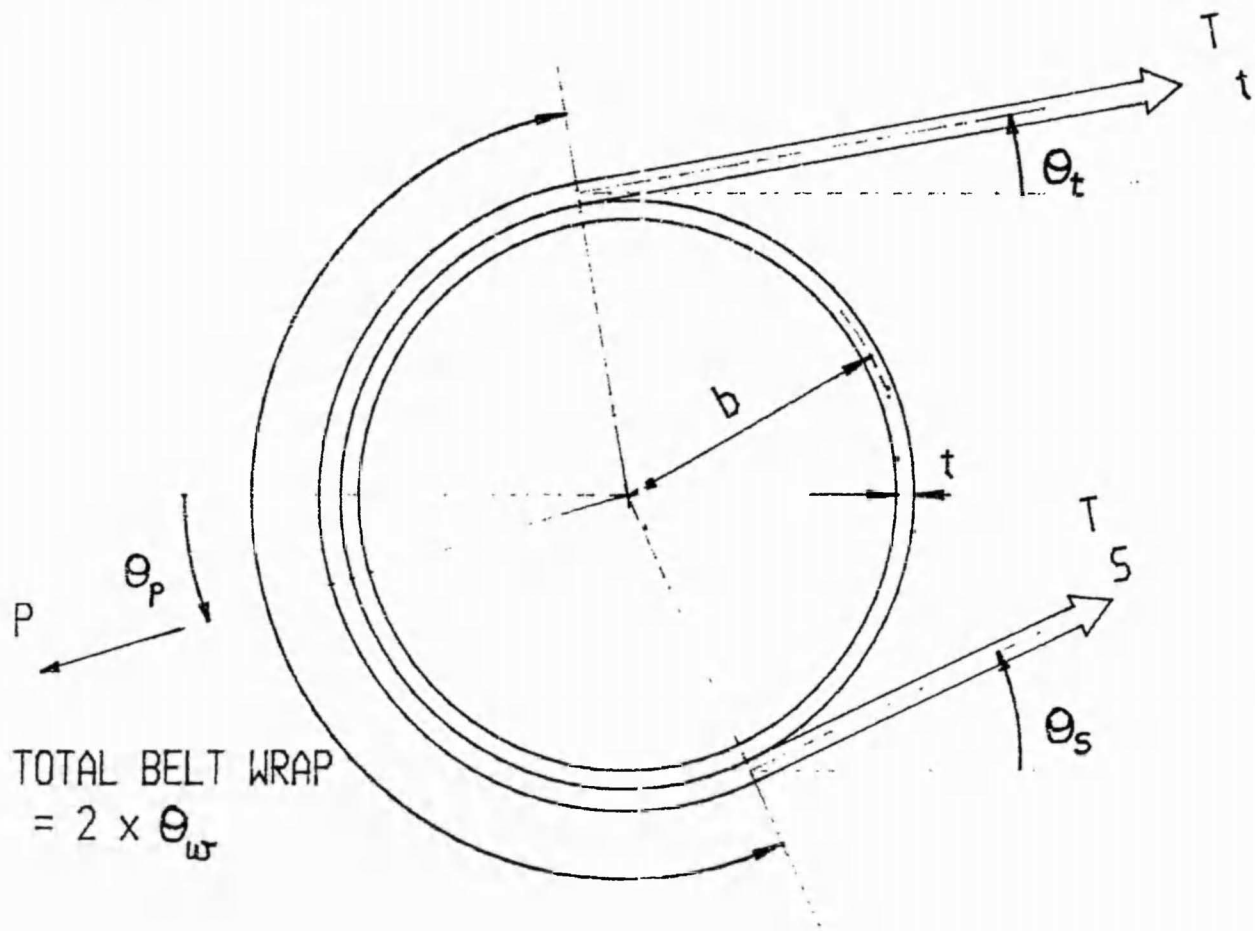
$$d_s = \left[\frac{16}{\pi \cdot \tau} \left[\left(K_b M_s \right)^2 + \left(K_t T \right)^2 \right]^{1/2} \right]^{1/3}$$

K_b ; K_t fatigue factors for bending & torsion respectively.

D d_s (min) is determined from limiting the stress σ_b (permissible bending), subject to non-drive only

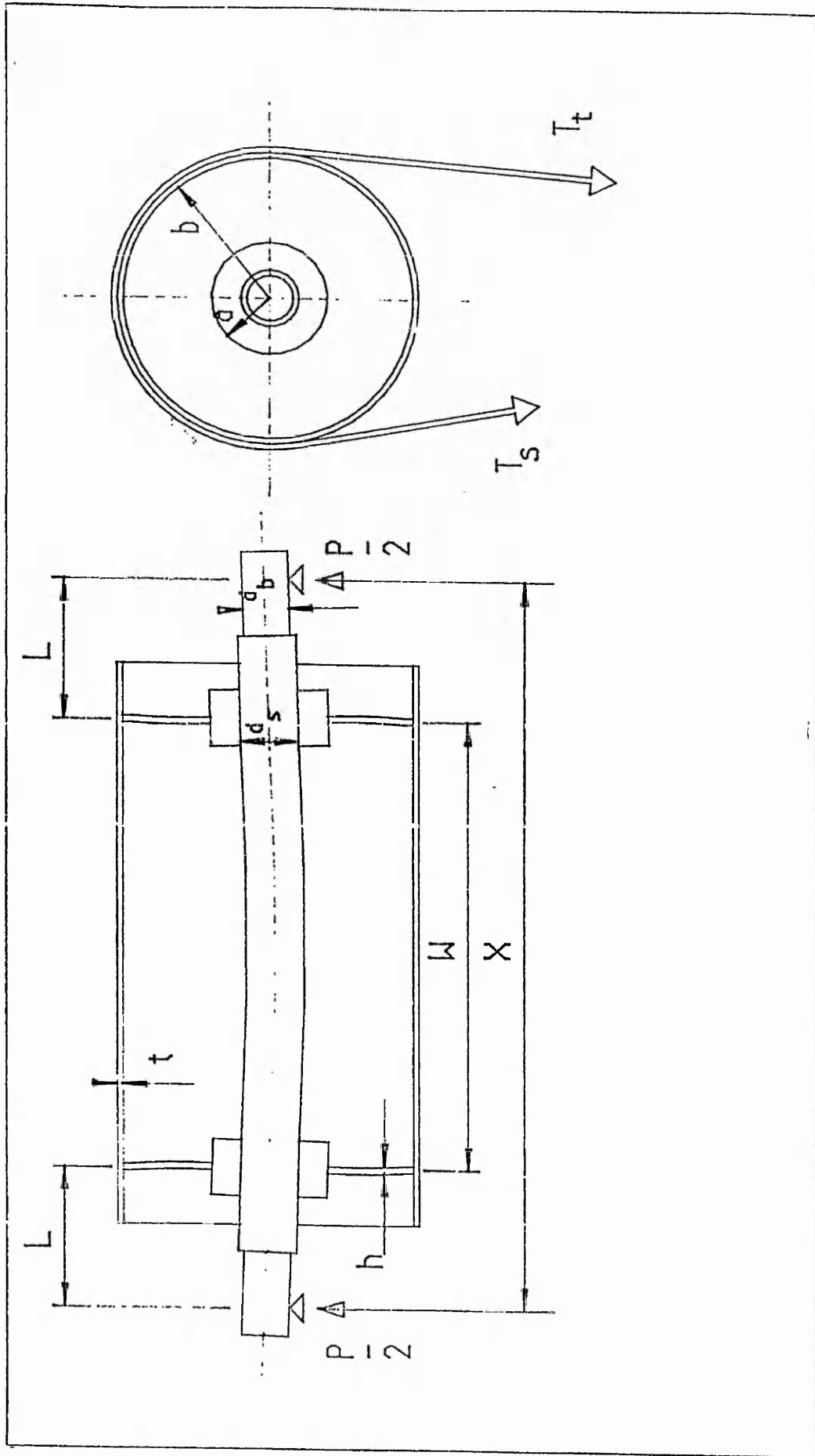
$$d_s = \left[\frac{32 M_s \cdot K_b}{\pi \cdot \sigma_b} \right]^{1/3}$$

K_b fatigue factor for bending only.



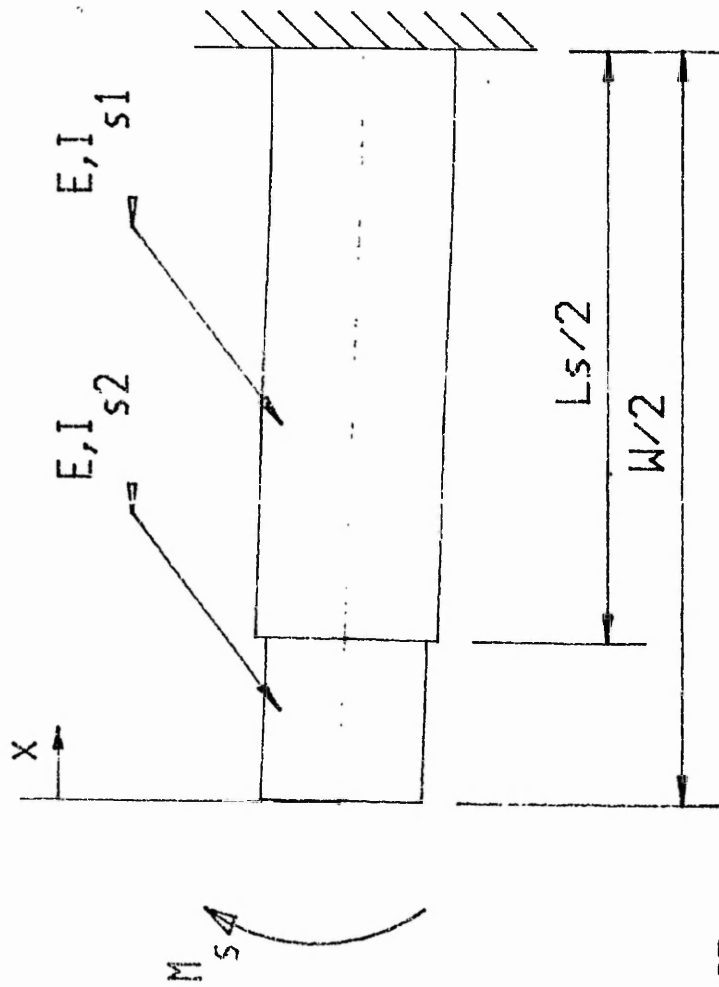
TITLE : SCHEMATIC DIAGRAM SHOWING MAGNITUDE & DIRECTION OF BELT PULL

FIGURE : 2.1



TITLE : SCHEMATIC DIAGRAM OF A CONVEYOR PULLEY

FIGURE : 2.2



L_s = LENGTH OF
BUILT-UP CENTRAL SECTION

TITLE : DIAGRAM SHOWING VARIABLE SECTION SHAFT

FIGURE : 2.3

CHAPTER 3

END DISC ANALYSIS

The end disc of a pulley is subject to both membrane and bending stresses. The bending stresses induced in the end disc result from the relative rotation of the shaft at the inner boundary. The membrane stresses in the end disc are due to the pressure of the belt on the shell at the outer radius, reacted by the pressure induced by the shaft fastener at the inner radius.

General assumptions concerning to the disc analysis

For the purpose of both membrane and bending analysis of the end disc, the disc is considered to be symmetrical about the centre line of its thickness. The disc material is assumed to be elastic, homogeneous and isotropic and the usual plate theory assumptions are invoked, namely

- (i). Deflections are small in comparison with disc thickness.
- (ii) All points of the plate lying on a normal-to-a-middle plane of the plate remain so before and after deformation.
- (iii) The normal stresses in the direction transverse to the plate can be disregarded ($\sigma_z = 0$).

3.1 OVERALL MOMENT DISTRIBUTION AND BOUNDARY CONDITIONS

3.1.1 OVERALL MOMENT DISTRIBUTION

The maximum bending moment (figure 3.1) produced just outside the end disc is given by $M = PL/2$. This moment is carried

by each of the components which make up a conveyor pulley and the relative distribution of this moment depends directly on each elements stiffness. The bending moment carried by each element is determined from the product of its stiffness k and rotation ϕ

$$\text{ie. } M = k \cdot \phi \quad (3.1)$$

The statically indeterminate system can be seen as a parallel connection of two springs, one representing the stiffness of the shaft k_s , the other representing the effective stiffness of the drum assembly k_p . They are bent by the same amount at the joint between the shaft and the fastener. The assumption that they both rotate by the same amount at this connection is derived from the fact that the fastener does not lift off the shaft. Compatibility of rotation is reflected in the following relationship.

$$\frac{M_s}{k_s} = \frac{M_p}{k_p} \quad (3.2)$$

where M_s and M_p are the moments carried by the shaft and drum assembly respectively.

The moment shared between the shaft and the drum assembly is written as,

$$M_t = M_s + M_p \quad (3.3)$$

The stiffness k_p is the equivalent stiffness of the drum assembly which represents a number of springs connected in series (figure 3.2). With symmetry considered, these components consist of a shaft fastener, hub, end disc and a shaft plus shell up to a plane which is central between the end discs.

Thus, the effective stiffness of the drum assembly is as follows:

$$k_p = \frac{1}{\left[\frac{1}{k_f} + \frac{1}{k_h} + \frac{1}{k_d} + \frac{1}{k_{sh}} \right]} \quad (3.4)$$

where k_f , k_h , k_d , k_{sh} represents the individual stiffnesses of the fastener, hub, end disc and shell respectively.

Substituting equations 3.2 and 3.4 into equation 3.3, yields the bending moment carried by the drum assembly.

$$M_p = \frac{M_t}{\left[k_s \cdot \left[\frac{1}{k_f} + \frac{1}{k_h} + \frac{1}{k_d} + \frac{1}{k_{sh}} \right] + 1 \right]} \quad (3.5)$$

As the drum assembly is constructed from a number of springs connected in series the moment carried by each component must be the same.

If each component of the drum assembly is examined more carefully it is possible to remove some of the stiffness from equation 3.5 with confidence. The large mass of the hub is very much stiffer than the other components, thus k_h is assumed to be infinite. The evaluation of the stiffness of a fastener has been considered previously Schmolzki [25], with limited success. However, a well designed and constructed device will allow very little relative rotation within itself: therefore its stiffness is regarded as very high. Hence, since the fastener and hub stiffnesses can be considered infinite, equation 3.5 can be written as

$$M_p = \frac{M_t}{\left[k_s \cdot \left(\frac{1}{k_d} + \frac{1}{k_{sh}} \right) + 1 \right]} = M_d \quad (3.6)$$

Such authors as Conway [3] [4] [5], Jackson [14], Lange [17] and Williams [29] considered the shell stiffness to be infinite when analysing the end disc, resulting in equation 3.6 further reducing to,

$$M_p = \frac{M_t}{\left[\frac{k_s}{k_d} + 1 \right]} \quad (3.7)$$

This leads to a very conservatively designed drum assembly, with too many components regarded as rigid leading to an unnecessarily imbalanced moment distribution within the assembly. Therefore, equation 3.6 will be used to form the basis of the present analysis.

3.1.2 BOUNDARY CONDITIONS

The relationship between the bending stiffnesses of the shaft and drum assembly is discussed above, where two equations describing the distribution of bending moment between these elements are derived. The first assumption considers the shell stiffness to be infinite, resulting in a rigid outer boundary to the disc (figure 3.3). The second assumption considers the shell's stiffness to be sufficiently low not to influence the bending moment distribution between the drum and shaft (figure 3.4). The bending of the shell will result in a reduction in the moment carried by the disc (see equation 3.6).

For a complete analysis therefore it is necessary to consider the following boundary conditions

CASE 1 Disc outer boundary fully-clamped to yield the disc stiffnesses required in the moment distribution in equation 3.7.

CASE 2 Outer boundary simply-supported, the results to be used as a comparison only with experimental data illustrated later in this chapter.

CASE 3 Outer boundary partially-restrained. The results from this analysis are to be used as a comparison against results from a static belt pull test on a complete pulley assembly. This boundary condition requires the determination of both disc and shell stiffnesses.

3.2 METHOD OF ANALYSIS

To achieve our ultimate aim of developing a technique to analyse variable-thickness (ie. minimum weight) discs, two analytical techniques will be considered. The method of Timoshenko and Woinowsky-Krieger [28] for the analysis of variable-thickness discs does not easily allow for a re-distribution of shear forces and internal moments, which may both significantly affect stress and deflexion results. It is necessary therefore to employ the Rayleigh-Ritz strain energy method (Richards [22]) to more accurately account for these variables. The first stage of the analysis however will be to analyse constant thickness discs using Rayleigh-Ritz against the method of Timoshenko and Woinowsky-Krieger to provide a benchmark to assess the accuracy of the former method in relation to the number of terms required in the

approximation.

3.2.1 ELASTIC RELATIONSHIPS FOR A PLATE SUBJECT TO BENDING

In order to describe the changes in shape due to the bending of either the constant or variable thickness discs, consider the element shown in figure 3.5, 3.6. The governing equations may be written down as [28]

$$\begin{aligned} \epsilon_r &= -z \cdot \frac{\delta^2 \omega}{\delta r^2} & \gamma_{r\theta} &= -2z \cdot \frac{\delta}{\delta r} \left(\frac{1}{r} \frac{\delta \omega}{\delta \theta} \right) \\ \epsilon_\theta &= -z \cdot \left(\frac{1}{r} \frac{\delta \omega}{\delta r} + \frac{1}{r^2} \frac{\delta^2 \omega}{\delta \theta^2} \right) \end{aligned} \quad (3.8)$$

$$\begin{aligned} \sigma_r &= \frac{E}{(1-\nu^2)} (\epsilon_r + \nu \cdot \epsilon_\theta) & \sigma_\theta &= \frac{E}{(1-\nu^2)} (\epsilon_\theta + \nu \cdot \epsilon_r) \end{aligned} \quad (3.9)$$

$$\tau_{r\theta} = G \cdot \gamma_{r\theta} \quad \text{where } 2G = \frac{E}{(1+\nu)}$$

The bending and twisting moments per unit length (M_{rr} , $M_{\theta\theta}$) and $M_{r\theta}$ respectively, along with the shearing forces Q_r , Q_θ may be expressed as

$$\begin{aligned} M_r &= \int_{-h/2}^{h/2} \sigma_r \cdot z \, dz = -D \cdot \left(\frac{\delta^2 \omega}{\delta r^2} + \nu \cdot \left(\frac{1}{r} \frac{\delta \omega}{\delta r} + \frac{1}{r^2} \frac{\delta^2 \omega}{\delta \theta^2} \right) \right) \\ M_\theta &= \int_{-h/2}^{h/2} \sigma_\theta \cdot z \, dz = -D \cdot \left(\nu \cdot \frac{\delta^2 \omega}{\delta r^2} + \frac{1}{r} \frac{\delta \omega}{\delta r} + \frac{1}{r^2} \frac{\delta^2 \omega}{\delta \theta^2} \right) \end{aligned} \quad (3.10)$$

$$M_{r\theta} = \int_{-h/2}^{h/2} \tau_{r\theta} \cdot z \, dz = -D(1-\nu) \left(\frac{1 \delta^2 \omega}{r \delta r \delta \omega} - \frac{1 \delta \omega}{r^2 \delta \theta} \right)$$

$$Q_r = \int_{-h/2}^{h/2} \tau_{rz} \cdot dz \quad ; \quad Q_\theta = \int_{-h/2}^{h/2} \tau_{\theta z} \cdot dz$$

$$D = \frac{E \cdot h^3}{12 \cdot (1-\nu^2)} \quad (3.11)$$

Thus, the stresses for the disc are as follows

$$\sigma_r(\max) = -\frac{6 \cdot M_r}{h^2} = -\frac{6 \cdot D}{h^2} \left(\frac{\delta^2 \omega}{\delta r^2} + \nu \cdot \left(\frac{1 \delta \omega}{r \delta r} + \frac{1 \delta^2 \omega}{r^2 \delta \theta^2} \right) \right) \quad (3.12)$$

$$\sigma_\theta(\max) = -\frac{6 \cdot M_\theta}{h^2} = -\frac{6 \cdot D}{h^2} \left(\frac{\nu \delta^2 \omega}{\delta r^2} + \frac{1 \delta \omega}{r \delta r} + \frac{1 \delta^2 \omega}{r^2 \delta \theta^2} \right)$$

$$\tau_{r\theta}(\max) = -\frac{6 \cdot M_{r\theta}}{h^2} = -\frac{6 \cdot D(1-\nu)}{h^2} \left(\frac{1 \delta^2 \omega}{r \delta r \delta \omega} - \frac{1 \delta \omega}{r^2 \delta \theta} \right)$$

where the flexural stiffness D is represented by D_c and $D(\rho)$ for constant and variable thickness discs respectively.

3.2.2 TRADITIONAL METHOD

The problem of twisting a constant-thickness annular disc with a rigid central boss along with various outer edge boundary conditions, has been considered previously [28]. This work derived solutions for the fully clamped (case 1) and simply supported (case 2) outer boundary conditions. An outline of the theory is reproduced here, together with a

solution for partially restrained (case 3) outer boundary condition.

The equilibrium equation for a plate free of distributed tractions, expressed in polar co-ordinates is:-

$$- \frac{1}{r^2} \frac{\delta M_{r\theta}}{\delta \theta} - 2 \frac{\delta^2 M_{r\theta}}{r \delta r \delta \theta} + \frac{1}{r^2} \frac{\delta^2 M_{\theta}}{\delta \theta^2} + \frac{\delta^2 M_r}{\delta \theta^2} + 2 \frac{\delta M_r}{r \delta r} = 0 \quad (3.13)$$

Substituting for the derivatives of the internal moments shown in section 3.2.1, and assuming that the thickness and hence the flexural stiffness, are independent of both r and θ , the following differential equation in terms of the transverse displacement ω can be obtained:-

$$\left[\frac{\delta^2}{\delta r^2} + \frac{1}{r} \frac{\delta}{\delta r} + \frac{1}{r^2} \frac{\delta^2}{\delta \theta^2} \right] \cdot \left[\frac{\delta^2 \omega}{\delta^2 r} + \frac{1}{r} \frac{\delta \omega}{\delta r} + \frac{1}{r^2} \frac{\delta^2 \omega}{\delta \theta^2} \right] = 0 \quad (3.14)$$

For this particular problem, a solution has been formulated [28], where a fundamental cosine variation only is considered. It may be verified by direct substitution that the following is a solution of (equation 3.1):-

$$\omega(\rho) = \left[\lambda_a \rho + \lambda_b \rho^3 + \lambda_c \rho^{-1} + \lambda_d \rho \cdot \log(\rho) \right] \cdot \cos(\theta) \quad (3.15)$$

where ρ is a non-dimensional radial co-ordinate ($\rho=r/b$). In order to establish the four arbitrary constants $\lambda_a, \lambda_b, \lambda_c, \lambda_d$ use must be made of the kinematic boundary conditions.

3.2.3 STRAIN ENERGY METHOD

The principles of the Rayleigh-Ritz method are reproduced here. The total strain energy stored in a plate (i.e. disc) is described in [22] and is given by

(3.16)

$$U = \iint \frac{K}{2} \left((u_x + v_y)^2 - 2(1-\nu) \left(u_x v_y - \frac{1}{4} (u_x + v_y)^2 \right) \right) dx dy$$

$$+ \iint \frac{D}{2} \left((\omega_{xx} + \omega_{yy})^2 - 2(1-\nu) (\omega_{xx} \omega_{yy} - \omega_{xy}^2) \right) dx dy$$

ie. $U = U_m + U_b$

where U_m and U_b are respectively the strain energy due to membrane and bending actions alone. Similarly, the total potential energy of a disc can be written down as

$$\Omega = \Omega_m + \Omega_b \tag{3.17}$$

where Ω_m and Ω_b are respectively the potential energy of the stress resultants associate with the in-plane and out-of-plane effects. Thus, the total energy of the system is

$$V = U + \Omega \tag{3.18}$$

The membrane and bending components of the total energy of the system are uncoupled and, for clarity, will be considered separately in the following sections.

The Rayleigh-Ritz method is applied determining the minimum of a function which describes the total energy of the system. A series is assumed to represent the deformations, for example

(3.19)

$$\omega = a_1 j_1(x,y) + a_2 j_2(x,y) + a_3 j_3(x,y) + \dots + a_N j_N(x,y)$$

where functions $j_1(x,y)$, $j_2(x,y)$, $j_3(x,y)$, $j_N(x,y)$ are chosen to represent the deformation of the system, and at the same time satisfy the boundary conditions. Once the solution of the double integral has been obtained the coefficient can

be determined by

$$\frac{\delta V}{\delta a_1} = 0 \quad \frac{\delta V}{\delta a_2} = 0 \quad \dots \quad \frac{\delta V}{\delta a_N} = 0 \quad (3.20)$$

Thus, a system of n linear equations $a_1, a_2, a_3, \dots, a_N$ are obtained which may readily be inverted. The number of terms taken in the series will have a direct bearing on the accuracy of the solution.

3.3 ANALYSIS OF A DISC WITH CONSTANT THICKNESS

(BENDING ONLY)

3.3.1 TRADITIONAL METHOD

Table 3.1 shows all the kinematic boundary conditions to be assumed. The solution of the constants in equation 3.15 for each boundary group can be obtained from equations 3.10, 3.11 and the kinematic boundary conditions listed in table 3.1. Table 3.2 lists the resulting transverse displacement w for any radius ($\beta < \rho < 1$) and corresponding values for the unknown constants.

Table 3.3 lists the disc stiffness for each set of boundary conditions considered, which may be inserted into equation 3.6. Figures 3.7, 3.8, 3.9 illustrate the variation in components of stress for both fully clamped and simply supported outer boundary conditions. Table 3.5 shows some important results of stress at the inner and outer boundaries for the fully clamped disc boundary condition.

3.3.2 STRAIN ENERGY METHOD

The analysis of a constant thickness disc is re-examined to determine the number of terms required for the strain energy

method. This is done by comparison of the results obtained from the method described in the previous section, the speed of convergence is tested. The outer boundary conditions 1 and 3 (section 3.1.2) are only discussed in this section. The same fundamental cosine variation of displacement with θ is retained, but a more complex variation with radius is adopted by choosing an arbitrary polynomial:-

$$\omega = \left[a_0 + a_1 \rho + a_2 \rho^2 + a_3 \rho^3 + \dots + a_N \rho^N \right] \cdot \cos(\theta) \quad (3.21)$$

No natural boundary conditions are invoked, but the imposition of kinematic restrictions listed in table 3.1 will result in the transverse displacements as listed in table 3.6.

The total strain energy due to bending actions alone is shown in the integral of equation 3.16. However, the contribution of the term containing the factor $(1 - \nu)$ is negligible for the boundary conditions considered, thus

$$U_b = \int_{\beta}^1 \int_0^{\pi/2} \frac{2 \cdot D(\rho)}{b^2} \left[\frac{\delta^2 \omega}{\delta \rho^2} + \frac{1}{\rho} \frac{\delta \omega}{\delta \rho} - \frac{\omega}{\rho^2} \right]^2 \rho \delta \rho \cdot d\theta \quad (3.22)$$

The potential energy of the stress resultants associated with the bending action only is

$$\Omega_b = - \left. \frac{M_d \delta \omega}{b \delta \rho} \right|_{\substack{\rho=\beta \\ \theta=0}} \quad (3.23)$$

Noting that $\cos(\theta)$ term appears in each derivative in 3.22 we may carry out the integration with respect to θ immediately and thus the total energy of the system can be written as

$$V_b = \frac{\pi}{2 \cdot b^2} \int_{\beta}^1 D(\rho) \cdot \left[\frac{\delta^2 \omega}{\delta \rho^2} + \frac{1}{\rho} \frac{\delta \omega}{\delta \rho} - \frac{\omega}{\rho^2} \right]^2 \rho \delta \rho - \left. \frac{M_d \delta \omega}{b \delta \rho} \right|_{\substack{\rho=\beta \\ \theta=0}} \quad (3.24)$$

Application of the Rayleigh-Ritz principle leads to a family of integral equations for $\delta V/\delta a_1 = 0$, $\delta V/\delta a_2 = 0$, .. $\delta V/\delta a_N = 0$. For clarity first let the transverse displacement listed in table 3.6 and their derivatives be written down in a generalised contracted form

(3.25)

$$\omega = \cos(\theta) \cdot \left[f'_1 + \sum_{s=1}^N a_n \cdot f_1(n) \right] \quad \text{ie. } \frac{\delta \omega}{\delta a_s} = f_1(s)$$

$$\frac{\delta \omega}{\delta \rho} = \cos(\theta) \cdot \left[f'_2 + \sum_{s=1}^N a_n \cdot f_2(n) \right] \quad \text{ie. } \frac{\delta^2 \omega}{\delta \rho \delta a_s} = f_2(s)$$

$$\frac{\delta^2 \omega}{\delta \rho^2} = \cos(\theta) \cdot \left[f'_3 + \sum_{s=1}^N a_n \cdot f_3(n) \right] \quad \text{ie. } \frac{\delta^3 \omega}{\delta \rho^2 \delta a_s} = f_3(s)$$

where $f_2(n)$, $f_3(n)$ are obtained by termwise differentiation of the second part (within the summation) of the equation representing the transverse displacement as listed in table 3.6. Similarly, f'_2 , f'_3 are obtained through termwise differentiation of the first term of the same equation. The first part of each of these equations is the influence of the partially restrained outer boundary, and would, in the case of the fully clamped outer boundary condition be zero. The bracketed term in equation 3.24 can also be represented in a contracted form

(3.26)

$$\sum_{n=1}^N a_n \left[f_3(n) - \frac{f_1(n)}{\rho^2} + \frac{f_2(n)}{\rho} \right] = \sum_{n=1}^N a_n \cdot G(n)$$

$$\frac{\delta}{\delta a_s} \left[\sum_{n=1}^N a_n \cdot G(n) \right] = G(s)$$

(3.27)

$$\left[\frac{f'_3}{\rho^2} - \frac{f'_1}{\rho^2} + \frac{f'_2}{\rho} \right] = G'$$

$$\frac{\delta}{\delta a_s} \left[G' \right] = 0$$

Thus, the reduced form of equation 3.24 is given by

(3.28)

$$0 = \pi \int_{\rho}^1 \frac{D(\rho) \cdot G' \cdot G(s) \rho \delta \rho}{b^2} + \pi \int_{\rho}^1 \frac{D(\rho) \cdot \sum_{n=1}^N a_n \cdot G(n) \cdot G(s) \rho \delta \rho}{b^2} - \frac{M_d \cdot f_2(s)}{b} \Bigg|_{\rho=\beta}^{\rho=0}$$

For the fully-clamped outer boundary condition the first integral of equation 3.28 is zero. The expansion of the bracketed term 3.26 is given by

$$G(z) = \rho^{z-2} \cdot g_1(z) + g_2(z) + \rho^{-2} \cdot g_3(z) \quad (3.29)$$

where $g_1(z) = z^2 - 1$

$$g_2(z) = -3 \cdot (z-1) \cdot \frac{(1-\beta^2)}{(1+\beta^2)}$$

$$g_2(z) = -(z-1) \cdot \frac{(\beta^2 - \beta^2)}{(1 - \beta^2)}$$

$z = n$ or s for $G(n)$, $G(s)$ respectively.

The second integral of equation 3.28 may be solved explicitly within the summation sign, if $D(\rho)$ is constant (i.e. independent of the integral) as in the case of constant thickness disc.

The fully-clamped outer boundary condition will be considered only to evaluate the rate of convergence towards the known results obtained from the plate theory discussed in section 3.3.1.

The convergence is rapid and the transverse displacement w (the summated term of the equation listed in table 3.6), is within 0.25% of the "known" answers, when N is taken to be 10, for β between the values of 0.25 and 0.80.

The variation of the stresses with respect to ρ is listed in table 3.7. With the introduction of the derivatives to establish the stresses σ_r , σ_θ and $\tau_{r\theta}$, a small difference occurred over a range of β between 0.25 and 0.4, and is corrected by increasing N to 20.

It can be concluded therefore that provided sufficient terms in the Rayleigh-Ritz approach are chosen the method will yield acceptable accuracies.

3.4 ANALYSIS OF A DISC WITH VARIABLE THICKNESS

(BENDING ONLY)

For variable thickness discs, let the thickness at any radius be $h(\rho) = h_o \cdot \lambda(\rho)$. The flexural stiffness (equation 3.11) can now be rewritten

$$D(\rho) = \frac{E \cdot h_o^3 \cdot \lambda(\rho)^3}{12(1-\nu^2)} = D_o \cdot \lambda(\rho)^3 \quad (3.30)$$

Substituting into equation 3.28 and re-arranging gives a new family of integral equations for $\delta V / \delta a_s = 0$

$$0 = \int_{\beta}^1 \lambda(\rho)^3 \cdot G' \cdot G(s) \rho \delta \rho + \int_{\beta}^1 \lambda(\rho)^3 \cdot \sum_{s=n}^N G(n) \cdot G(s) \rho \delta \rho - \frac{M_d \cdot b \cdot f_2(s)}{\pi \cdot D_o} \Bigg|_{\substack{\rho=\beta \\ \theta=0}} \quad (3.31)$$

$\lambda(\rho) = \text{constant}$ will result in the solution found in section 3.3.2.

There are an infinite number of possible choices for modelling the disc profile by the function $\lambda(\rho)$, such as

$$\lambda(\rho) = \begin{bmatrix} \beta \\ - \\ \rho \end{bmatrix}, \quad \lambda(\rho) = \begin{bmatrix} \beta \\ - \\ \rho \end{bmatrix}^{3/2}; \quad \lambda(\rho) = \begin{bmatrix} \beta \\ - \\ \rho \end{bmatrix}^{5/4} \quad (3.32)$$

also illustrated graphically on figure 3.10.

In order to make optimum use of material used in manufacture, extra material should be concentrated near the inner and outer boundaries whilst near the point of contraflexure, a "necking" portion (thinnest section) may be incorporated. To allow this, a more complicated function of the disc's profile

is needed. However, the majority of ideal functions which can be chosen are totally impractical to manufacture. Lengthy discussions with several United Kingdom steel foundries led to the following conclusions:-

- (i) Large blending curves at the sharp sectional changes should be used at the hub to disc and shell to disc boundaries. These blending curves are essential to ensure good material flow during the casting process and will assist in eliminating shrinkage cracks at section changes.
- (ii) Minimum thicknesses must be retained at the "necking" portion (thinnest section) of the disc and is dependent on the distance between the inner and outer radius of the disc.
- (iii) The complexity of the disc profile should be kept as simple as possible because, in practice, ideal theoretical functions describing the disc thickness are often impossible for the foundry to reproduce.

Therefore, to enable these constraints to be incorporated into the analysis for variable thickness discs, cubic spline functions are adopted to enable any disc profile to be modelled. Any particular disc profile function would have the above mentioned inadequacies removed by choosing collocation points (figure 3.11 illustrates) and fitting a spline function according to the following:-

$$\lambda(\rho) = A_i + B_i \cdot (\rho - \rho_i) + C_i \cdot (\rho - \rho_i)^2 + D_i \cdot (\rho - \rho_i)^3 \quad (3.33)$$

where $A_i = \lambda(\rho)$

$$B_i = \frac{[\lambda(\rho)_{i+1} - \lambda(\rho)_i] - H_i(Z_{i+1} + Z_i)}{H_i} \quad 6$$

$$C_i = \frac{Z_i}{2}$$

$$D_i = \frac{(Z_{i+1} - Z_i)}{6 \cdot H_i}$$

$$E_i = \rho_{i+1} - \rho_i$$

ρ_i represents the radial co-ordinate ρ at the i th collocation point (figures 3.12). A_i , B_i , C_i , D_i , H_i and Z_i can be solved for use with any variable thickness disc profile.

The variation of the stresses α_r , α_θ , $\tau_{r\theta}$ with respect to ρ is listed in table 3.8. Experimental verification of the Rayleigh-Ritz technique for variable thickness discs is presented in section 3.6.

3.5 ANALYSIS OF A DISC (IN-PLANE LOADING ONLY)

It can be shown that the stresses induced by purely in-plane loading of the disc, for the thickness of plate under consideration, are small in comparison to bending stress components (see Finite Element and experimental results in chapter 5). The in-plane membrane stresses are therefore disregarded further in this analysis.

3.6 EXPERIMENTAL VERIFICATION (BENDING ONLY)

The Rayleigh-Ritz approximate theory for bending stresses in both constant- and variable-thickness discs was further

tested experimentally using equipment shown in figure 3.13. The rig was designed such that the disc outer boundary could be taken to be encastred (case 1 (section 3.1.2)).

3.6.1 EXPERIMENTAL FRAME

Figures 3.14, 3.15 show schematically the experimental frame set up for parallel and profiled end disc respectively. The apparatus consists of two heavy-gauge steel outer plates (figure 3.14 item A) and two heavy gauge steel centre plates (figure 3.14 item C) used to sandwich the test discs (item B) to stimulate encastre boundary conditions at the outer edge. The radius b (figure 3.14, 3.15) is 250mm. A shaft was secured between the two central plates, to which the moment was applied.

3.6.2 MODELLED DISCS

Four steel discs were manufactured for this study, two of constant 3mm thickness and two variable thickness discs as illustrated by figure 3.16. The relatively thin plate used can be accounted for by the necessity to provide measurable

out-of-plane deflections. Any thinner plate would have a very high slenderness ratio and non-linear, large deflections may have resulted.

The strain gauges were attached to the steel discs, using general purpose gauges of the self-temperature compensation 90 degrees rosette type (Welwyn Strain

Measurement_CEA-06-125TQ-120ohm) glued and sealed to the surface of the disc at intervals (figure 3.14_item D). All the gauges were wired into a strain bridge in a

quarter-bridge arrangement.

The radial and tangential strains obtained from loading all the model discs will be used in conjunction with the elastic relationship (equation 3.13) to determine the stresses.

The values of Poisson's ratio and Young's Modulus used were 0.3 and 210KN/m^2 respectively.

3.6.3 RESULTS

By means of a DTI attached to the securing plate, the deflection of the model disc was monitored at various radii from the inner to the outer boundaries. The correlation between theory and experimentally measured deflections, for a constant thickness disc ($\beta = 0.3$), is given in figures 3.17. Figures 3.18, 3.19, 3.20 and 3.21 illustrate the comparison between the experimental and theoretical stresses for all the discs considered. Strains were stable to within 1% during the loading period.

Figure 3.17 illustrates that the variation of deflection w w.r.t θ follows a simple cosine function. During the experiment it was found that the test rig deformed slightly, thus a small amount of compensation was necessary to obtain the actual deflection between the shaft and the disc.

Figures 3.18 and 3.19 illustrate the variation of stress with respect to ρ on the end disc's surface at $\theta = 0$ for the end disc concerned. The theoretical and experimental stresses compare favourably, with a difference of less than 6% between the two sets of results. Similarly, figures 3.20 and 3.21 illustrate the variation of stress with respect ρ on the disc's surface at $\theta = 0$ for the two variable thickness disc's

concerned (figure 3.16). Again, the correlation between theoretical and experimental results was good, with a difference of less than 8%. The theoretical stresses were greater (ie. safer) than the experimental for all disc's concerned.

The errors indicated above are mainly associated with the tangential stress at the inner boundary of the disc. It was concluded that these discrepancies were due to slight losses in tangential strains at the inner radius caused by ineffective clamping of the disc by the centre boss. Both theoretical stress and deflection results show sufficient correlation with the experimental results to conclude that the disc behaviour with respect to pure bending is adequately prescribed and that the Rayleigh-Ritz technique is sound.

3.7 EXPERIMENTAL VERIFICATION (IN-PLANE LOADING ONLY)

To confirm the assumption that the stress produced by in-plane loading was negligible the experimental test rig used previously was re-used as shown in the figure 3.22. Figure 3.22 shows schematically the equipment details.

3.7.1 EXPERIMENTAL FRAME

The apparatus consisted of a heavy-gauge steel central plate (figure 3.22 item A) and shaft (figure 3.22 items C). The central plate was pressed into the bore of the disc (item B) at the inner edge and the outer boundary was clamped to provide encastre conditions. The load was applied by means

of weights attached to the shaft (figure 3.22 item E) symmetrically about the plane of the plane.

3.7.2 MODELLED DISCS

The constant-thickness discs used as described in section 3.6.2 were used for this test (ie. $\beta = 0.22$ figure 3.22(a) and $\beta = 0.41$ figure 3.22(b)).

3.7.3 RESULTS

The strains recorded with a maximum 25kg. load were too small to measure, which was also reinforced by F.E. analysis. It can be concluded therefore that for the disc slenderness ratios used in-plane loading can be neglected.

TABLE 3.1

The kinematic boundary conditions:-

CASE 1 Clamped outer boundary

$$\omega = 0, \quad \frac{\delta\omega}{\delta\rho} = 0 \quad @ \rho = 1 \text{ for all } \theta$$

$$M_d = b \int_{-\pi}^{\pi} \left(M_r \cdot \rho \cdot \cos(\theta) + M_{r\theta} \cdot \rho \cdot \sin(\theta) - Q_r \cdot b \cdot \rho^2 \cos(\theta) \right) \cdot d\theta$$

@ $\rho = 1$

CASE 2 Simply supported outer boundary

$$\omega = 0, \quad M_r = 0 \quad @ \rho = 1 \text{ for all } \theta$$

$$M_d = b \int_{-\pi}^{\pi} \left(M_{r\theta} \cdot \rho \cdot \sin(\theta) - Q_r \cdot b \cdot \rho^2 \cos(\theta) \right) \cdot d\theta$$

@ $\rho = 1$

CASE 3 Partially restrained outer boundary

$$\omega = 0, \quad \frac{\delta\omega}{\delta\rho} = \phi_{sh} \cdot \cos(\theta) \quad @ \rho = 1 \text{ for all } \theta$$

$$M_d = b \int_{-\pi}^{\pi} \left(M_r \cdot \rho \cdot \cos(\theta) + M_{r\theta} \cdot \rho \cdot \sin(\theta) - Q_r \cdot b \cdot \rho^2 \cos(\theta) \right) \cdot d\theta$$

@ $\rho = 1$

The boundary condition applicable to all cases, ie. rigid central boss.

$$\frac{\delta\omega}{\delta\rho} = \omega \quad @ \rho = \beta \text{ for } \theta = 0$$

TABLE 3.2

The transverse displacement w :-

$$w = \frac{M_d \cdot b \cdot \lambda \cdot \left[\lambda_a \rho + \lambda_b \rho^3 + \lambda_c \rho^{-1} + \lambda_d \rho \cdot \log(\rho) \right] \cdot \cos(\theta)}{D_o}$$

where λ , λ_a , λ_b , λ_c ; λ_d are listed below.

CASE 1 Clamped outer boundary

$$\lambda_a = 1 - \beta^2, \quad \lambda_b = -1, \quad \lambda_c = \beta^2, \quad \lambda_d = 2 \cdot \left(1 + \beta^2 \right)$$

$$\lambda = \left[8\pi \cdot \left(1 + \beta^2 \right) \right]^{-1}$$

CASE 2 Simply supported outer boundary

$$\begin{aligned} \lambda_a &= (1+\nu) \left[\beta^2 - 1 \right]^2 & \lambda_b &= - \left[\beta^2(1-\nu) + (1+\nu) \right] \\ \lambda_c &= \beta^2 \left[(3+\nu) - \beta^2(1+\nu) \right] & \lambda_d &= 2 \cdot \left[\beta^4(1-\nu) + (3+\nu) \right] \end{aligned}$$

$$\lambda = \left[8\pi \cdot \left[\beta^4(1-\nu) + (3+\nu) \right] \right]^{-1}$$

CASE 3 Partially restrained outer boundary

$$\lambda_a = \left[\frac{\left[1 - \beta^2 \right]}{8\pi \left[1 + \beta^2 \right]} + \frac{D_o \left[1 + \beta^2 \right]}{2 \cdot b \cdot k_{sh} \left[1 - \beta^2 \right]} \right]$$

$$\lambda_b = - \left[\frac{1}{8\pi \left[1 + \beta^2 \right]} - \frac{D_o}{2 \cdot b \cdot k_{sh} \left[1 - \beta^2 \right]} \right]$$

$$\lambda_c = \left[\frac{\beta^2}{8\pi \left[1 + \beta^2 \right]} - \frac{D_o \beta^2}{2 \cdot b \cdot k_{sh} \left[1 - \beta^2 \right]} \right] \quad \lambda_d = \frac{1}{4\pi}$$

$$\lambda = 1$$

where shell stiffness k_{sh} is established in section 4.3

TABLE 3.3

Disc stiffness k_d for constant thickness discs :-

$$k_d = \frac{M_d}{\phi_d} = \frac{M_d \cdot b}{\left. \frac{\delta \omega}{\delta \rho} \right|_{\rho=\beta}}$$

$$k_d = \frac{D_o}{\lambda} \frac{1}{\left[\lambda_a + 3 \cdot \lambda_b \beta - \lambda_c \beta^{-2} + \lambda_d \cdot (\log(\beta) + 1) \right]}$$

where $\lambda, \lambda_a, \lambda_b, \lambda_c, \lambda_d$ are listed in table 3.2

TABLE 3.4

The important stresses σ_r , σ_θ ; $\tau_{r\theta}$ are listed :-

$$\sigma_r = - \frac{12.M_d}{b.h^2} \lambda \left[(3+\nu)\lambda_b \cdot \rho + (1-\nu)\lambda_c \cdot \rho^{-3} + \frac{(1+\nu)\lambda_d \cdot \rho^{-1}}{2} \right] \cdot \cos(\theta)$$

$$\sigma_\theta = - \frac{12.M_d}{b.h^2} \lambda \left[(1+3\nu)\lambda_b \cdot \rho - (1-\nu)\lambda_c \cdot \rho^{-3} + \frac{(1+\nu)\lambda_d \cdot \rho^{-1}}{2} \right] \cdot \cos(\theta)$$

$$\tau_{r\theta} = - \frac{12.M_d}{b.h^2} \lambda \cdot (1-\nu) \left[\lambda_b \cdot \rho - \lambda_c \cdot \rho^{-3} + \lambda_d \cdot \rho^{-1} \right] \cdot \sin(\theta)$$

where λ , λ_a , λ_b , λ_c ; λ_d are listed in table 3.2

TABLE 3.5

Some important variations for $\theta = 0$ showing behaviour of a constant thickness disc, with clamped outer boundary.

Parameter	$\rho = \beta$	$\rho = 1$
$\frac{\alpha_r \cdot h^2 b}{M_d}$	$-\frac{3}{\pi \beta} \frac{(\beta^2 - 1)}{(\beta^2 + 1)}$	$\frac{3}{\pi} \frac{(1 - \beta^2)}{(1 + \beta^2)}$
$\frac{\alpha_\theta \cdot h^2 b}{M_d}$	$-\frac{3\nu}{\pi \beta} \frac{(\beta^2 - 1)}{(\beta^2 + 1)}$	$\frac{3\nu}{\pi} \frac{(1 - \beta^2)}{(1 + \beta^2)}$
$\frac{(\alpha_r - \alpha_\theta) \cdot h^2 b}{M_d}$	$-\frac{3(1 - \nu)}{\pi \beta} \frac{(\beta^2 - 1)}{(\beta^2 + 1)}$	$\frac{3(1 - \nu)}{\pi} \frac{(1 - \beta^2)}{(1 + \beta^2)}$
$\frac{\phi_s \cdot h^2 b}{M_d}$	$\frac{3(1 - \nu^2)}{\pi} \left[\frac{(\beta^2 - 1)}{(\beta^2 + 1)} - \log(\beta) \right]$	0

TABLE 3.6

The transverse displacement ω :-

$$\omega = \left[\lambda_e \cdot (\rho^2 - \beta^2 \rho + \beta^2) + \sum^N a_n \cdot (\rho^n + \lambda_f \rho^2 - \lambda_g \rho + \lambda_h) \right] \cdot \cos(\theta)$$

where $\lambda_e, \lambda_f, \lambda_g, \lambda_h$ are listed below.

CASE 1 Clamped outer boundary.

$$\lambda_e = 0$$

CASE 3 Partially restrained outer boundary.

$$\lambda_e = \frac{\phi_{sh}}{(1-\beta^2)}$$

Variables applicable for both cases :-

$$\lambda_f = (n-1) \frac{(\beta^n - 1)}{(1-\beta^2)}, \quad \lambda_g = n + 2(n-1) \frac{(\beta^n - 1)}{(1-\beta^2)} ;$$

$$\lambda_h = (n-1) \frac{(\beta^n - \beta^2)}{(1-\beta^2)}$$

TABLE 3.7

The important stresses σ_r , σ_θ ; $\tau_{r\theta}$ (constant thickness disc only)

$$\sigma_r = \frac{M_d \cdot b}{h^2} (I_1 + I_4) \cdot \cos(\theta) \qquad \sigma_\theta = \frac{M_d \cdot b}{h^2} (I_2 + I_5) \cdot \cos(\theta)$$

$$\tau_{r\theta} = \frac{M_d \cdot b}{h^2} (I_3 + I_6) \cdot \sin(\theta)$$

$$I_1 = -\frac{6}{\pi} \sum_3^N a_n \cdot \left[\frac{(n-1)(n+\nu) \cdot g_1(n)}{\rho^{2-n}} + \frac{(2+\nu) \cdot g_2(n)}{3} - \frac{\nu \cdot g_3(n)}{\rho^2} \right]$$

$$I_2 = -\frac{6}{\pi} \sum_3^N a_n \cdot \left[\frac{(n-1)(\nu n+1) \cdot g_1(n)}{\rho^{2-n}} + \frac{(2\nu+1) \cdot g_2(n)}{3} - \frac{1 \cdot g_3(n)}{\rho^2} \right]$$

$$I_3 = -\frac{6}{\pi} \sum_3^N a_n \cdot \left[\frac{(n-1) \cdot g_1(n)}{\rho^{2-n}} + \frac{g_2(n)}{3} - \frac{g_3(n)}{\rho^2} \right]$$

CASE 1 Clamped outer boundary.

$$I_4 = I_5 = I_6 = 0$$

CASE 3 Partially restrained outer boundary.

$$I_4 = -D_o \cdot \frac{[2 + \nu \cdot (1 - \beta^2 \rho^{-2})]}{b^2 k_{sh} [1 - \beta^2]} \qquad I_5 = -D_o \cdot \frac{[2\nu + 1 - \beta^2 \rho^{-2}]}{b^2 k_{sh} [1 - \beta^2]}$$

$$I_6 = -D_o \cdot \frac{(1-\nu) [1 - \beta^2 \rho^{-2}]}{b^2 k_{sh} [1 - \beta^2]}$$

TABLE 3.3

The important stresses α_r , α_θ ; $\tau_{r\theta}$ (variable thickness disc only)

$$\alpha_r = \frac{M_d \cdot b \lambda(\rho) \cdot (I_1 + I_4) \cdot \cos(\theta)}{h_o^2}$$

$$\alpha_\theta = \frac{M_d \cdot b \lambda(\rho) \cdot (I_2 + I_5) \cdot \cos(\theta)}{h_o^2}$$

$$\tau_{r\theta} = \frac{M_d \cdot b \lambda(\rho) \cdot (I_3 + I_6) \cdot \sin(\theta)}{h_o^2}$$

where I_1 , I_2 ; I_3 are listed in table 3.7 and $\lambda(\rho)$ may be determined using equation 3.33.

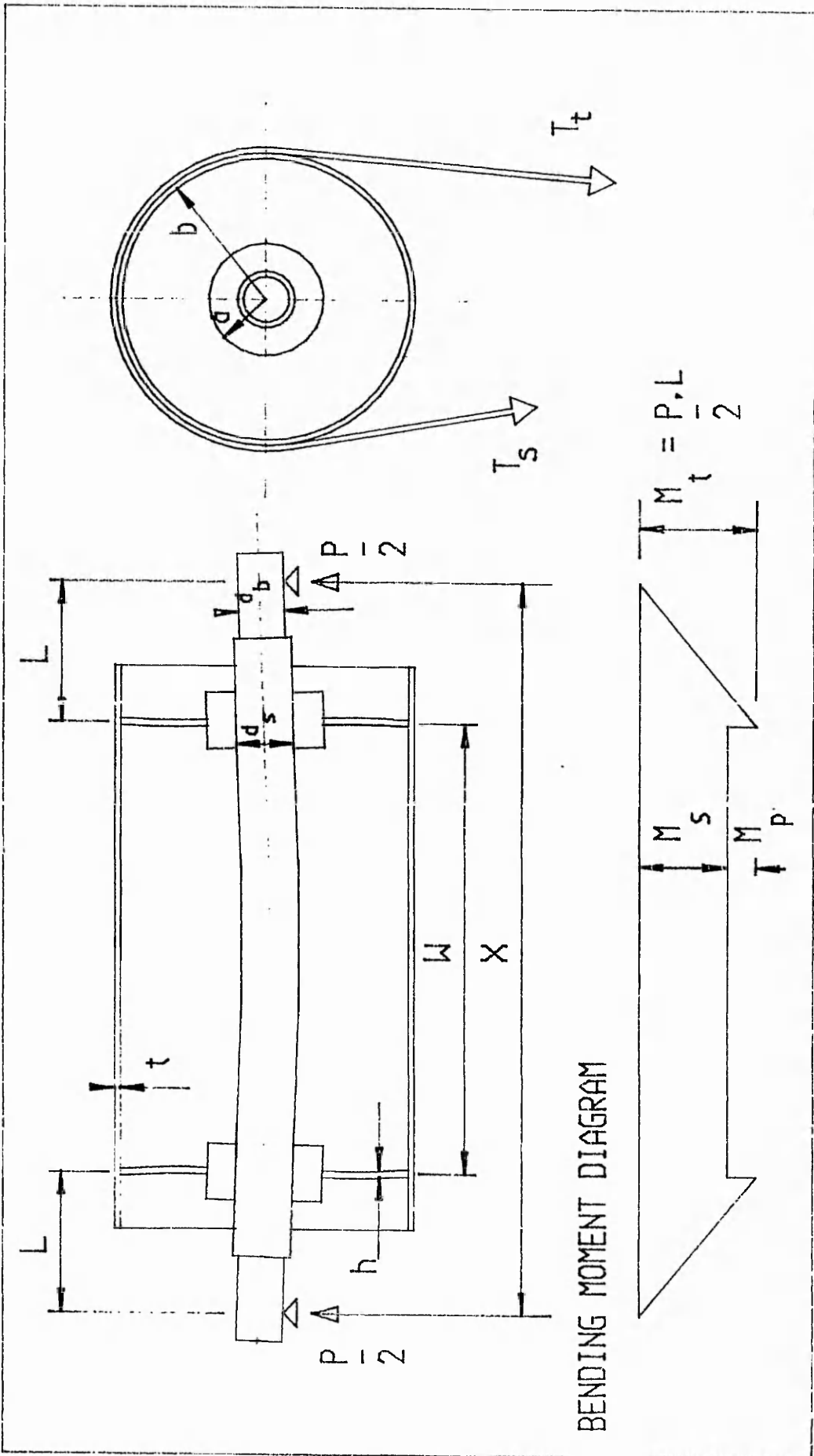
CASE 1 Clamped outer boundary.

$$I_4 = I_5 = I_6 = 0$$

CASE 3 Partially restrained outer boundary.

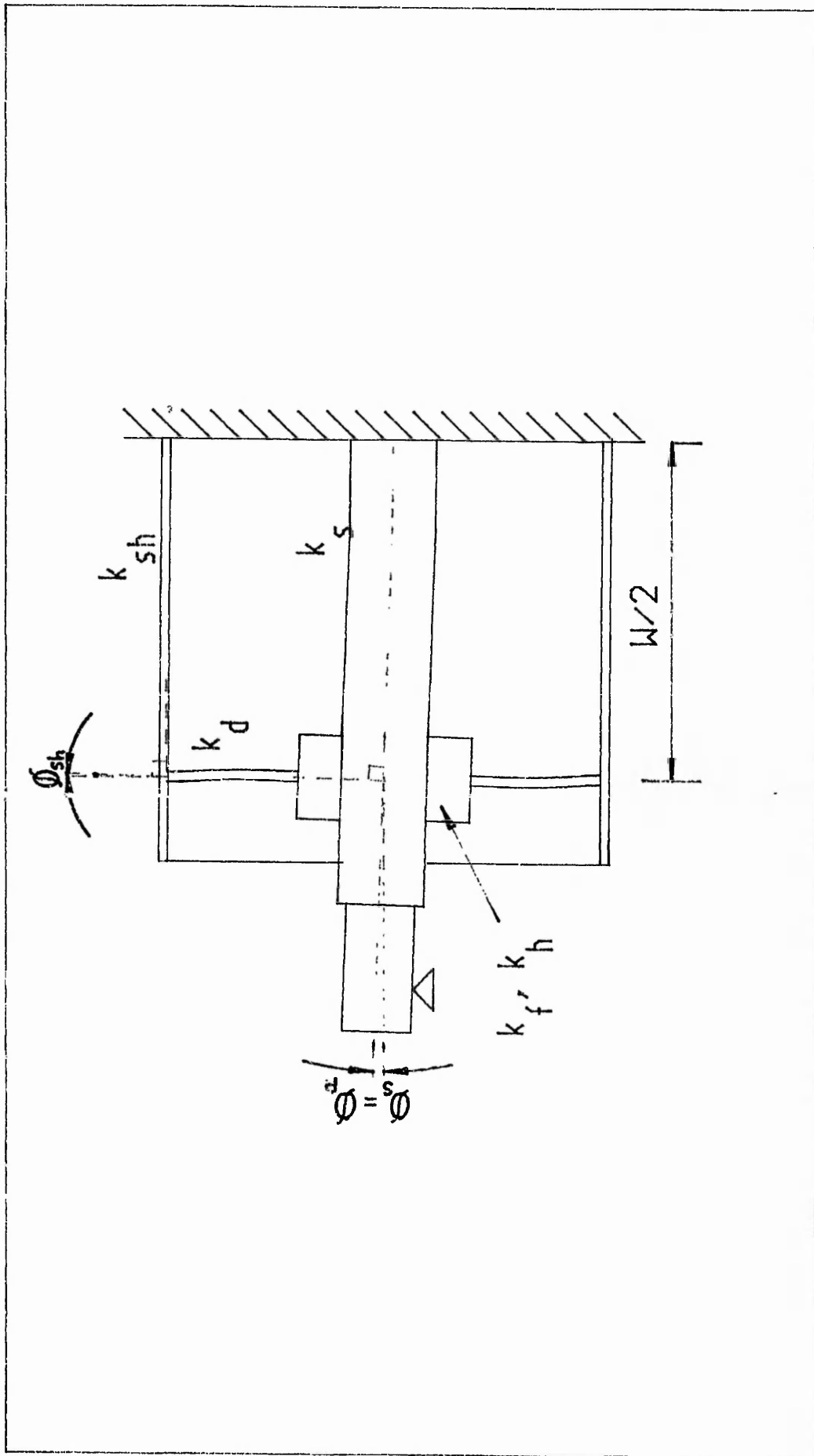
$$I_4 = -D_o \cdot \frac{[2 + \nu \cdot (1 - \beta^2 \rho^{-2})]}{b^2 k_{sh} (1 - \beta^2)} \quad I_5 = -D_o \cdot \frac{[2\nu + 1 - \beta^2 \rho^{-2}]}{b^2 k_{sh} (1 - \beta^2)}$$

$$I_6 = -D_o \cdot \frac{(1 - \nu) (1 - \beta^2 \rho^{-2})}{b^2 k_{sh} (1 - \beta^2)}$$



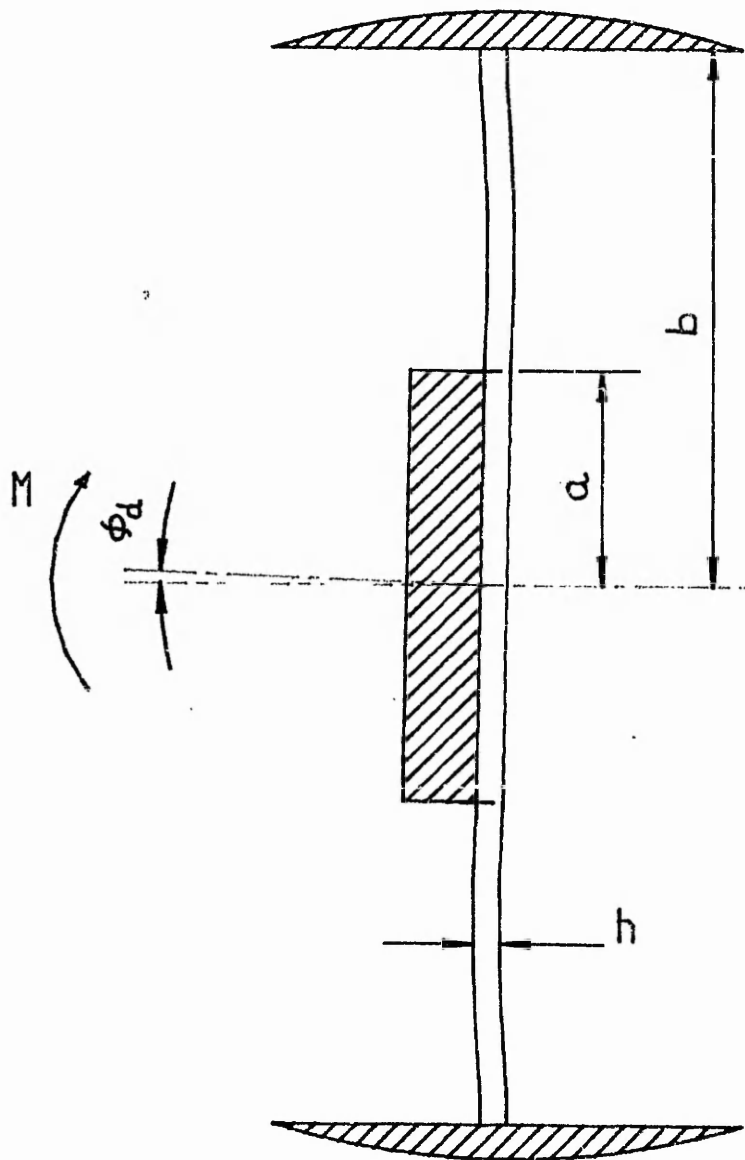
BENDING MOMENT DIAGRAM

TITLE : SCHEMATIC DIAGRAM OF A CONVEYOR PULLEY WITH B.M DIAGRAM FIGURE : 3.1



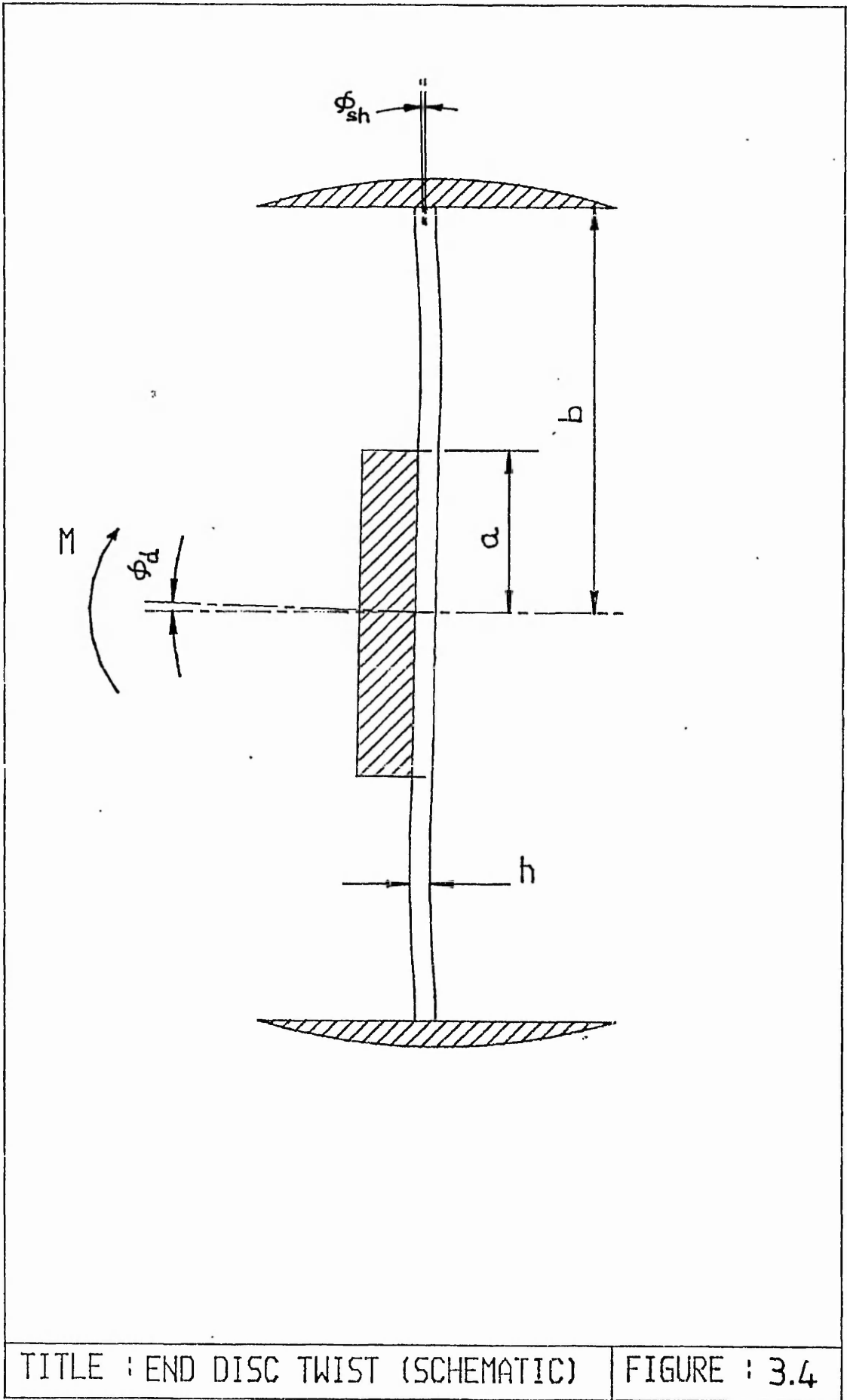
TITLE : DIAGRAM SHOWING STIFFNESS WITHIN A CONVEYOR PULLEY

FIGURE : 3.2



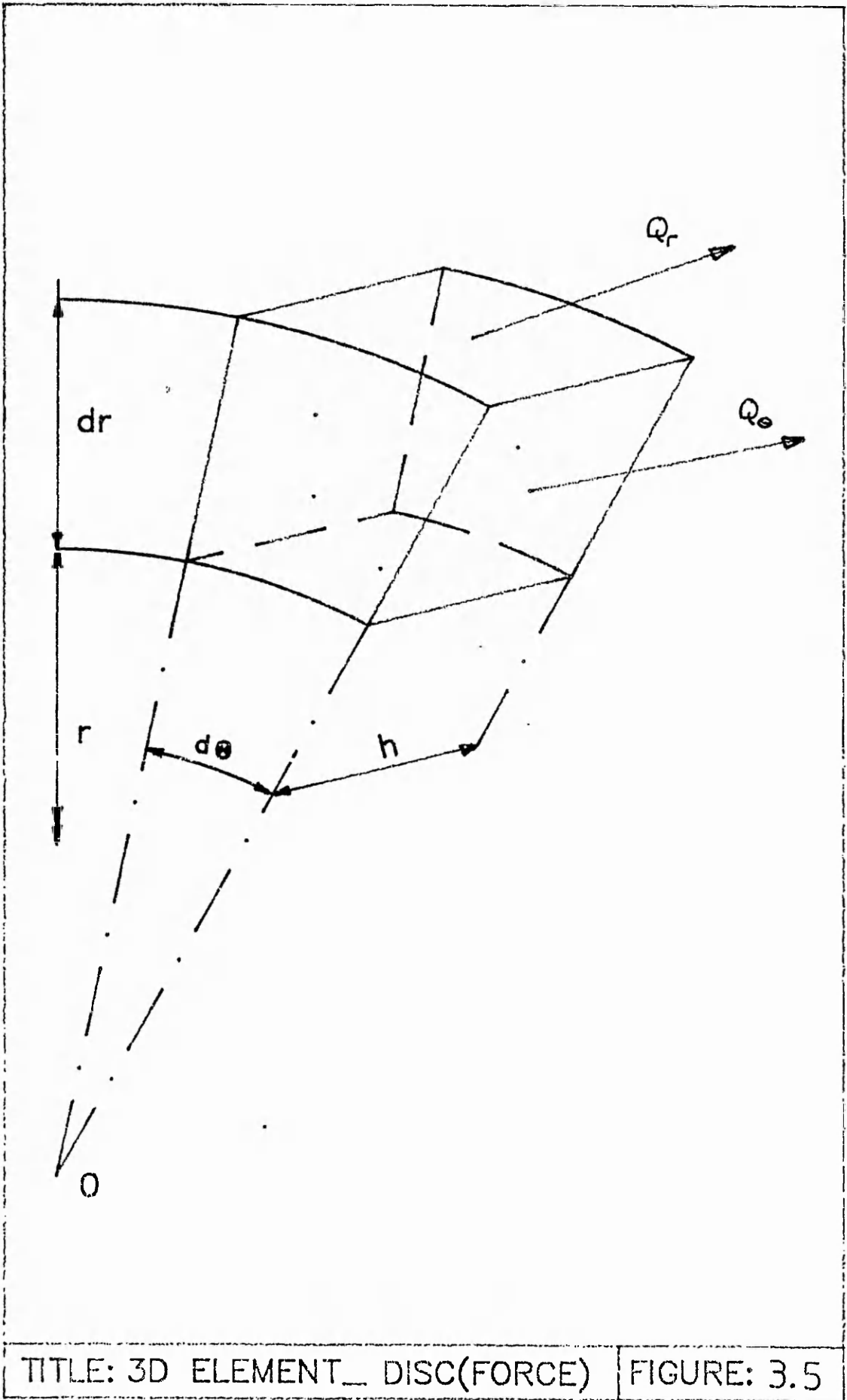
TITLE : END DISC TWIST (SCHEMATIC)

FIGURE : 3.3



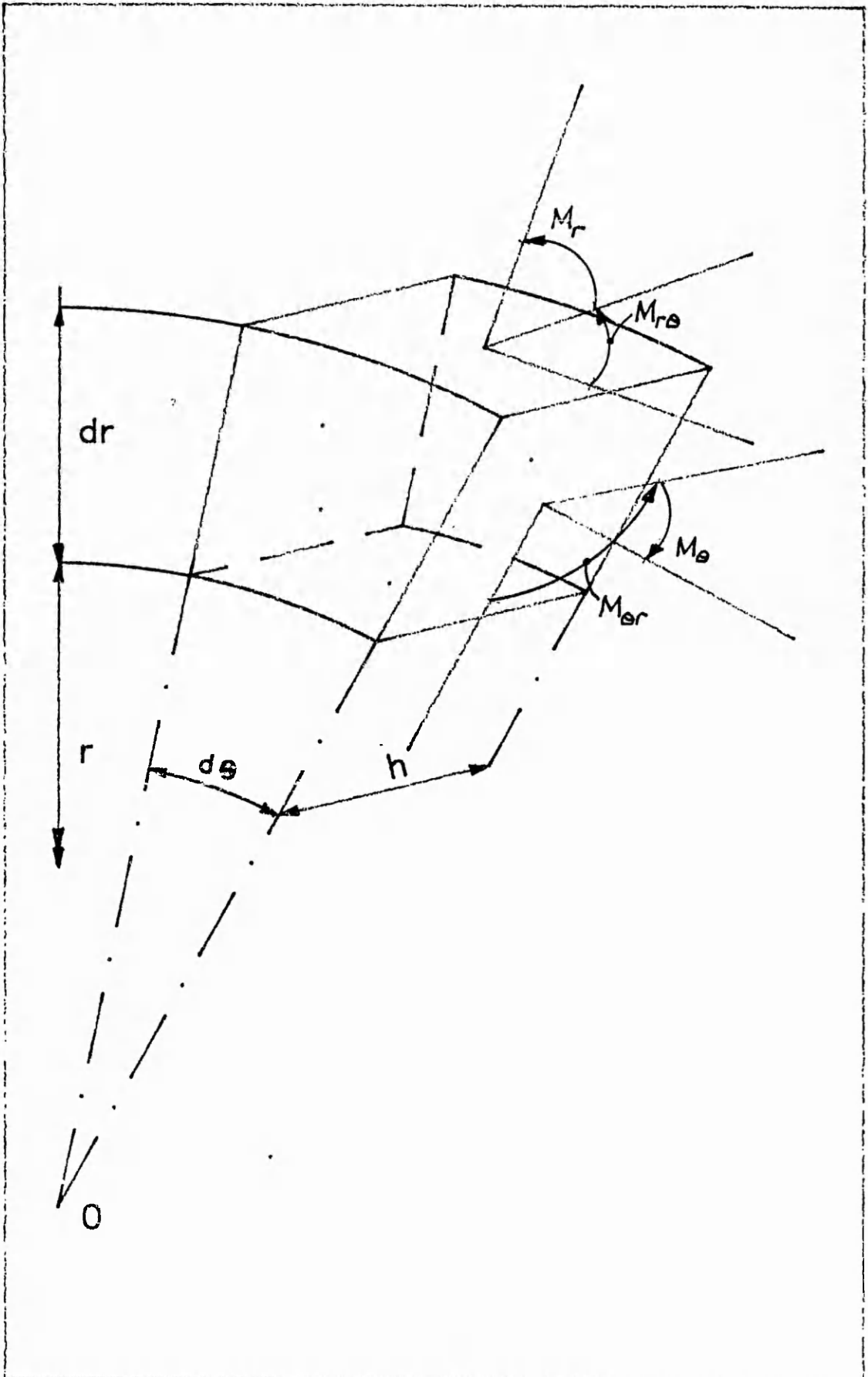
TITLE : END DISC TWIST (SCHEMATIC)

FIGURE : 3.4



TITLE: 3D ELEMENT_ DISC(FORCE)

FIGURE: 3.5



TITLE: 3D ELEMENT_DISC(MOMENT) | FIGURE: 3.6

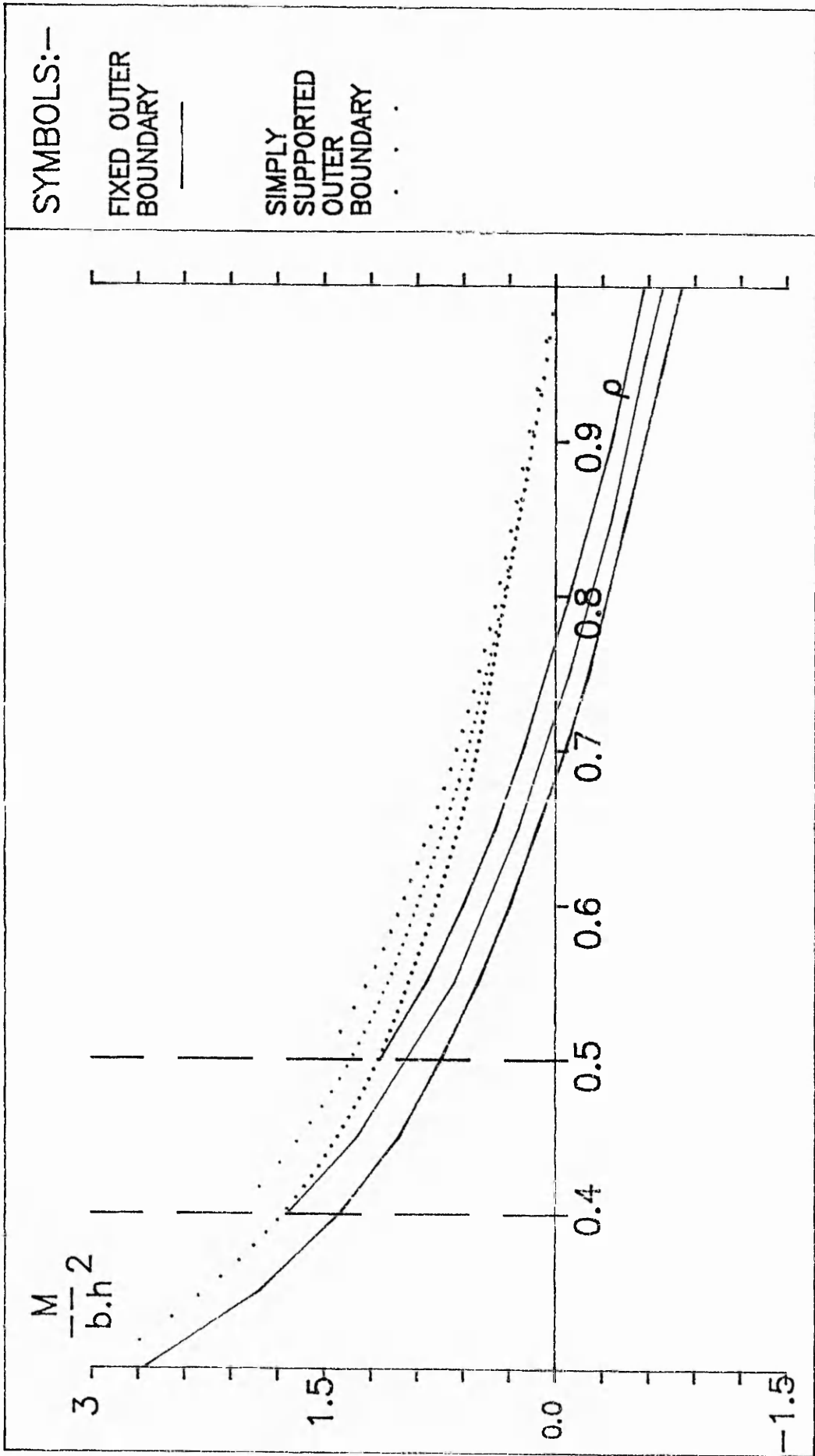
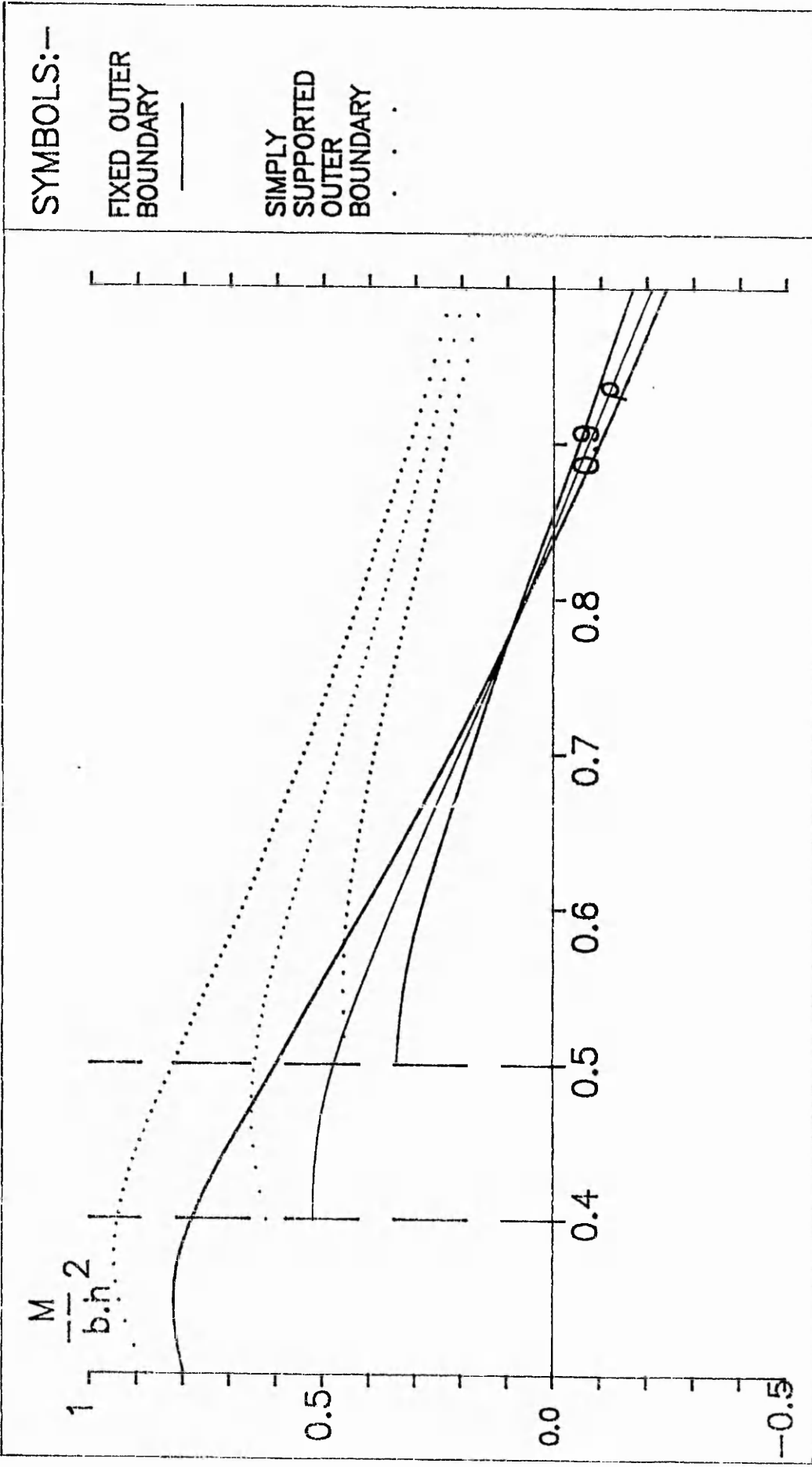


FIGURE: 3.7

TITLE: VARIATION IN STRESS σ_{rr} FOR VARIOUS RATIOS OF β



TITLE: VARIATION IN STRESS σ_{00} FOR VARIOUS RATIOS OF β FIGURE: 3.8

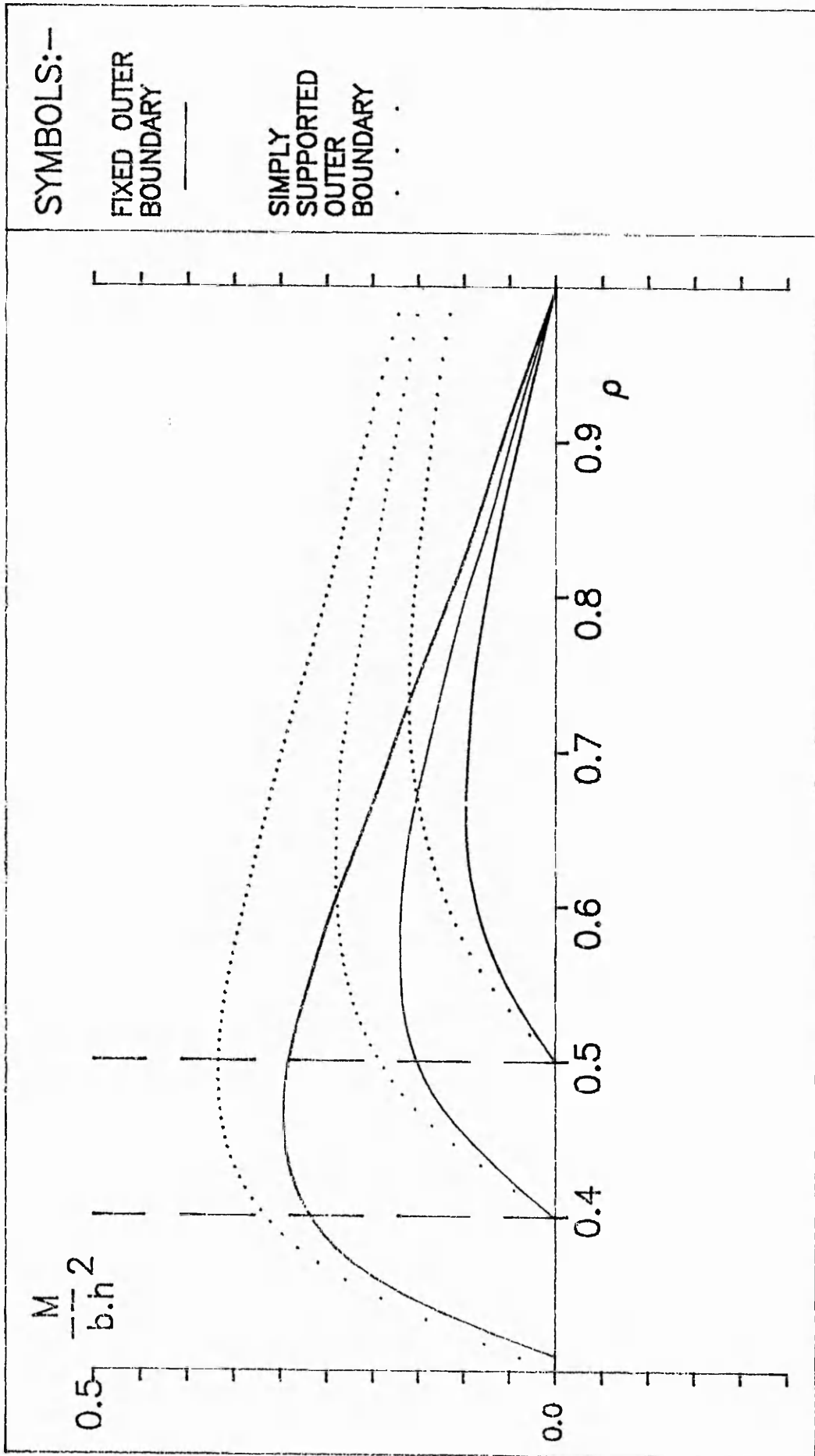
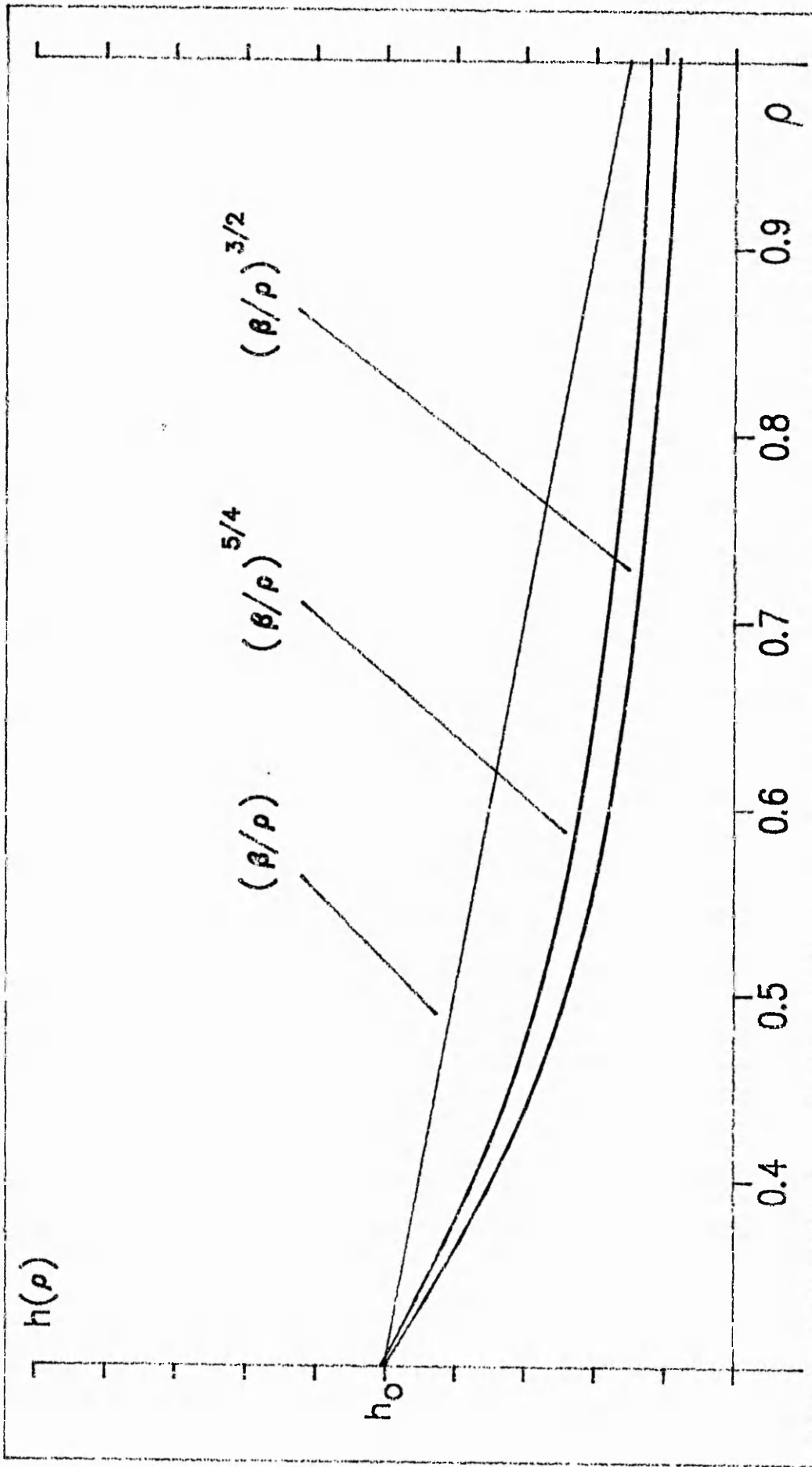


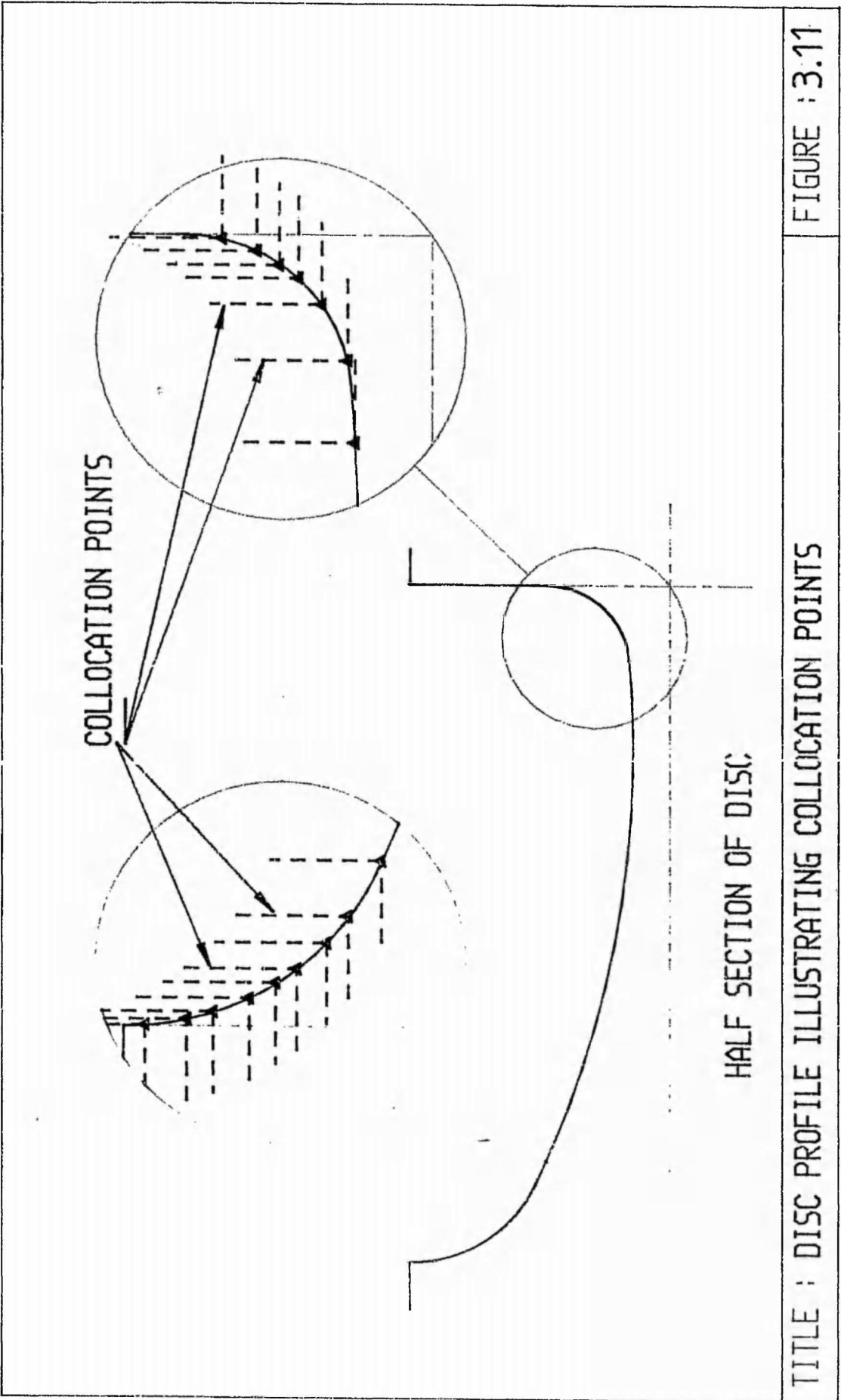
FIGURE: 3.9

TITLE: VARIATION IN STRESS $\tau_{r\theta}$ FOR VARIOUS RATIOS OF β



TITLE: EXAMPLES OF VARIOUS DISC PROFILES (HALF-SECTION)

FIGURE: 3.10



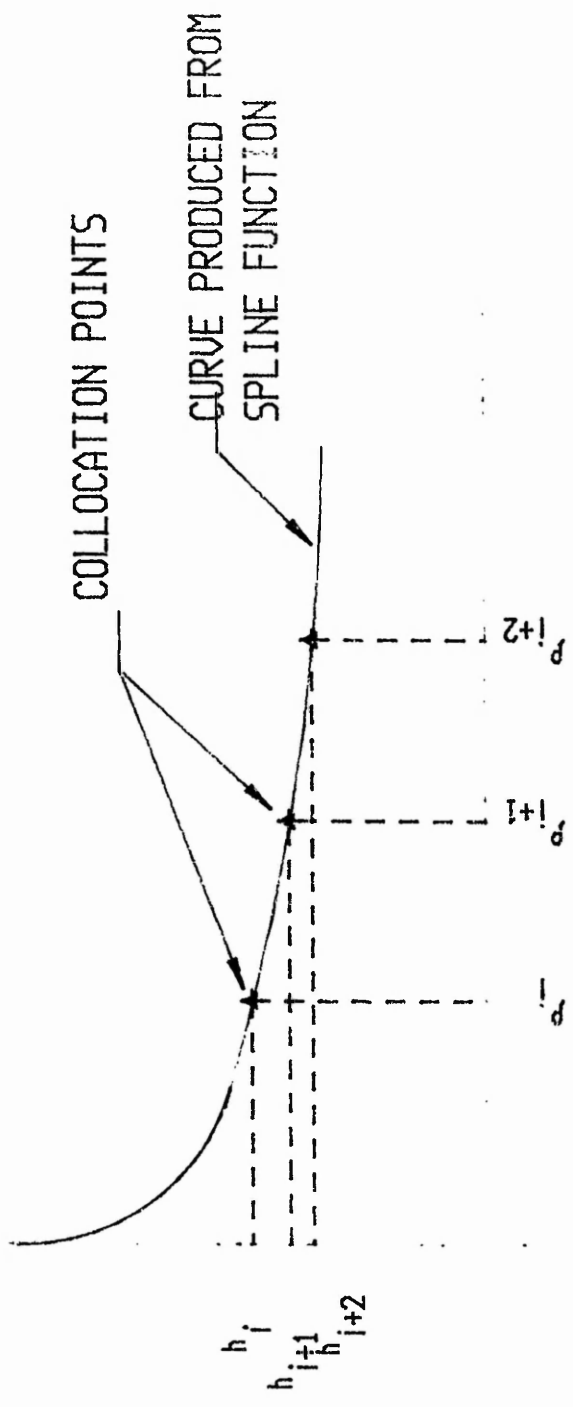
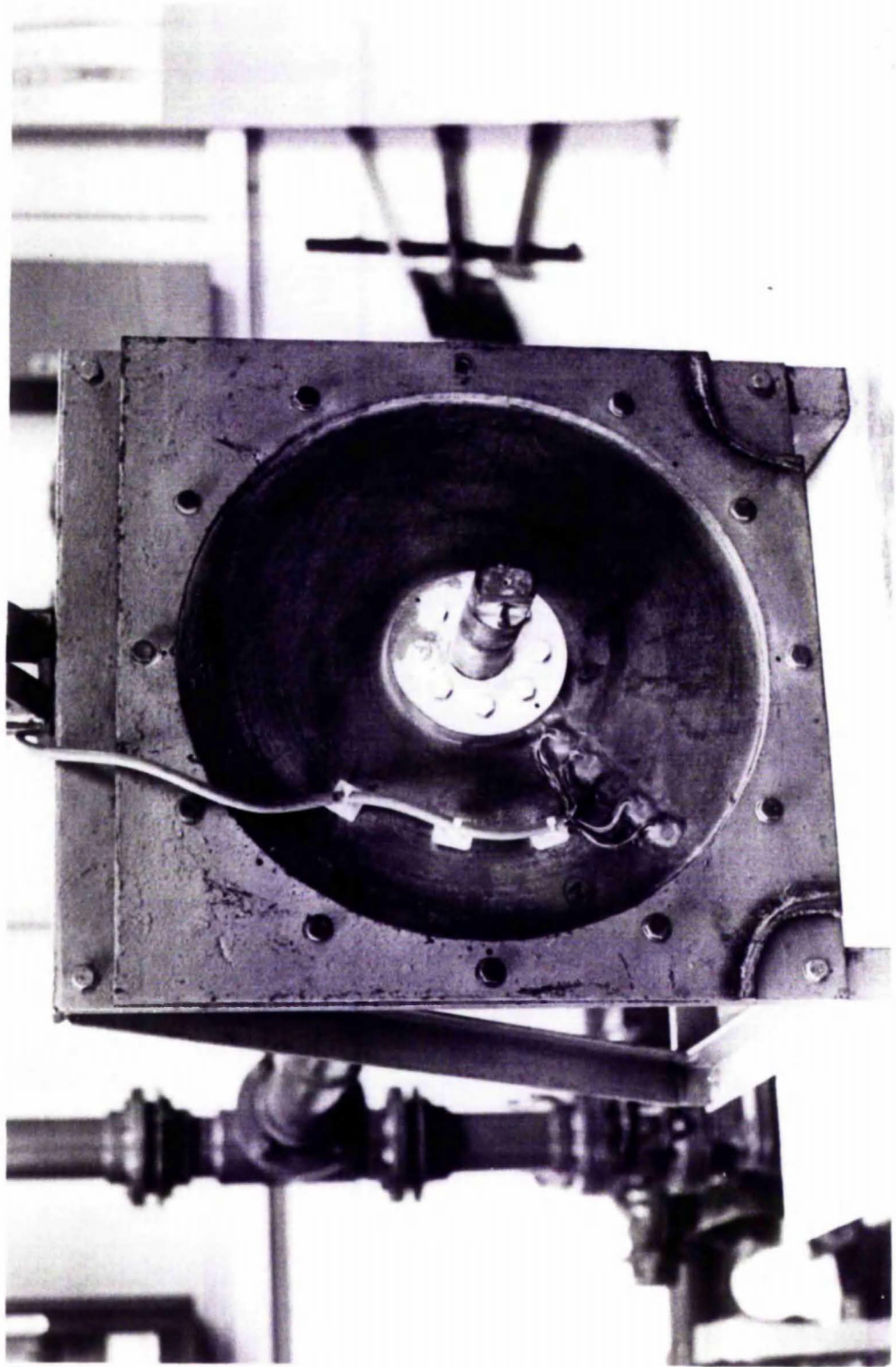


FIGURE : 3.12

TITLE : COORDINATES SYSTEM FOR COLLOCATION POINTS IN SPLINE FUNCTION



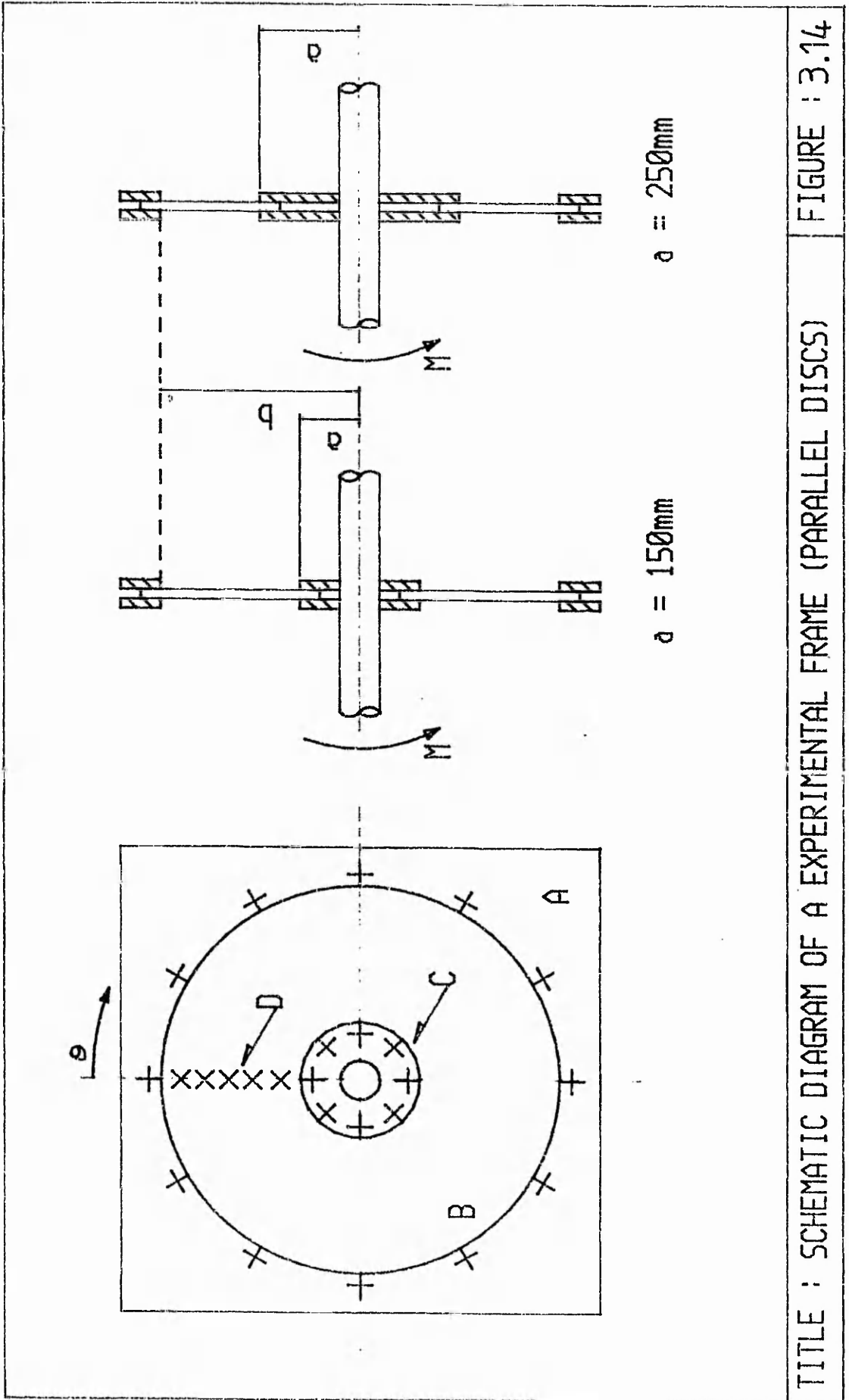
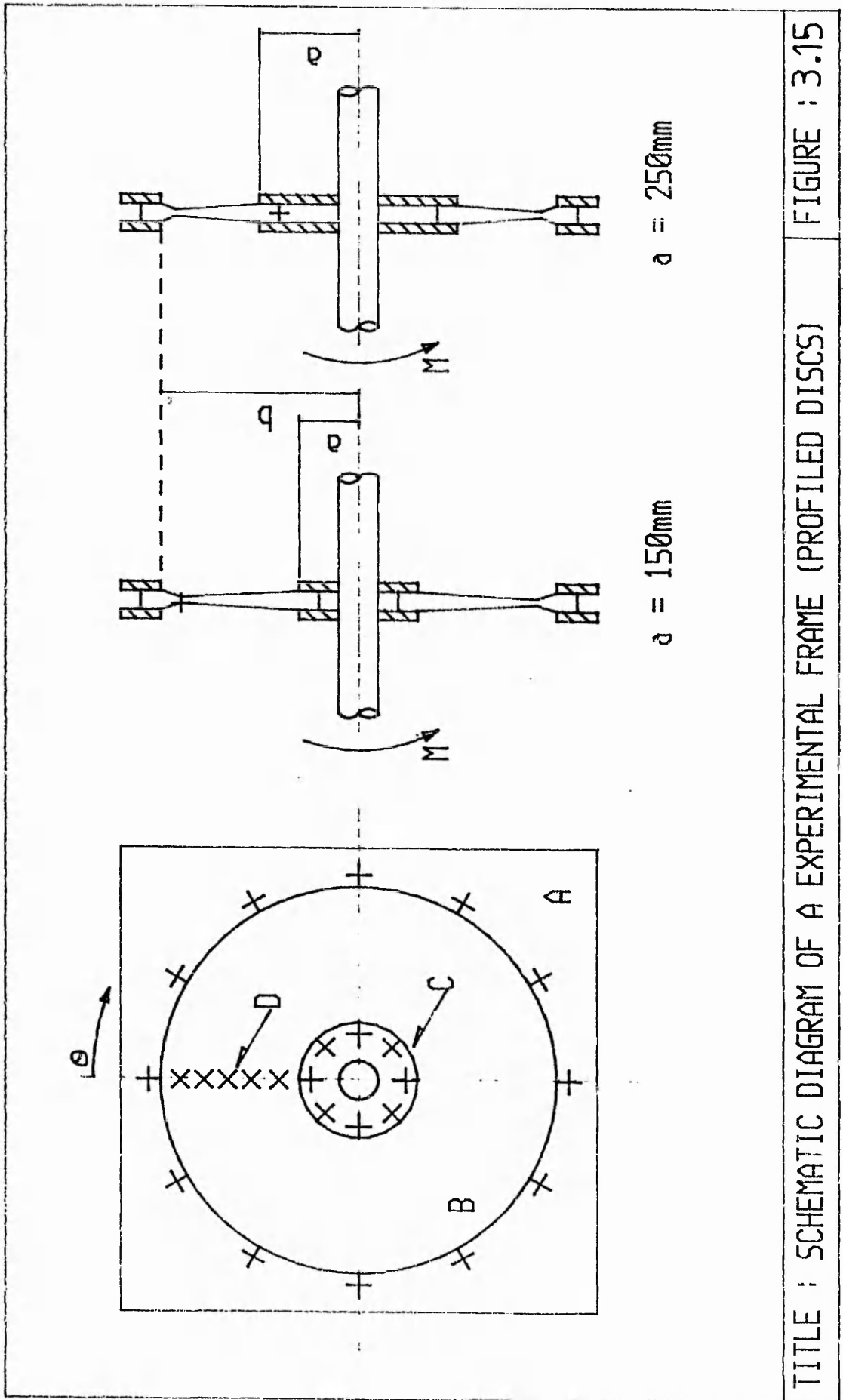
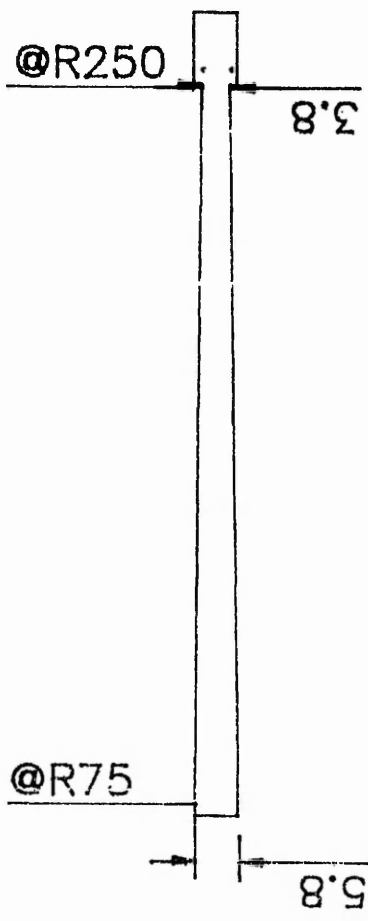


FIGURE : 3.14

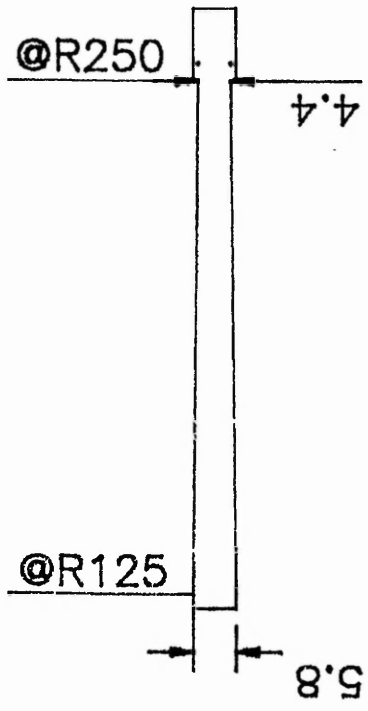
TITLE : SCHEMATIC DIAGRAM OF A EXPERIMENTAL FRAME (PARALLEL DISCS)



TITLE : SCHEMATIC DIAGRAM OF A EXPERIMENTAL FRAME (PROFILED DISCS) FIGURE : 3.15



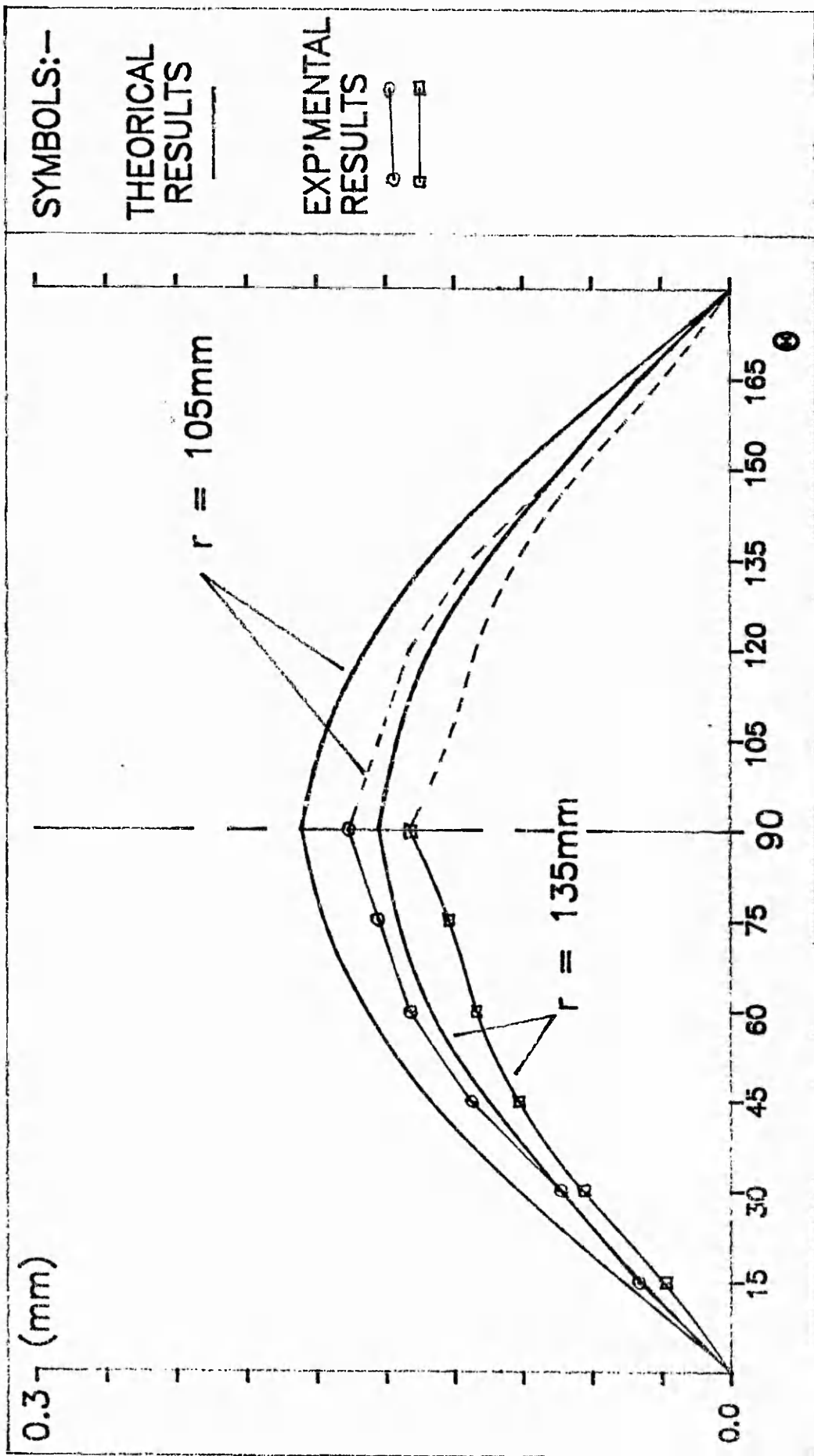
STEEL PROFILED DISC(a)



STEEL PROFILED DISC(b)

SCHEMATIC DIAGRAM OF EXPERIMENTAL PROFILED DISCS

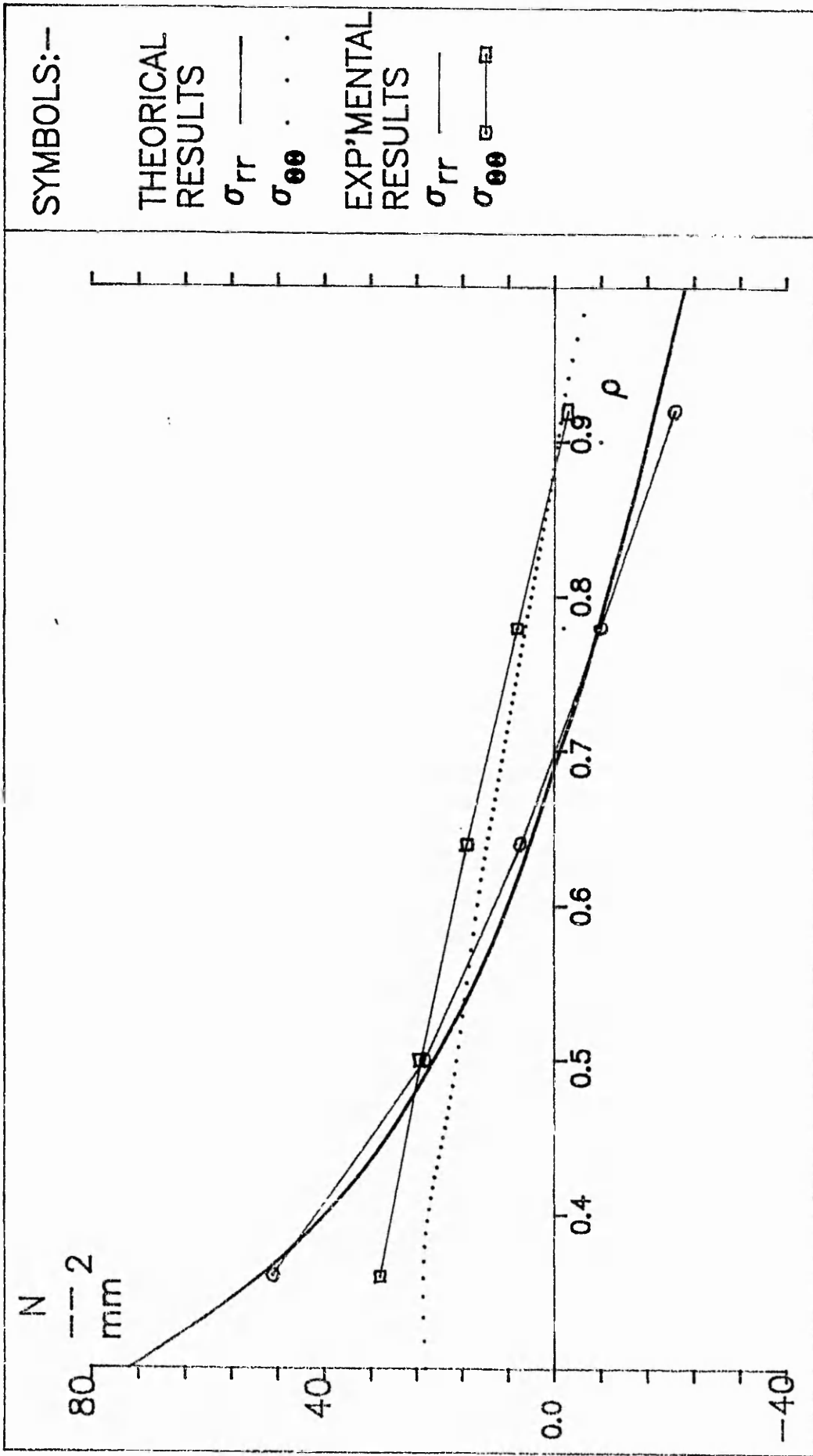
FIGURE:3.16



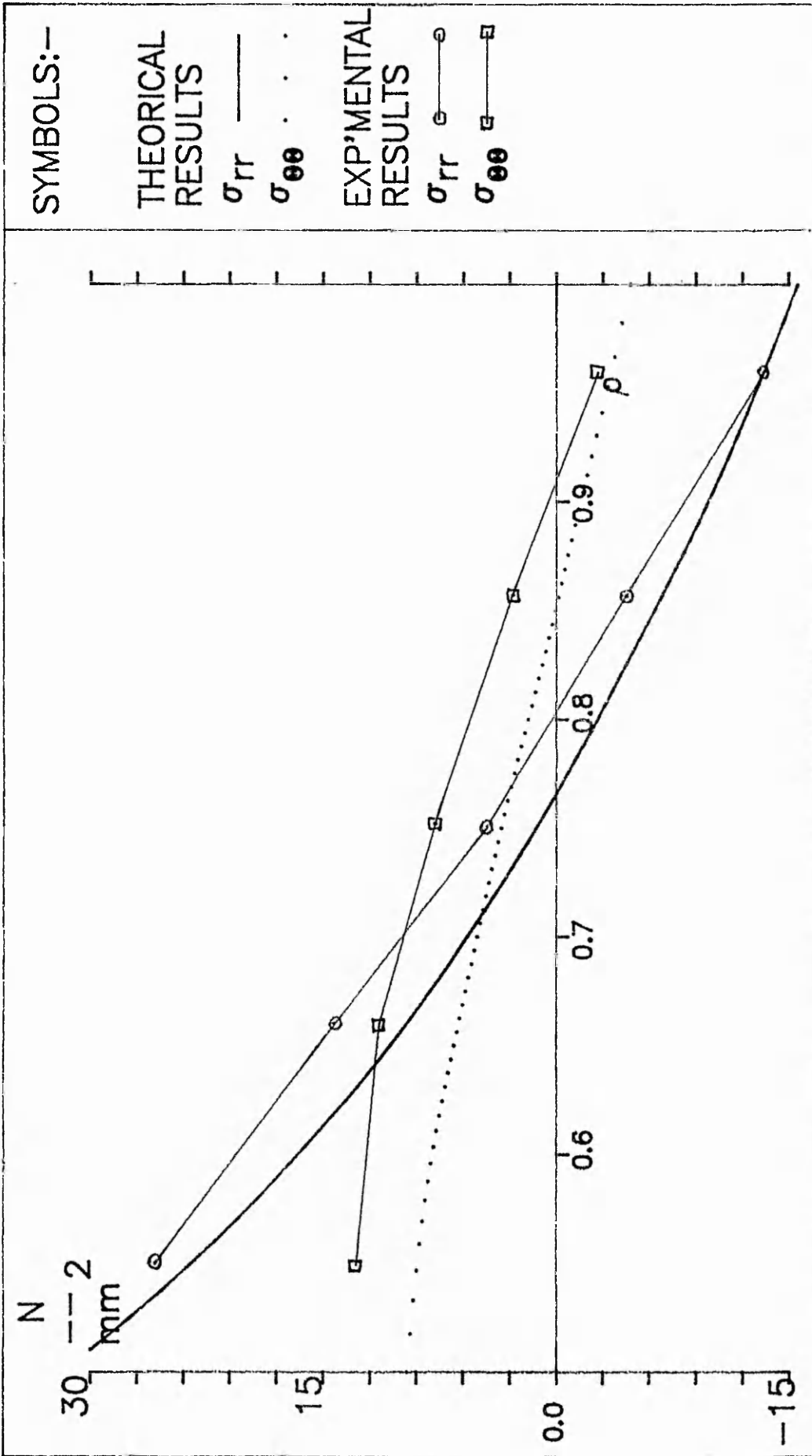
SYMBOLS:—
 THEORETICAL RESULTS ———
 EXP'MENTAL RESULTS ○ □

FIGURE: 3.17

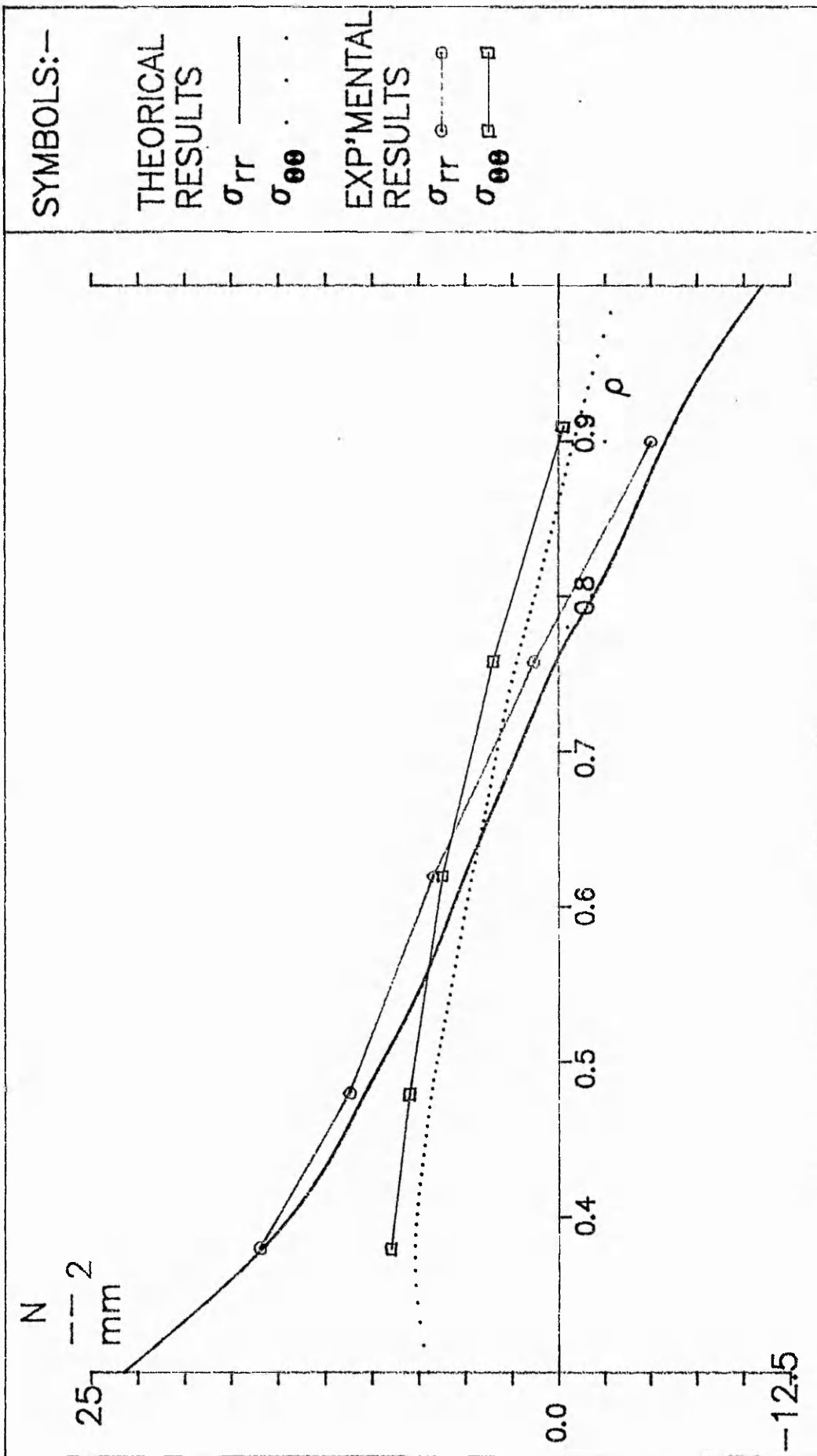
TITLE: DISPLACEMENT ω COMPARISONS FOR STEEL DISC (CONSTANT)



TITLE: STRESS COMPARISONS FOR STEEL DISC(CONSTANT) ($\beta=0.3$) FIGURE: 3.18



TITLE: STRESS COMPARISONS FOR STEEL DISC(CONSTANT) ($\beta=0.5$) FIGURE: 3.19



SYMBOLS:—

THEORETICAL RESULTS

σ_{rr} ———

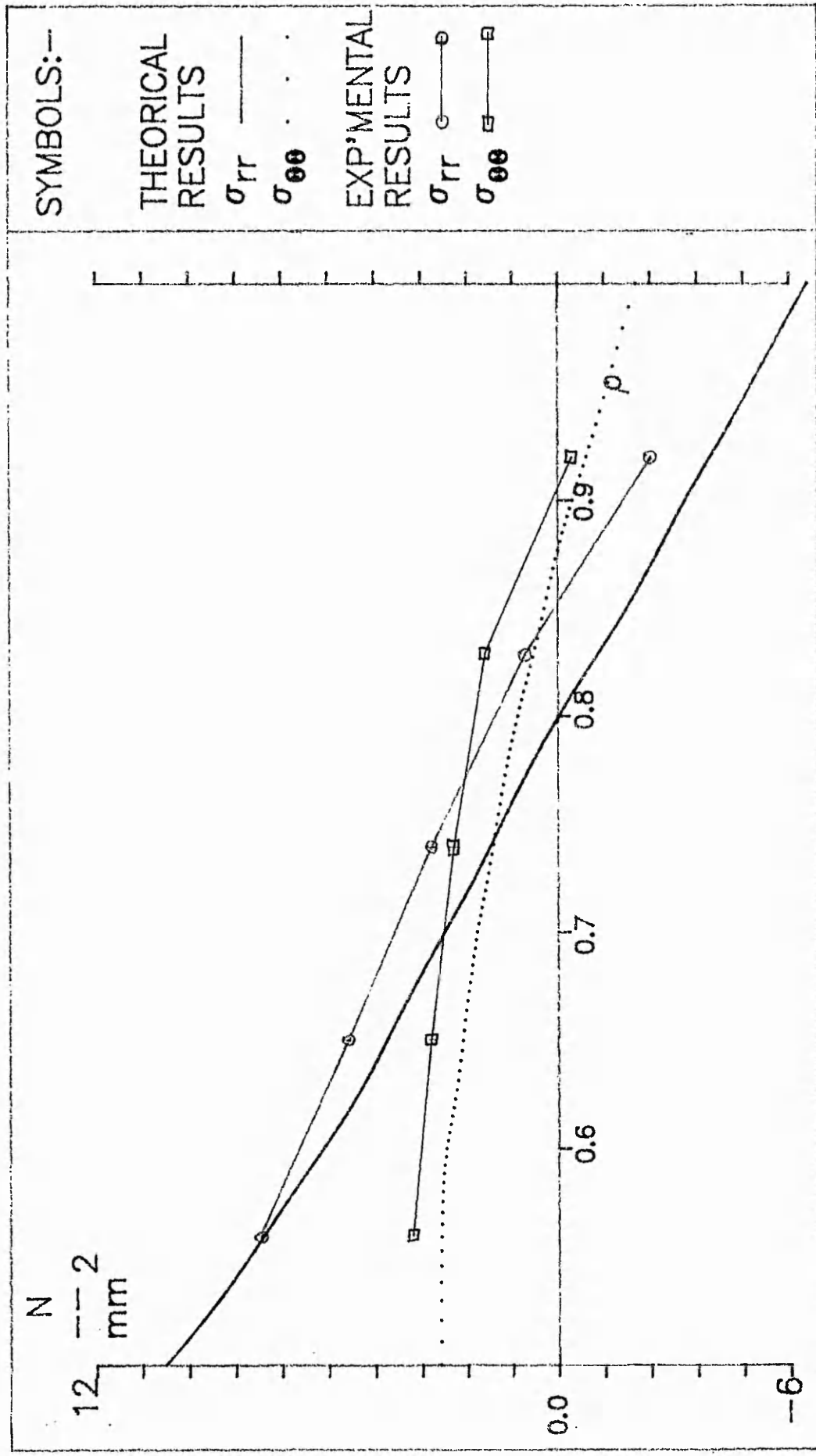
$\sigma_{\theta\theta}$

EXP'IMENTAL RESULTS

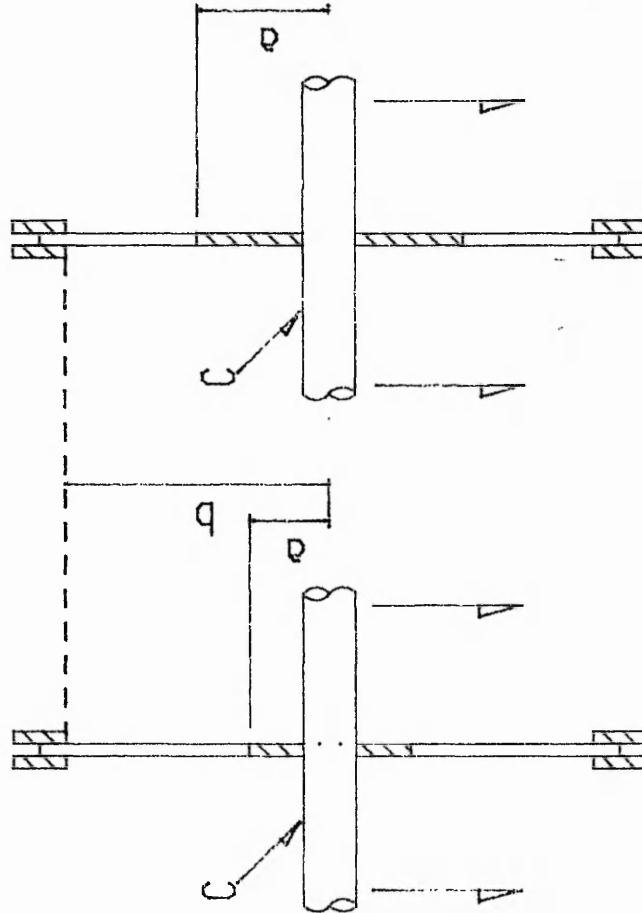
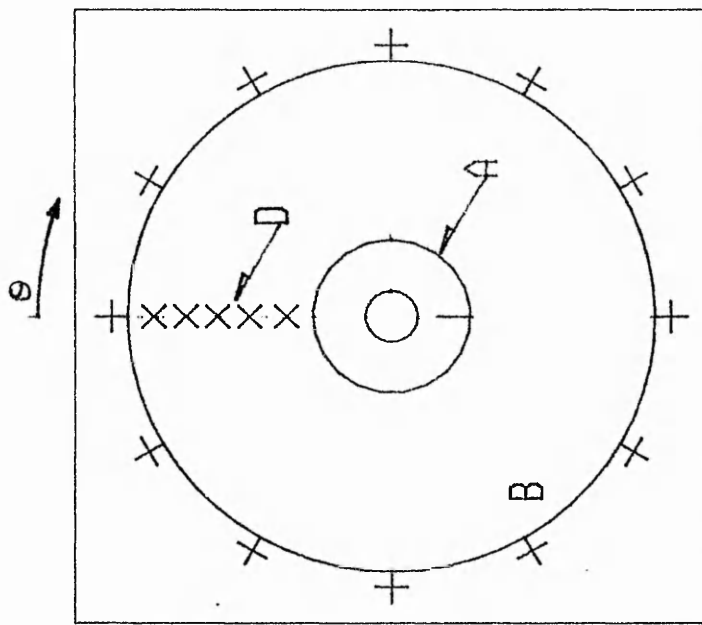
σ_{rr} ○ ———○

$\sigma_{\theta\theta}$ □ ———□

TITLE: STRESS COMPARISONS FOR STEEL DISC (PROFILED) ($\beta=0.3$) FIGURE: 3.20



TITLE: STRESS COMPARISONS FOR STEEL DISC (PROFILED) ($\beta=0.5$) FIGURE: 3.21



$d = 205\text{mm}$

$d = 110\text{mm}$

FIGURE : 3.22

TITLE : SCHEMATIC DIAGRAM OF A/ EXPERIMENTAL FRAME (PARALLEL DISCS)

CHAPTER 4

SHELL ANALYSIS

The shell of a conveyor pulley is subject to two components of stress viz membrane and bending stresses, induced by external loading and internal reactions. The external load is due totally to the conveyor belt traction, whereas the internal reactions are due to the in-plane pressure transmitted by the end discs and localised bending at the disc to shell connection. In order to analyse a pulley shell, it is necessary to develop two sets of equilibrium equations which represent its shape due to (1) external load and (2) internal reactions. The analysis for both loading conditions will, for clarity be developed separately below.

General assumptions applied to the shell analysis.

For the purpose of both membrane and bending analysis, the shell is considered to be a thin elastic, homogeneous cylinder, with isotropic material of constant thickness t and mean radius b (figure 4.1). The following assumptions also apply:

- (i) The thickness t is small compares to the radius b and shell length W .
- (ii) All points of the plate initially on a normal-to-a-middleplane of the plate remain so before and after deformation.
- (iii) The normal stresses in the direction transverse to the plate can be disregarded ($\sigma_z = 0$).

- (iv) The shell is sufficiently long for the ends not to have any mutual influence on each other

For the purpose of analysing the shell subject only to the belt pressure, it is assumed that the shell is supported at each end by a rigid disc which allows no deformation in its own plane. Therefore, the ends of the cylinder will be constrained to move only perpendicularly to this rigid plane. Thus, displacements v and w , and stress resultants N_x and M_x vanish at the shell edges.

4.1 METHOD OF ANALYSIS (BELT LOADING ONLY)

4.1.1 BELT LOADING CHARACTERISTICS

The pulley is subject to a tight side tension T_1 and a slack side tension T_2 (figure 4.1). The belt is wrapped around the shell between the angles of belt entry $\phi = \theta_v$ and the belt exit $\phi = -\theta_v$, with respect to a datum (i.e. $\phi = 0$). The direction (figure 4.1) and the magnitude of the resultant belt pull is calculated using equation group 2.1.

To establish the belt traction distribution between the belt and a drive pulley, consider figure 4.1, which illustrates four distinct zones. Firbank [9] regards these as the important regions of belt contact as it passes over the outer surface of a drive pulley.

- (i) Arc of "running on"
- (ii) Arc of "stick" or "adhesion"
- (iii) Arc of "slip"
- (iv) Arc of "running off"

The phenomenon of the "running on" and "running off" arcs are not well documented. However their presence is mainly

associated with the process of 'bending' the belt around the pulley. The degree of bending is dependent on how well the belt runs onto and off a pulley, which is a function of its stiffness, pulley diameter and the operating environment. It is assumed that the belt as been selected in accordance with belt manufacturers recommendations, so that these bending effects are minimal and therefore are ignored.

During the belt's passage through the arc of "stick" the velocity of the belt surface assumes the same velocity as the pulley surface. Within this region the belt effectively sticks to the pulley. As rotation continues towards the angle θ_c , shear strains develop in the belt cover resulting in a steadily decreasing tension in the belt strand. This decline in the belt is equilibrated by the interfacial shear traction. This state of equilibrium is preserved until $\phi = \theta_c$, where the contact pressure is insufficient to maintain stick and slip will result. Within the arc of slip ($-\theta_w > \phi > \theta_c$), the belt tension falls exponentially to the exit tension T_s in accordance with elementary theory of belt mechanics, Johnson [15].

$$T(\phi) = T_s e^{-\mu\phi} \quad -\theta_w > \phi > \theta_c \quad (4.1)$$

where T is the belt tension as it enters the arc of "slip".

In a conveyor idler pulley, the regions of belt contact as it passes over the outer surface are shown on figure 4.2. With the entry belt tension T_s equal to the exit belt tension T_t . The velocity of the belt surface will assume the same velocity as the pulley surface for the region between the arc's of "running on" and "running off". Within this region the belt will effectively stick to the pulley and there will

be no slip zone.

The belt tension variation with respect to ϕ can be written as:

(4.2)

For Drive pulleys only

$$\begin{aligned} \text{Arc of "Stick"} \quad T(\phi) &= T_L & \theta_c > \phi > \theta_v \\ \text{Arc of "Slip"} \quad T(\phi) &= T_c \cdot e^{-\mu\phi} & -\theta_v > \phi > \theta_c \end{aligned}$$

For Idler pulleys only

$$\text{Arc of "Stick"} \quad T(\phi) = T_c \quad -\theta_v > \phi > \theta_v$$

where T_c is the belt tension at $\phi = \theta_c$.

μ is the coefficient of friction between the belt and the pulley surfaces; a typical value given by belt manufacturers is 0.25 for an unlagged pulley.

The normal ($P(\phi, x)$) and tangential ($P'(\phi, x)$) components of the belt traction for both drive and idler pulleys may be written as:

For Drive pulleys only

(4.3)

$$P(\phi, x) = \frac{T(x) \cdot T_L}{W.b} \quad ; \quad P'(\phi, x) = \frac{d(P(\phi, x))}{d\phi} = 0 \quad \theta_c > \phi > \theta_v$$

$$P(\phi, x) = \frac{T(x) \cdot T_c \cdot e^{-\mu\phi}}{W.b} \quad ; \quad P'(\phi, x) = \frac{-T(x) \cdot T_c \cdot \mu \cdot e^{-\mu\phi}}{W.b} \quad -\theta_v > \phi > \theta_c$$

For Idler pulleys only

(4.4)

$$P(\phi, x) = \frac{T(x) \cdot T_i}{W \cdot b} \quad ; \quad P'(\phi, x) = \frac{d(P(\phi, x))}{d\phi} = 0 \quad -\theta_v > \phi > \theta_v$$

Distribution of the belt load across the pulley face is dependent on the type of construction of the belt and the way it enters and exits the pulley (i.e. bend and take-up pulleys as illustrated in figure 1.1) the pressure is constant across the width (curve a, figure 4.3). If the belt is troughed as it enters or exits the pulley (i.e. drive and tail pulleys as illustrated with figure 1.1) the pressure is non-uniform across the width and depends mainly on the relative position (i.e. height) of the pulley to the trough of the belt. If the point of contact between the belt and pulley is higher than the centre of the trough, then the pressure distribution will be in accordance with curve b, figure 4.3. Whereas, if the same contact point is lower than the centre of the trough then the pressure distribution will be as curve c, figure 4.3. To enable any of these variations in pressure to be represented, a Fourier series is used

(4.5)

$$T(x) = \sum_n^N a_n \cdot \sin(n\lambda \cdot x) \quad 0 < x < W$$

$$\text{where } a_n = \frac{2}{W} \int_0^W f'(x) \cdot \sin(n\lambda \cdot x) dx \quad \text{and } \lambda = \pi/W$$

The pressure generating function $f'(x)$ is assigned the value of unity to represent constant pressure across the belt width (curve "a", figure 4.3) which gives

$$T(x) = 4 \sum_{n=1}^N \frac{\sin(n\lambda \cdot x)}{\pi n} \quad n = 1, 3, 5, \dots, N \quad (4.6)$$

This variation of pressure with respect to x will be inserted into equations 4.3 and 4.4 for drive and idler pulleys respectively.

4.1.2 EQUILIBRIUM CONDITIONS

In order to describe the changes in the shell shape due to the belt traction, consider the element shown in figure 4.4 and 4.5. The first of these figures displays all the external and internal forces on the element and the second shows the internal moments. These equilibrium conditions have previously been documented, Flugge [10] and Timoshenko [28] and is detailed as follows

$$a \frac{\delta N_x}{\delta x} + \frac{\delta N_{\phi x}}{\delta \theta} = - a \cdot X(\phi, x) \quad (4.7)$$

$$\frac{\delta N_{\phi}}{\delta \phi} + a \frac{\delta N_{x\phi}}{\delta x} + \frac{\delta M_{x\phi}}{\delta x} - \frac{1 \cdot \delta M_{\phi}}{a \delta \phi} = - a \cdot Y(\phi, x)$$

$$N_{\phi} + \frac{\delta^2 M_{\phi x}}{\delta x \delta \phi} + a \frac{\delta^2 M_x}{\delta x^2} - \frac{\delta^2 M_{x\phi}}{\delta x \delta \phi} + \frac{1 \cdot \delta^2 M_{\phi}}{a \delta \phi^2} = - a \cdot Z(\phi, x)$$

where $X(\phi, x)$, $Y(\phi, x)$; $Z(\phi, x)$ are external force components acting on the shell and u , v , w are displacements, all parallel to the x , y , z axes respectively (figure 4.6).

For the determination of the shell displacements u , v , and w consider the components of stress and strain

(4.8)

$$\epsilon_x = u_x - z \cdot w_{xx} \quad , \quad \epsilon_\phi = \frac{1}{b} (v_\phi - w) - \frac{z}{b^2} (v_\phi - z \cdot w_{xx})$$

$$\chi_{x\phi} = \frac{1}{b} u_\phi + v_x - \frac{2z}{b} (v_x + w_{x\phi})$$

$$\text{where } ()_x = \frac{\delta()}{\delta x} \quad \text{and} \quad ()_\phi = \frac{\delta()}{\delta \phi}$$

(4.9)

$$\sigma_x = \frac{E}{1-\nu^2} (\epsilon_x + \nu \cdot \epsilon_\phi) \quad , \quad \sigma_\phi = \frac{E}{1-\nu^2} (\epsilon_\phi + \nu \cdot \epsilon_x)$$

$$\tau_{x\phi} = \frac{E}{2(1+\nu)} \cdot \chi_{x\phi}$$

Substituting these expressions for strain into the stress equations, the resultant loads (ie. N_x , N_ϕ , $N_{x\phi}$, etc.) and the moments (i.e. M_x , M_ϕ , etc.) can be expressed in terms of displacement only

(4.10)

$$N_x = \int_{-l/2}^{l/2} \sigma_x \cdot I_x \, dz = K \cdot \left[u_x + \frac{\nu}{b} (v_\phi - w) \right]$$

$$N_\phi = \int_{-l/2}^{l/2} \sigma_\phi \cdot dz = K \cdot \left[\frac{1}{b} (v_\phi - w) + \nu \cdot u_x \right]$$

$$M_x = \int_{-l/2}^{l/2} \sigma_x \cdot I_x \cdot z \, dz = -D \cdot \left[w_{xx} + \frac{\nu}{b^2} (v_\phi + w_{\phi\phi}) \right]$$

$$M_{\phi} = \int_{-t/2}^{t/2} \sigma_x \cdot z \, dz = -D \cdot \left[\frac{1}{b^2} \left(v_{\phi} + w_{\phi\phi} \right) + \nu \cdot w_{\phi\phi\phi} \right]$$

$$\text{where } I_x = \frac{1}{b}, \quad D = \frac{E \cdot t^3}{12(1-\nu^2)} \quad \text{and } K = \frac{E \cdot t}{1-\nu^2}$$

As stated earlier, the thickness t of the shell is small in comparison with the radius b . Thus the quantity z/b is neglected, giving

(4.11)

$$N_{x\phi} = N_{\phi x} = \int_{-t/2}^{t/2} \tau_{x\phi} \, dz = \frac{K(1-\nu)}{2} \left[\frac{u_{\phi}}{b} + v_x \right]$$

$$M_{x\phi} = -M_{\phi x} = - \int_{-t/2}^{t/2} \tau_{x\phi} \cdot z \, dz = \frac{D(1-\nu)}{b} \left[v_x + w_{x\phi} \right]$$

The equilibrium equation can now be rewritten in terms of displacements and external force components only

(4.12)

$$b^2 u_{xx} + \frac{(1-\nu) \cdot u_{\phi\phi}}{2} + \frac{(1+\nu)b \cdot v_{x\phi}}{2} - \nu \cdot b^2 w_x = - \frac{b^2 \cdot X(\phi, x)}{D} \quad (a)$$

$$\frac{(1+\nu)b \cdot u_{x\phi}}{2} + \frac{(1-\nu)b^2 v_{\phi\phi}}{2} + v_{\phi\phi} - w_{\phi} + \frac{t^2}{12} \left[w_{\phi\phi\phi\phi} + (1-\nu) \cdot v_{\phi\phi\phi} \right] = - \frac{b^2 \cdot Y(\phi, x)}{D} \quad (b)$$

$$\nu b \cdot u_x + v_{\phi} - w - \frac{t^2}{12 \cdot b^2} \left[b^4 w_{\phi\phi\phi\phi} + 2 \cdot b^2 w_{\phi\phi\phi\phi} + w_{\phi\phi\phi\phi} \right] = - \frac{b^2 \cdot Z(\phi, x)}{D} \quad (c)$$

4.1.3 MODEL BELT LOADING

To study the stress state induced by a shell subject to the belt loading only, allow the components of load and displacement to be formed using a double Fourier series. The resulting coefficients of these series can be determined using the functions for belt traction described in section 4.1.1. Consider the external force components to be distributed according to the following set of equations

$$\begin{aligned}
 X(\phi, x) &= \sum_{m=0}^M \sum_{n=0}^N \bar{X}_{mn} \cos(m\phi) \cos(n\lambda \cdot x) + \sum_{m=0}^M \sum_{n=0}^N X_{mn} \sin(m\phi) \cos(n\lambda \cdot x) \\
 Y(\phi, x) &= \sum_{m=0}^M \sum_{n=0}^N \bar{Y}_{mn} \sin(m\phi) \sin(n\lambda \cdot x) + \sum_{m=0}^M \sum_{n=0}^N Y_{mn} \cos(m\phi) \sin(n\lambda \cdot x) \\
 Z(\phi, x) &= \sum_{m=0}^M \sum_{n=0}^N \bar{Z}_{mn} \cos(m\phi) \sin(n\lambda \cdot x) + \sum_{m=0}^M \sum_{n=0}^N Z_{mn} \sin(m\phi) \sin(n\lambda \cdot x)
 \end{aligned}
 \tag{4.13}$$

where \bar{X}_{mn} , X_{mn} , \bar{Y}_{mn} , Y_{mn} , \bar{Z}_{mn} ; Z_{mn} are determined independently from the equations representing the modelled belt traction described in section 4.1.1. Let \bar{X}_{mn} , \bar{Y}_{mn} ; \bar{Z}_{mn} be representative of the symmetric components of the belt traction for both drive and idler pulleys and X_{mn} , Y_{mn} ; Z_{mn} correspond to the anti-symmetric components of the belt traction relevant only to drive pulleys. Consider the components of displacement to be distributed according to the following set of equations

$$u(\phi, x) = \sum_{m, n=0}^{M, N} \bar{u}_{mn} \cos(m\phi) \cos(n\lambda \cdot x) + \sum_{m, n=0}^{M, N} u_{mn} \sin(m\phi) \cos(n\lambda \cdot x)$$

$$v(\phi, x) = \sum_{m, n=0}^{M, N} \bar{v}_{mn} \sin(m\phi) \sin(n\lambda \cdot x) + \sum_{m, n=0}^{M, N} v_{mn} \cos(m\phi) \sin(n\lambda \cdot x)$$

$$w(\phi, x) = \sum_{m, n=0}^{M, N} \bar{w}_{mn} \cos(m\phi) \sin(n\lambda \cdot x) + \sum_{m, n=0}^{M, N} w_{mn} \sin(m\phi) \sin(n\lambda \cdot x)$$

where \bar{u}_{mn} , u_{mn} , \bar{v}_{mn} , v_{mn} , \bar{w}_{mn} ; w_{mn} are the unknown displacements coefficients. Let \bar{u}_{mn} , \bar{v}_{mn} ; \bar{w}_{mn} be representative of the symmetric components of displacement and u_{mn} , v_{mn} ; w_{mn} correspond to anti-symmetric components of displacement.

The first terms of equations 4.13 and 4.14 reflect the symmetric components of load and displacements respectively, whereas the second terms are the anti-symmetric components of load and displacements.

For clarity the symmetric and anti-symmetric elements of load and deflection will be considered separately, with the resulting displacements superimposed at a later stage.

For the symmetrical loading of the pulley shell it is necessary to introduce the first terms of 4.13 and 4.14 and their derivatives into the equilibrium equation 4.12. The trigonometric constants are common to all elements of the equations, and are therefore omitted, resulting in the following set of three linear equations in terms of \bar{u}_{mn} , \bar{v}_{mn} ; \bar{w}_{mn} .

$$\begin{bmatrix} \left[\frac{-(b_n^*)^2 - (1-\nu)m^2}{2} \right] & \left[\frac{(1+\nu)b_n^*m}{2} \right] & - \left[\nu \cdot b_n^* \right] \\ \left[\frac{(1+\nu)b_n^*m}{2} \right] & - \left[\frac{m^2 + (1-\nu)(b_n^*)^2(1+2k)}{2} \right] & \left[1 + k(b_n^*)^2 \right] \\ - \left[\nu \cdot b_n^* \right] & \left[m \right] & - \left[1 + k \left[(b_n^*)^2 + m^2 \right]^2 \right] \end{bmatrix} \begin{bmatrix} \bar{u}_{mn} \\ \bar{v}_{mn} \\ \bar{w}_{mn} \end{bmatrix} = \begin{bmatrix} 0 \\ 0 \\ -\frac{b^2 Z_{mn}}{D} \end{bmatrix}$$

$$\text{where } b_n^* = \frac{b \cdot n}{w} \quad \text{and} \quad k = \frac{12 \cdot b^2}{t^2}$$

Similarly, for the anti-symmetric loading case it is necessary to introduce the second terms of 4.13 and 4.14 and derivatives into the equilibrium equation 4.12 to arrive at a further set of linear equations in the terms of \bar{u}_{mn} , \bar{v}_{mn} ; \bar{w}_{mn} .

$$\begin{bmatrix} \left[\frac{-(b_n^*)^2 - (1-\nu)m^2}{2} \right] & - \left[\frac{(1+\nu)b_n^*m}{2} \right] & - \left[\nu \cdot b_n^* \right] \\ - \left[\frac{(1+\nu)b_n^*m}{2} \right] & - \left[\frac{m^2 + (1-\nu)(b_n^*)^2(1+2k)}{2} \right] & - \left[1 + k(b_n^*)^2 \right] \\ - \left[\nu \cdot b_n^* \right] & - \left[m \right] & - \left[1 + k \left[(b_n^*)^2 + m^2 \right]^2 \right] \end{bmatrix} \begin{bmatrix} \bar{u}_{mn} \\ \bar{v}_{mn} \\ \bar{w}_{mn} \end{bmatrix} = \begin{bmatrix} 0 \\ -\frac{b^2 Y_{mn}}{D} \\ -\frac{b^2 Z_{mn}}{D} \end{bmatrix}$$

To solve each set of linear equations, consider first the load constants X, Y, Z for both symmetric and anti-symmetric load conditions.

Loads transmitted from the belt to the pulley in the axial

direction are assumed to be negligible because any significant axial force would lead to the belt moving from side to side (ie tracking off line), hence the force components in the X direction vanish, i.e. $\bar{X}_{mn} = \bar{X}_{mn} = 0$. Constants \bar{Y}_{mn} , \bar{Y}_{mn} , \bar{Z}_{mn} and \bar{Z}_{mn} are determined by considering the external forces applied by the belt traction, consisting only of the pressure normal to the surface $p(\phi, x)$ and a tangential component $p'(\phi, x)$, which were both defined in section 4.1.1.

4.1.4 SYMMETRIC LOADING CONDITIONS

As the symmetric loading conditions are subject only to pressure normal to the surface, $\bar{Y}_{mn} = 0$ and \bar{Z}_{mn} may be resolved using the following integral

$$\bar{Z}_{mn} = \frac{2}{\pi.W} \int_0^W \int_{-\theta_v}^{\theta_v} \bar{P}(\phi, x) \cdot \cos(m\phi) \sin(n\lambda.x) dx d\phi \quad (4.17)$$

$P(\phi, x)$ and $T(x)$ were evolved for symmetric belt traction in section 4.1.1. However they are confirmed to be

$$P(\phi, x) = \frac{T(x) \cdot T_t}{b.W} \quad \text{and} \quad T(x) = \frac{a}{n} \sin(n\lambda.x) \quad (4.18)$$

The loading constant \bar{Z}_{mn} is easily determined for all values of m and n , which leads to the following

$$\bar{Z}_{mn} = \frac{T_t}{b.W} \frac{a \sin(m \cdot \theta_v)}{n} \quad \begin{array}{l} m = 1, 3, 5, \dots, M \\ n = 1, 3, 5, \dots, N \end{array} \quad (4.19)$$

$$\bar{Z}_{0n} = \frac{T}{\pi} a_n \theta_v$$

b.W

$$m = 0$$

$$n = 1, 3, 5, \dots, N$$

where $a_n = \frac{4}{n\pi}$

Substituting 4.19 into 4.15, the displacement coefficients

\bar{u}_{mn} , \bar{v}_{mn} ; \bar{w}_{mn} are established by computation.

4.1.5 ANTI-SYMMETRIC LOADING CONDITIONS

The anti-symmetric loading conditions are subject to pressure normal to the surface and its tangential component. Thus, \bar{Y}_{mn} and \bar{Z}_{mn} are determined using the same method described in section 4.1.3.

$$\bar{Y}_{mn} = \frac{2}{\pi.W} \int_0^W \int_{-\theta_v}^{\theta_c} P'(\phi, x) \cdot \sin(m\phi) \cos(n\lambda \cdot x) \, dx d\phi$$

(4.20)

$$\bar{Z}_{mn} = \frac{2}{\pi.W} \int_0^W \int_{-\theta_v}^{\theta_c} P(\phi, x) \cdot \sin(m\phi) \sin(n\lambda \cdot x) \, dx d\phi$$

The components of the belt traction stated for drive pulleys only (equation 4.3 contain both symmetric and anti-symmetric elements. Therefore, since both components of belt traction are being considered separately and later superimposed, it is necessary to remove the symmetric element by subtracting equation 4.18 from the expression for $P(\phi, x)$ which was derived in section 4.1.1, equation 4.3. Thus, resulting in the following equation for the anti-symmetric load element of $P(\phi, x)$ and $P'(\phi, x)$,

(4.21)

$$P(\phi, x) = \frac{T(x)}{b.W} \left[T_s \cdot e^{\mu(\theta_v + \phi)} - T_t \right]$$

$$P(\phi, x) = \frac{T(x)}{b.W} \left[\mu \cdot T_s \cdot e^{\mu(\theta_v + \phi)} \right] \quad \text{and } T(x) = a_n \sin(n\lambda \cdot x)$$

Loading constants Y_{mn} and X_{mn} are easily determined for all values of m and n , which gives

(4.22)

$$Y_{mn} = \frac{a_n}{\pi \cdot b.W} \frac{\mu}{\mu^2 + m^2} \left[T_t \left[\mu \cdot \cos(m \cdot \theta_c) - m \cdot \sin(m \cdot \theta_c) \right] + T_s \left[\mu \cdot \cos(m \cdot \theta_c) - m \cdot \sin(m \cdot \theta_c) \right] \right]$$

$$m = 1, 2, 3, 4, \dots, M$$

$$n = 1, 3, 5, \dots, N$$

$$Y_{on} = \frac{a_n}{\pi \cdot b.W} \frac{(T_t - T_s)}{2}$$

$$m = 0$$

$$n = 1, 3, 5, \dots, N$$

where $a_n = \frac{4}{n\pi}$

$$Z_{mn} = \frac{a_n}{\pi \cdot b \cdot W} \left[\frac{1}{\mu^2 + m^2} \left[T_t \left[\mu \cdot \sin(m \cdot \theta_c) - m \cdot \cos(m \cdot \theta_c) \right] \right. \right. \\ \left. \left. + T_s \left[\mu \cdot \sin(m \cdot \theta_c) - m \cdot \cos(m \cdot \theta_c) \right] \right] \right. \\ \left. + \frac{T_t}{m} \left[\mu \cdot \cos(m \cdot \theta_c) - m \cdot \cos(m \cdot \theta_c) \right] \right]$$

$$m = 1, 2, 3, 4, \dots, M \quad n = 1, 3, 5, \dots, N$$

$$\text{where } a_n = \frac{4}{n\pi}$$

Substituting 4.22, 4.23 into 4.16 the displacement coefficients u_{mn} , v_{mn} ; w_{mn} are established by computation

4.1.6 RESULTANT STRESSES

The displaced shape of the shell (i.e. u, v, w) is determined by substituting the symmetric and anti-symmetric displacement coefficients computed in sections 4.1.4 and 4.1.5 (for drive pulleys only) into equation 4.14. Thus, the important stresses for inner (+ve sign) and outer surfaces are

$$\sigma_{ii}(\max) = \left[\frac{6 \cdot M_{ii}}{t^2} \right] \pm \left[\frac{N_i}{t} \right] \quad i = \phi, x \quad (4.24)$$

The resultant moments and forces were established in section 4.1.3.

How well the load and displacement series converge greatly depends on the magnitude of certain dimensionless ratios, such as b/t . If b/t is large (greater than 20), the series for the N -forces converge quickly, whereas the series for

M-forces require a larger number of terms. In any event, for the typical sizes expected with heavy duty conveyor pulleys 15 terms are found to be sufficient to permit the series to converge.

Figure 4.7, 4.8, 4.9 illustrate the variation of stress for various belt wraps subjected to an idler pulley. Figure 4.10 illustrates the maximum stress variation (belt wrap 65 degrees) along the shells length for the case of a belt wrap of 180 degrees (figure 4.8). Similarly, the figure 4.11 illustrates the variation of stress for a drive pulley with a typical belt wrap of 210 degrees. Verification of this technique is carried out by experimental and finite element analysis comparisons in chapter 5.

4.2 METHOD OF ANALYSIS (SHELL END EFFECTS)

The shell of a conveyor pulley is subject to additional loads which were not accounted for in the previous sections, namely, radial expansion of the end discs due to a shaft fastener and the reaction forces at any connection between the shell and supporting end discs.

CASE 1 Reaction between the end discs and shell

It was assumed in the previous sections that the shell was supported at each end by a rigid plane, where the displacements v and w and stress resultants N and M vanish at the shell edges. In fact, there will be a very small displacement in the end discs caused by the belt pressure generating a reaction force Q and

bending moment M at the disc/shell connection (figure 4.12).

CASE 2 Reaction between the centre supporting discs and shell

Central annular disc are often used to support the pulley shell and assist in providing even wear of the shell during operation. Very small displacements in the shell caused by the belt pressure will be restrained by the centre supporting discs which will generate a reaction force Q and bending moment M at the disc/shell connection (figure 4.12).

CASE 3 End disc expansion due to shaft fastener expansion

The compressive shaft fasteners commonly used with conveyor pulleys as discussed in chapter 1, generates a pressure at the inside diameter of the end disc, which is normally dissipated through the central boss and end disc. Therefore, any displacements that remain at the shell can be safely ignored.

4.2.1 EQUILIBRIUM CONDITIONS

The study of shells with stiffeners is not well documented, mainly because the analysis is very complex and should only be dealt with in three dimensions, in terms of both loading and geometry.

The literature reviewed assumed gross approximations on how the bending moments and forces are distributed between the shell and stiffeners. Also the previous work only considered shells subjected to uniformly distributed internal pressure.

A conservative analysis will be presented to demonstrate key areas of stress. This analysis will be further discussed in chapter 5 with the aid of finite element analysis and experimental comparisons.

Timoshenko and Woinowsky-Krieger [28] and Hartenburg [12] discussed the equilibrium of a shell with supporting discs which is subject to forces distributed symmetrically with respect to the axis. To account for the three load conditions described above, it is assumed that the generated pressure is uniform around, and normal to, the shell surface. Thus, the three equations of equilibrium (equation 4.7) will be reduce to

$$N_{\phi} + a \cdot \frac{\delta^2 M_x}{\delta x^2} = - a \cdot Z(\phi, x) \quad (4.25)$$

From symmetry it is assumed that in the circumferential direction the displacement component v vanishes and the change of curvature is negligible. The expressions for the strain components (equation 4.8) will also reduce to

$$\epsilon_x = u_x - z \cdot w_{xx} \quad ; \quad \epsilon_{\phi} = - \frac{w}{b} \quad (4.26)$$

Hence, by invoking Hooke's law (equation 4.9) and substituting into the integrals in equation 4.10

$$(4.27)$$

$$N_x = K \cdot \left[\begin{array}{c} u_x - \nu \cdot w \\ - \\ b \end{array} \right] = 0 \quad u_x = \frac{\nu \cdot w}{b}$$

$$N_{\phi} = K \cdot \left[\begin{array}{c} \nu \cdot u_x - w \\ - \\ b \end{array} \right] \quad N_{\phi} = - \frac{E \cdot t \cdot w}{b}$$

$$M_{xx} = -D \cdot w_{xxxx} \quad ; \quad M_{\phi} = \nu \cdot M_{xx}$$

The equilibrium equation may now be written only in terms of displacements and external force components.

$$w_{xxxx} + 4 \cdot \beta^4 w = \frac{Z}{D} \quad \text{where } \beta^4 = \frac{E \cdot t}{4 \cdot b^2 D} = \frac{3(1-\nu^2)}{b^2 \cdot t^2} \quad (4.28)$$

The general solution of this equation is

$$w = e^{\beta x} \left[C_1 \cos(\beta x) + C_2 \sin(\beta x) \right] + e^{-\beta x} \left[C_3 \cos(\beta x) + C_4 \sin(\beta x) \right] + f(x) \quad (4.29)$$

where $f(x)$ is a particular solution 4.28, and $C_1 \dots C_4$ are the constants of integration. Since the forces applied at the end $x = 0$ produce local bending which vanishes rapidly as x increases, it is concluded that the first term of equation 4.29 must also vanish. Introducing M and Q at the load point $x = 0$ and assuming the $f(x)$ will be independent of x for all examples considered, the two constants C_3 and C_4 may be established

$$M = M_{xx} \Big|_{x=0} = -D \cdot w_{xxxx} \Big|_{x=0} \quad (4.30)$$

$$Q = Q_{xx} \Big|_{x=0} = \frac{\delta M_{xx}}{\delta x} \Big|_{x=0} = -D \cdot w_{xxxxx} \Big|_{x=0}$$

$$C_3 = -\frac{1}{2 \cdot \beta^3 D} \left(Q + \beta M \right) \quad ; \quad C_4 = \frac{M}{2 \cdot \beta^2 D}$$

Thus, the final general expression for w is

$$w = \frac{e^{-\beta x} \left[\beta \cdot M \cdot (\sin(\beta x) - \cos(\beta x)) - Q \cdot \cos(\beta x) \right] + f(x)}{2 \cdot \beta^3 D} \quad (4.31)$$

4.2.2 MODEL LOADING

To study the stress state induced by localised bending, it is necessary to first described the shell's displacement for each of the three load conditions described above.

To define the displacement w and particular solution $f(x)$ (i.e. $f(x)$ at $x = 0$) for case 1, which is subject to an

assumed uniformly distributed pressure P' , and thrust Q , let

$$w = \left[P' \cdot h_d + 2 \cdot Q \right] \cdot \frac{b^2}{A_d \cdot E} \quad f(x) = \frac{P' \cdot b^2 (2 - \nu)}{2 \cdot E \cdot t} \quad (4.32)$$

where h_d and A_d are end supporting disc thickness and cross-sectional area respectively.

Also, assuming that the slope at $x = 0$ is zero, and substituting the result of this along with equation 4.32 into 4.31, M and Q may be resolved

$$M = \frac{P' \cdot b^2 \left[\frac{h_d}{A_d} - \frac{(2 - \nu)}{2t} \right]}{E} = \phi_d \quad Q = -2\beta \cdot \phi_d \quad (4.33)$$

$$\left[\frac{1}{2\beta^2 D} + \frac{4 \cdot b^2 \beta}{A_d E} \right]$$

Thus, the displacement w for case 1 may be written as

$$w = \frac{e^{-\beta x} \phi_d \left[\sin(\beta x) + \cos(\beta x) \right]}{2 \cdot \beta^2 D} \quad (4.34)$$

Similarly, w and $f(x)$ for case 2 may be defined as

$$w = \left[P' \cdot h_c + 2 \cdot Q \right] \cdot \frac{b^2}{A_c \cdot E} \quad f(x) = \frac{P' \cdot b^2 (2 - \nu)}{2 \cdot E \cdot t} \quad (4.35)$$

where h_c and A_c are centre supporting disc thickness and cross-sectional area respectively.

Again, assuming that the slope at $x = 0$ is zero, and substituting the result of this along with equation 4.35 into equation 4.31, M and Q may again be resolved

$$M = \frac{P' \cdot b^2 \left[\frac{h_c}{A_c} - \frac{(2-\nu)}{2t} \right]}{E \left[\frac{1}{2\beta^2 D} + \frac{4 \cdot b^2 \beta}{A_c E} \right]} = \phi_c \quad Q = -2\beta \cdot \phi_c \quad (4.36)$$

4.2.3 RESULTANT STRESSES

The important stresses are determined by substituting the resultant moments and forces (equation 4.27) into equation 4.24. These stresses are superimposed onto the resultant stresses determined in section 4.1.6. Figure 4.13 illustrates the localised nature of the stress produced by the above shell end effects, whilst table 4.1 shows some important results of stress.

Verification of these results are carried out by experimental and finite element analysis comparisons in chapter 5.

4.3 SHELL STIFFNESS

The shell can be regarded as a tube, to which a moment is applied at the ends. For the purpose of calculating the stiffness of the shell it will also be assumed that the ends will remain in plane. Thus, using elementary beam theory the stiffness of the shell is written as

$$k_{sh} = \frac{2.E.I_{sh}}{W} = \frac{M_{sh}}{\phi_{sh}} \frac{M_p}{\phi_{sh}}$$

$$I_{sh} = \frac{\pi}{64} \left[D^4 - (D - 2t)^4 \right]$$

This simple beam theory ignores the effect of the shear stress distribution on the strains and hence the deflections. The deflections caused by shear in a pulley shell, is only of real practical influence on its stiffness when the ratio b/t becomes large (greater than 40) and the ratio W/b becomes small (less than 1). For the typical sizes expected with heavy duty conveyor pulleys it is assumed that the shear influences will not produce any significant discrepancies in the overall bending moment distributions between the shaft and pulley.

TABLE 4.1

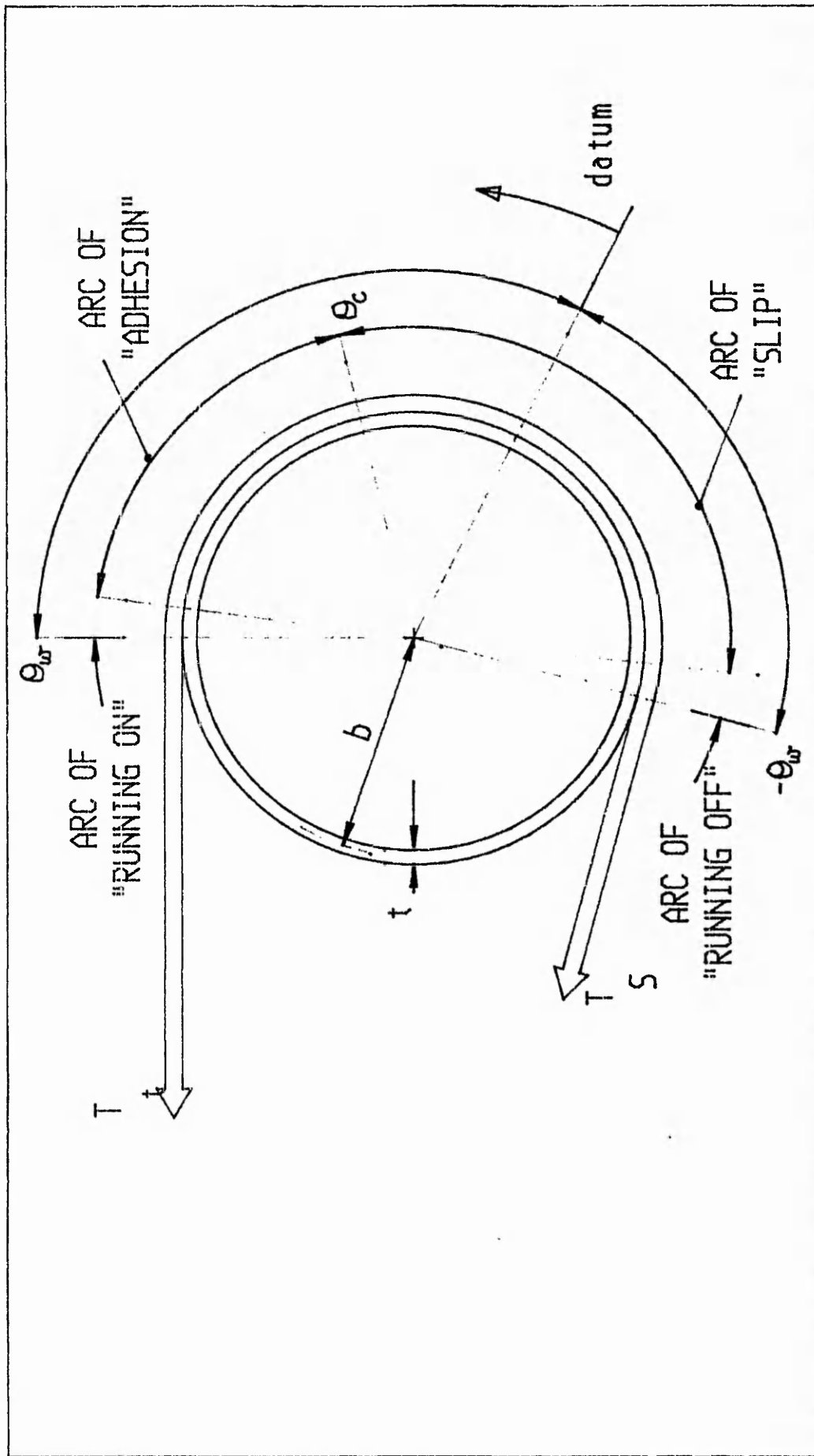
Some important shell stresses due to shell end effects.

Parameter	Variation
-----------	-----------

$$\sigma_{xx}(\max) = \frac{-6 \phi_x}{t^2} \cdot e^{-\beta x} \cdot [\cos(\beta x) - \sin(\beta x)]$$

$$\sigma_{\phi\phi}(\max) = -\sigma_x \cdot e^{-\beta x} \cdot \left[\left(\frac{6 \cdot \nu}{t^2} + \frac{E}{b \cdot t} \right) \cos(\beta x) + \left(\frac{6 \cdot \nu}{t^2} - \frac{E}{b \cdot t} \right) \sin(\beta x) \right]$$

$\phi_x = \phi_d$ or ϕ_c shown by equations 4.33 and 4.36 respectively.



TITLE : IMPORTANT REGIONS OF BELT CONTACT AROUND A DRIVE PULLEY

FIGURE : 4.1

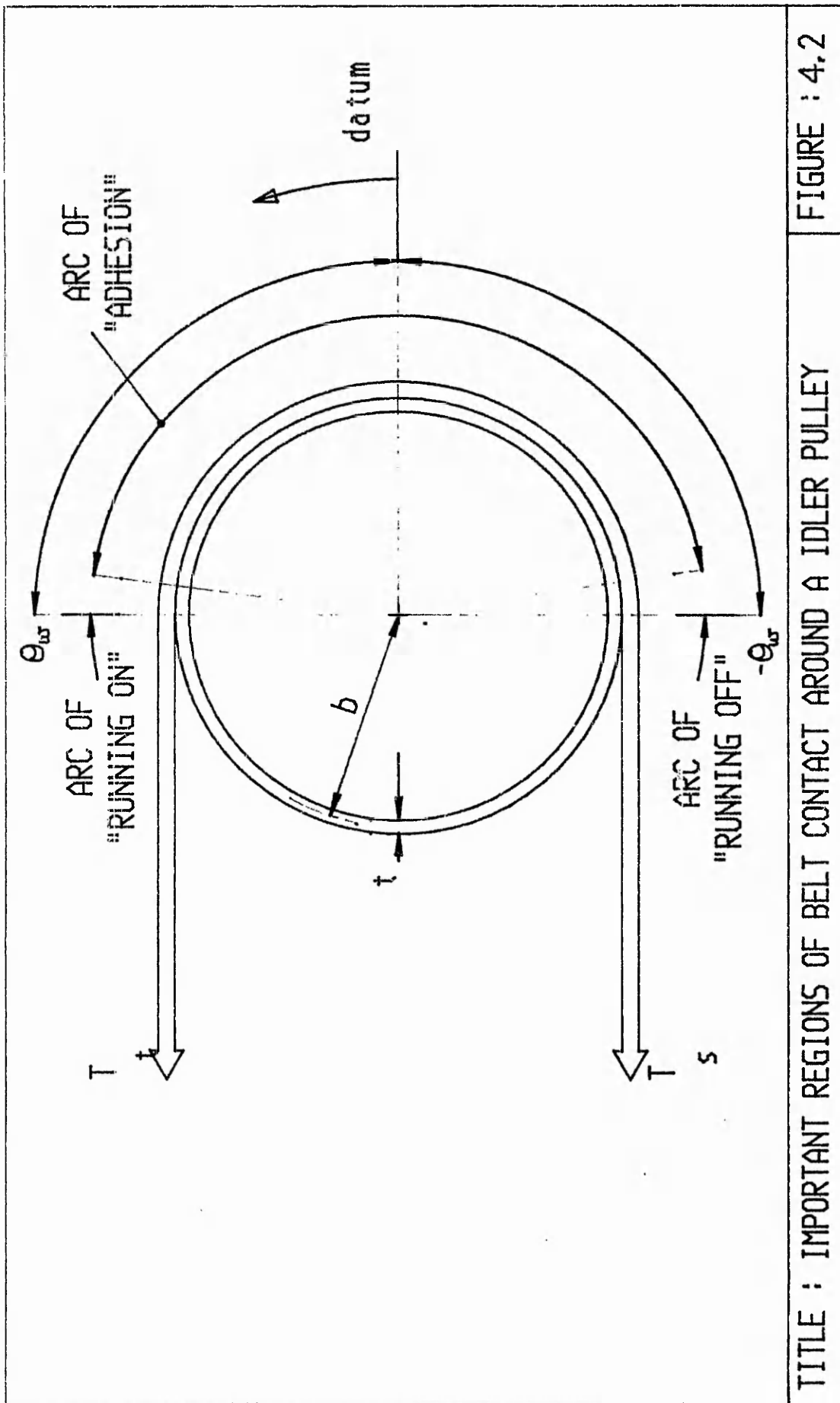


FIGURE : 4.2

TITLE : IMPORTANT REGIONS OF BELT CONTACT AROUND A IDLER PULLEY

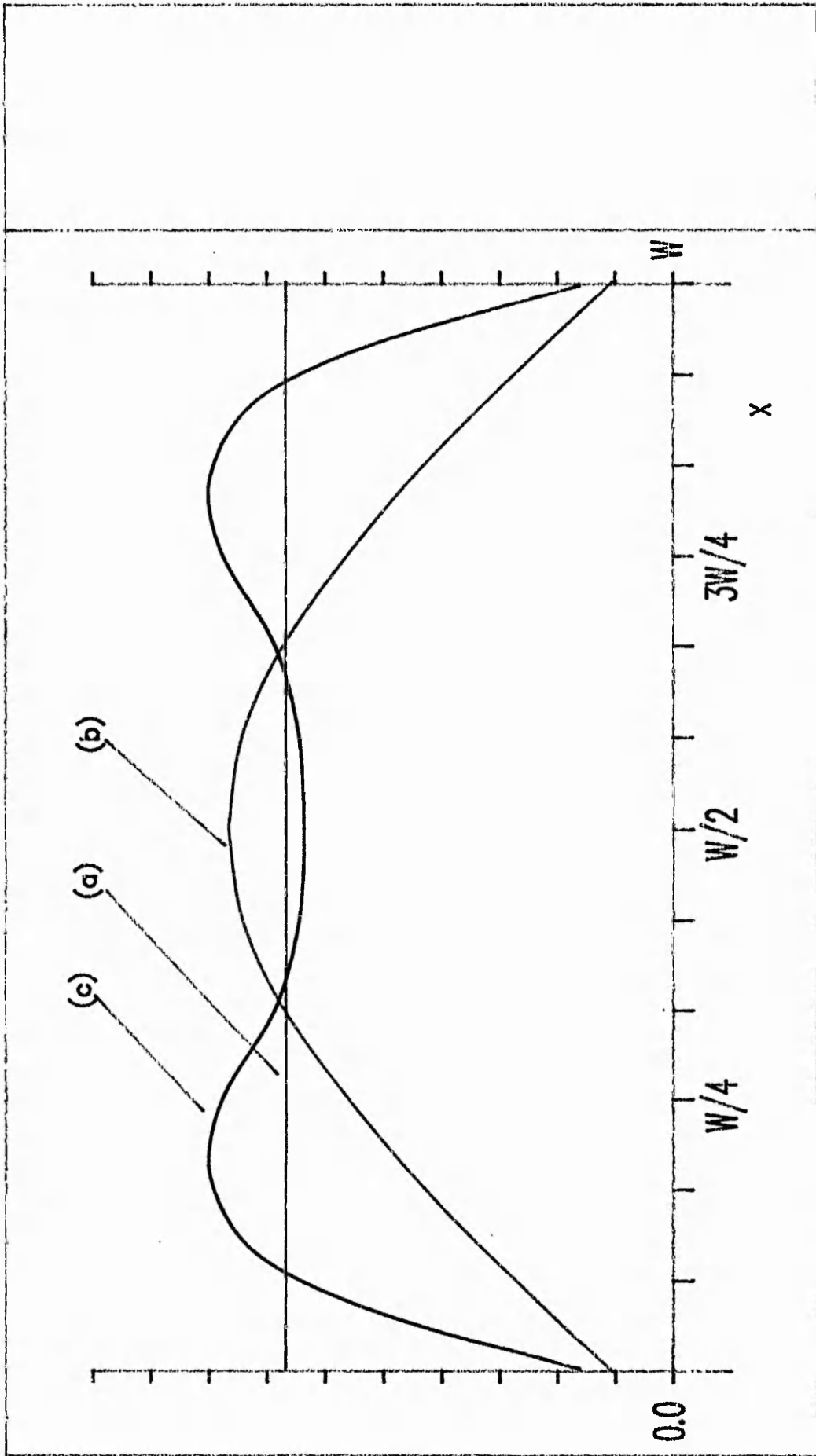
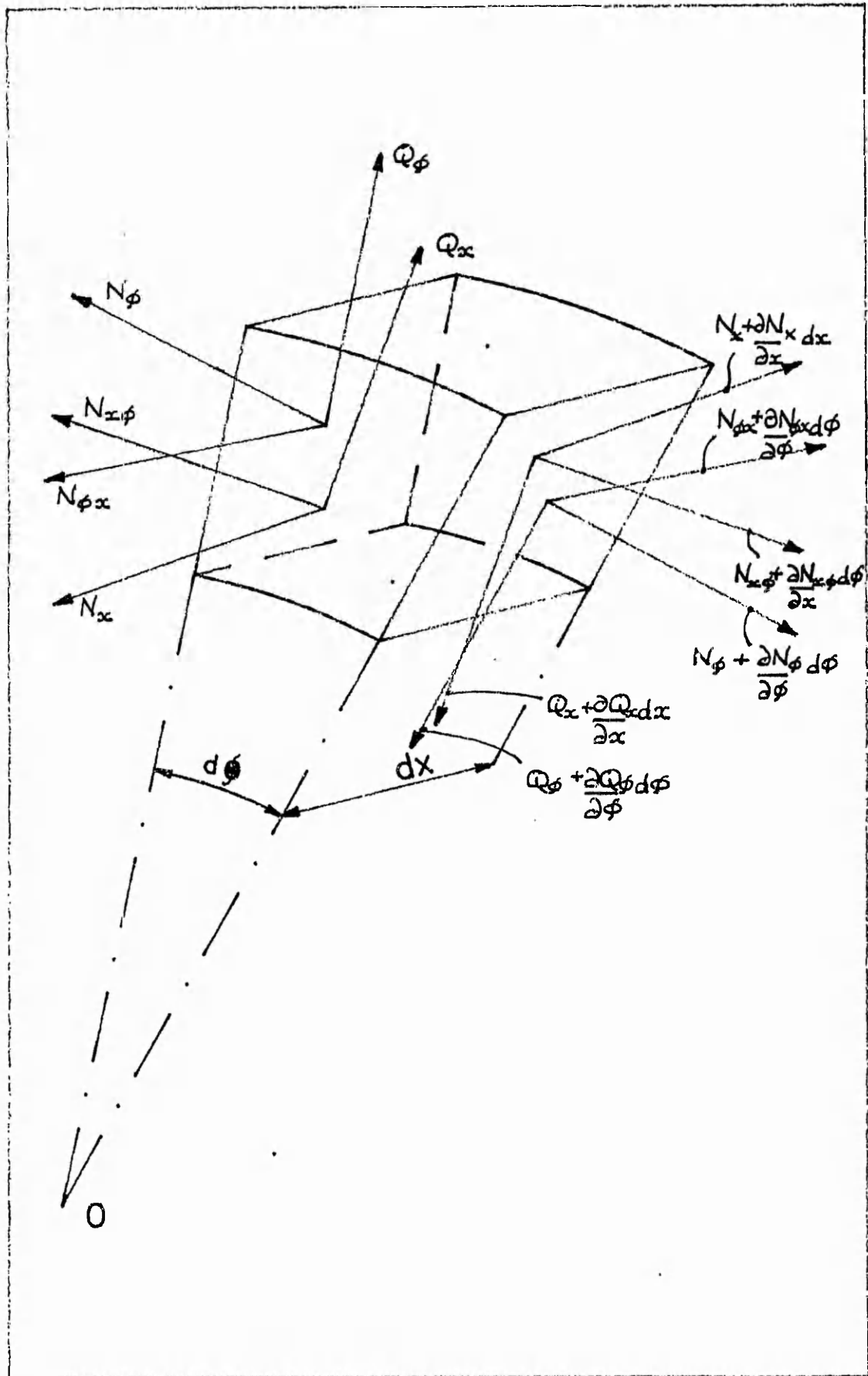
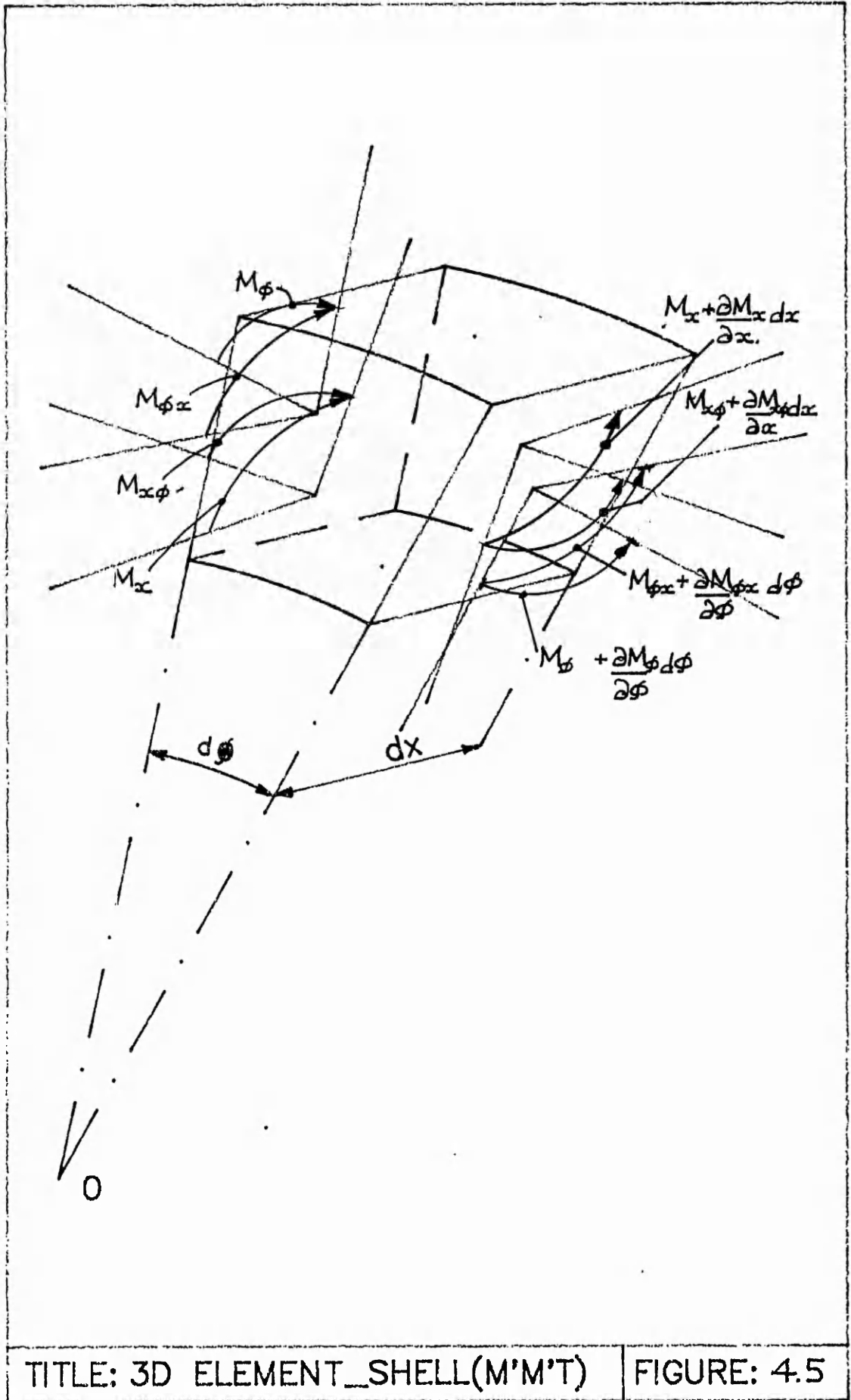


FIGURE: 4.3

TITLE: DISTRIBUTION OF BELT TRACTION ACROSS THE PULLEY FACE



TITLE: 3D ELEMENT_SHELL(FORCE) | FIGURE: 4.4



TITLE: 3D ELEMENT_SHELL(M'M'T)

FIGURE: 4.5

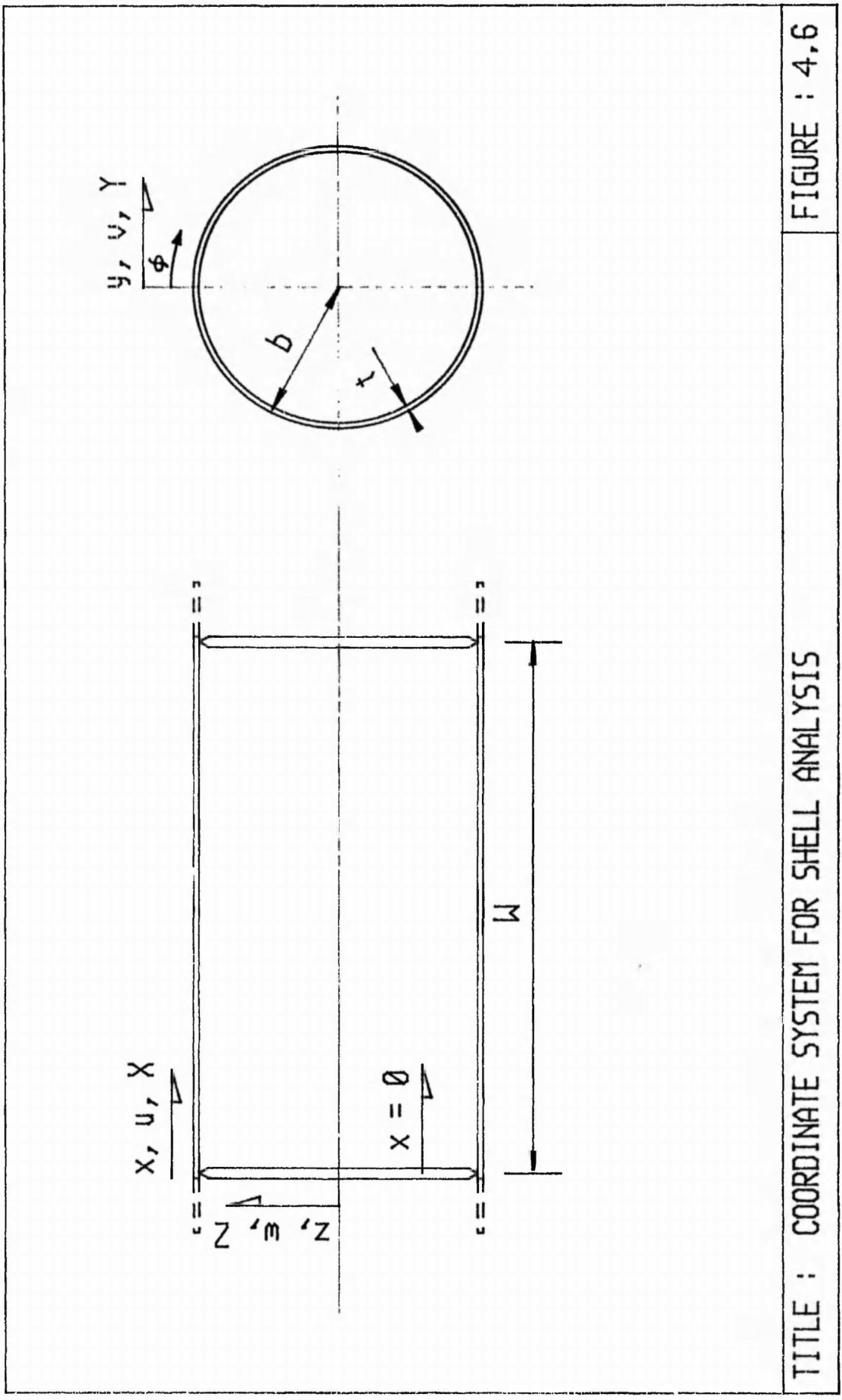
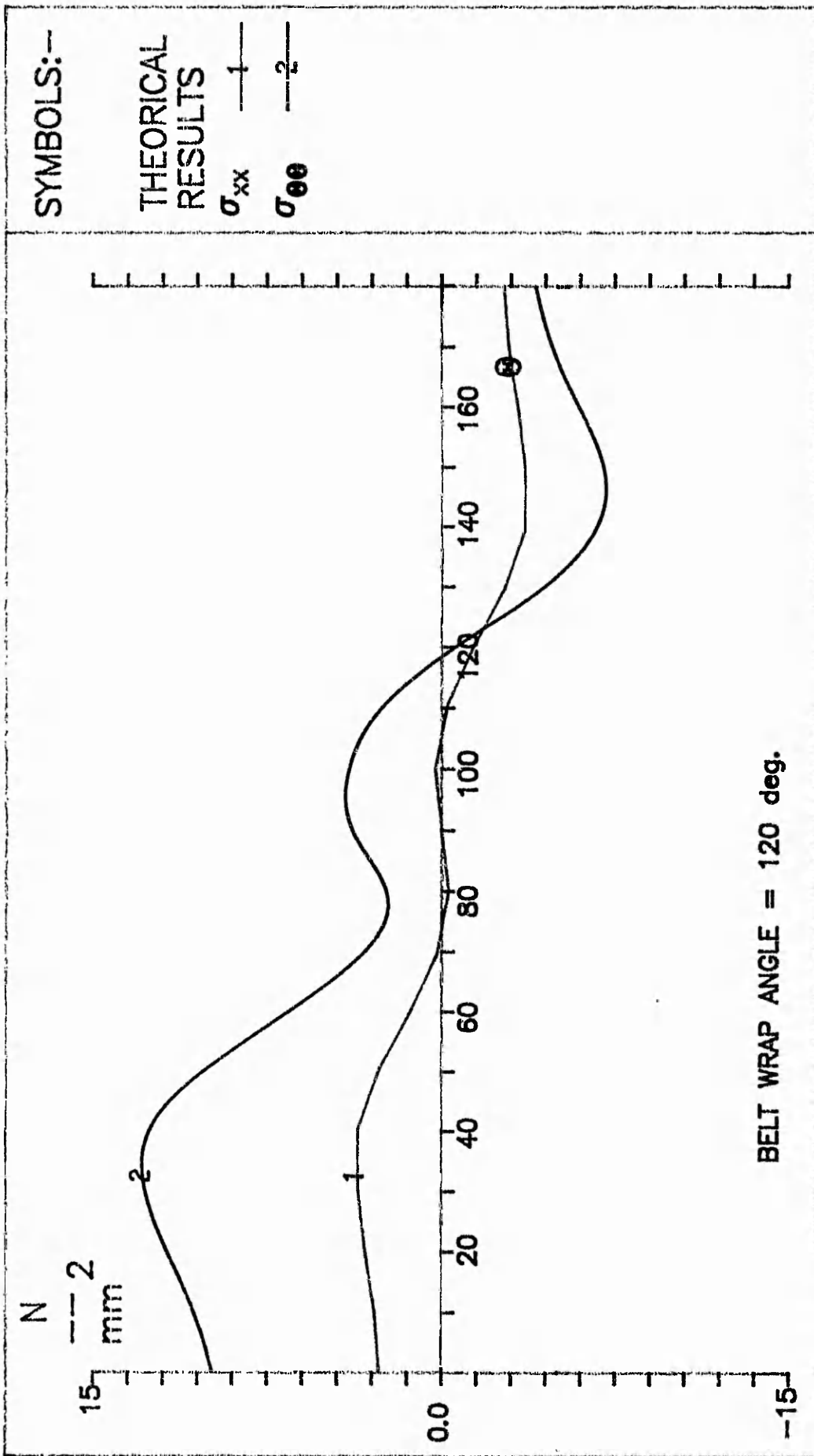


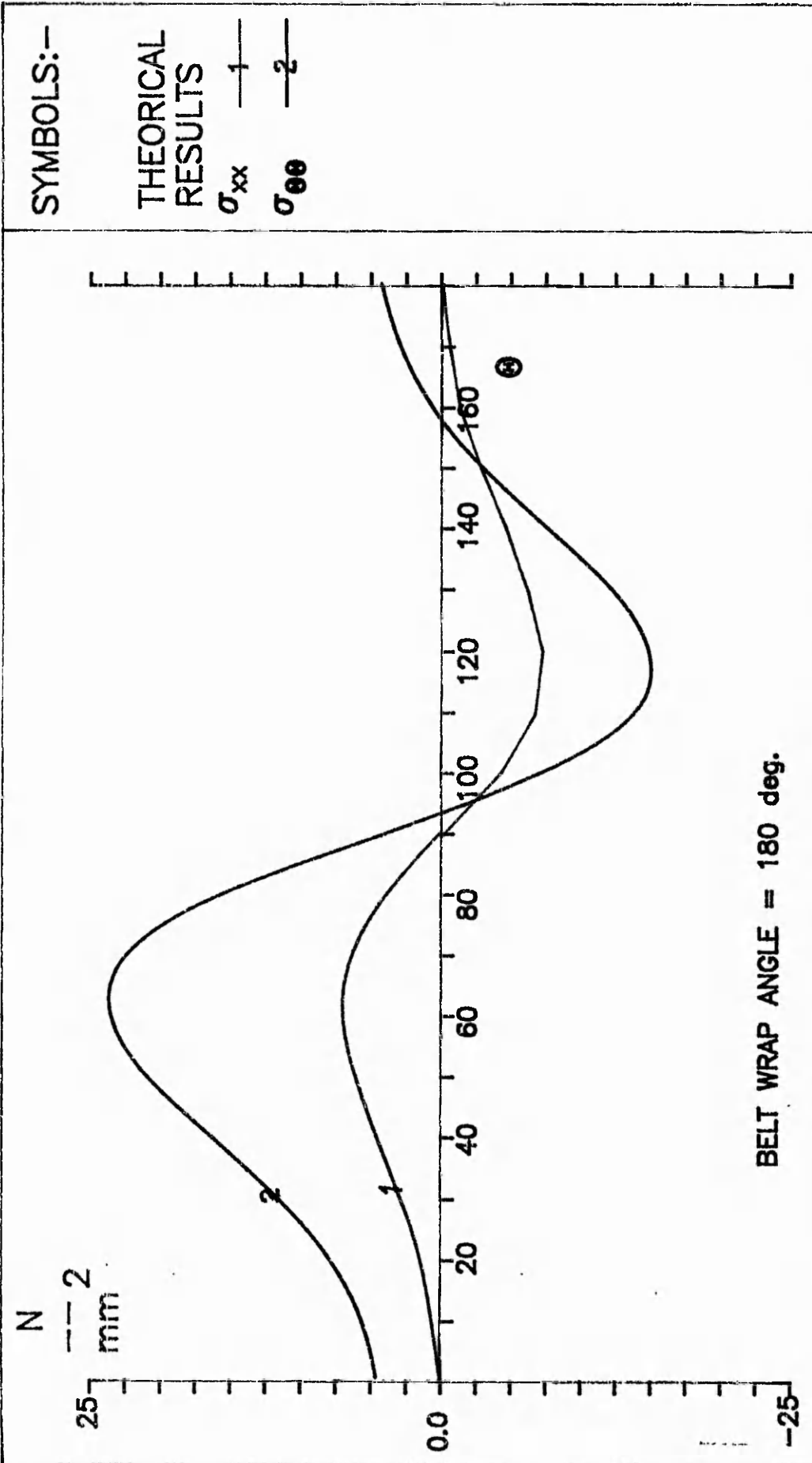
FIGURE : 4.6

TITLE : COORDINATE SYSTEM FOR SHELL ANALYSIS



TITLE: STRESS COMPARISONS FOR THE SHELL AT $x = W/2$

FIGURE: 4.7



TITLE: STRESS COMPARISONS FOR THE SHELL AT $x = w/2$

FIGURE: 4.8

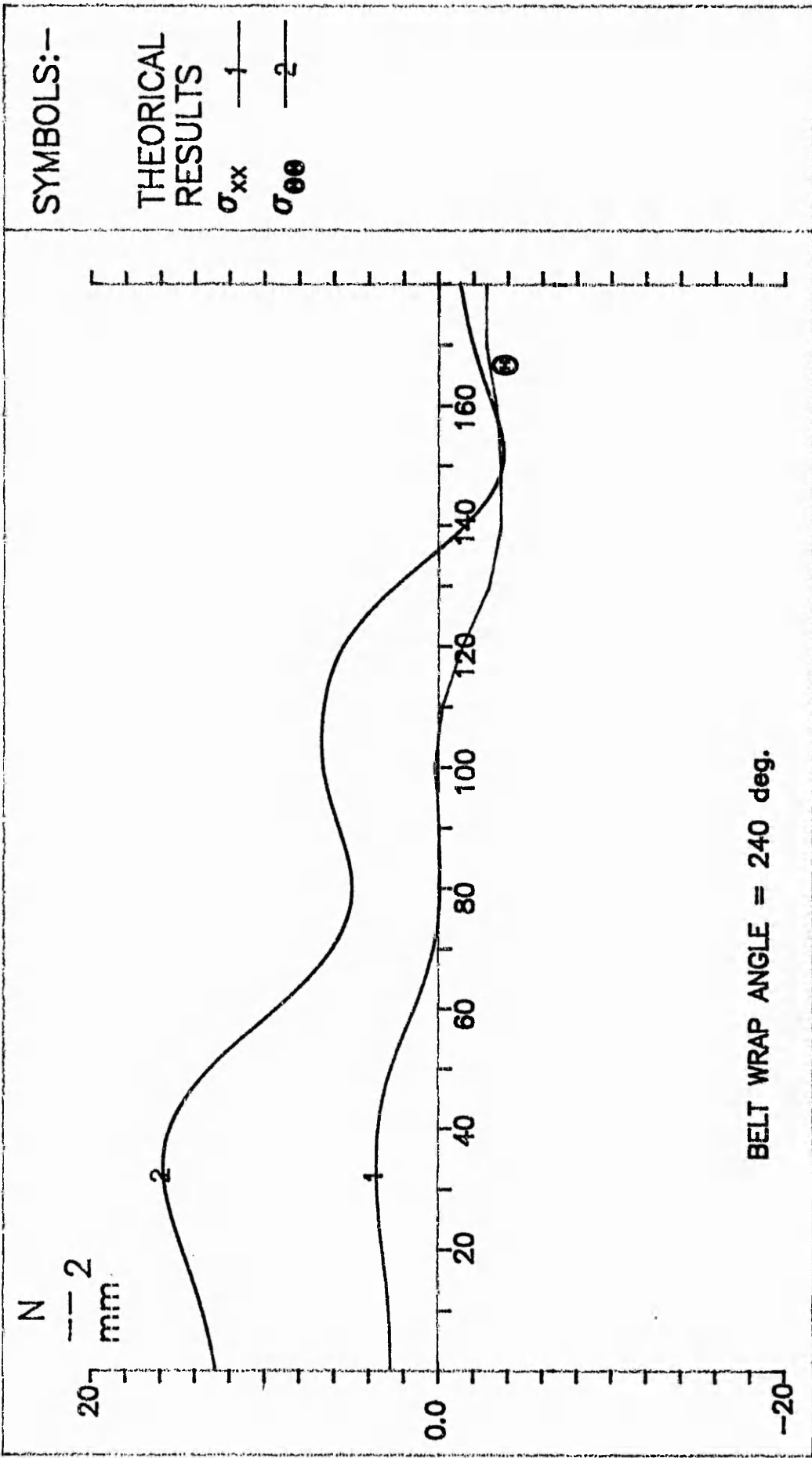
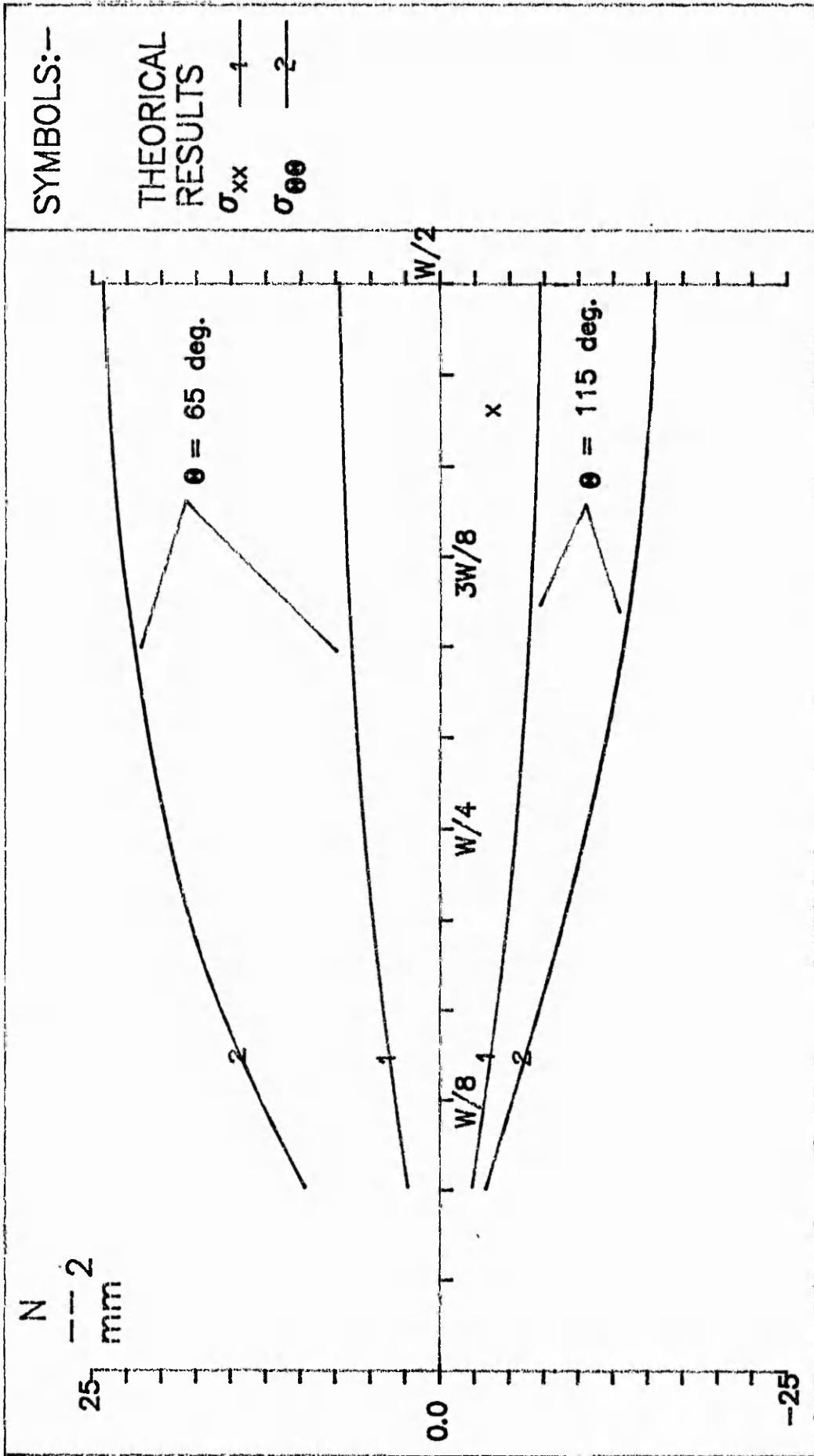


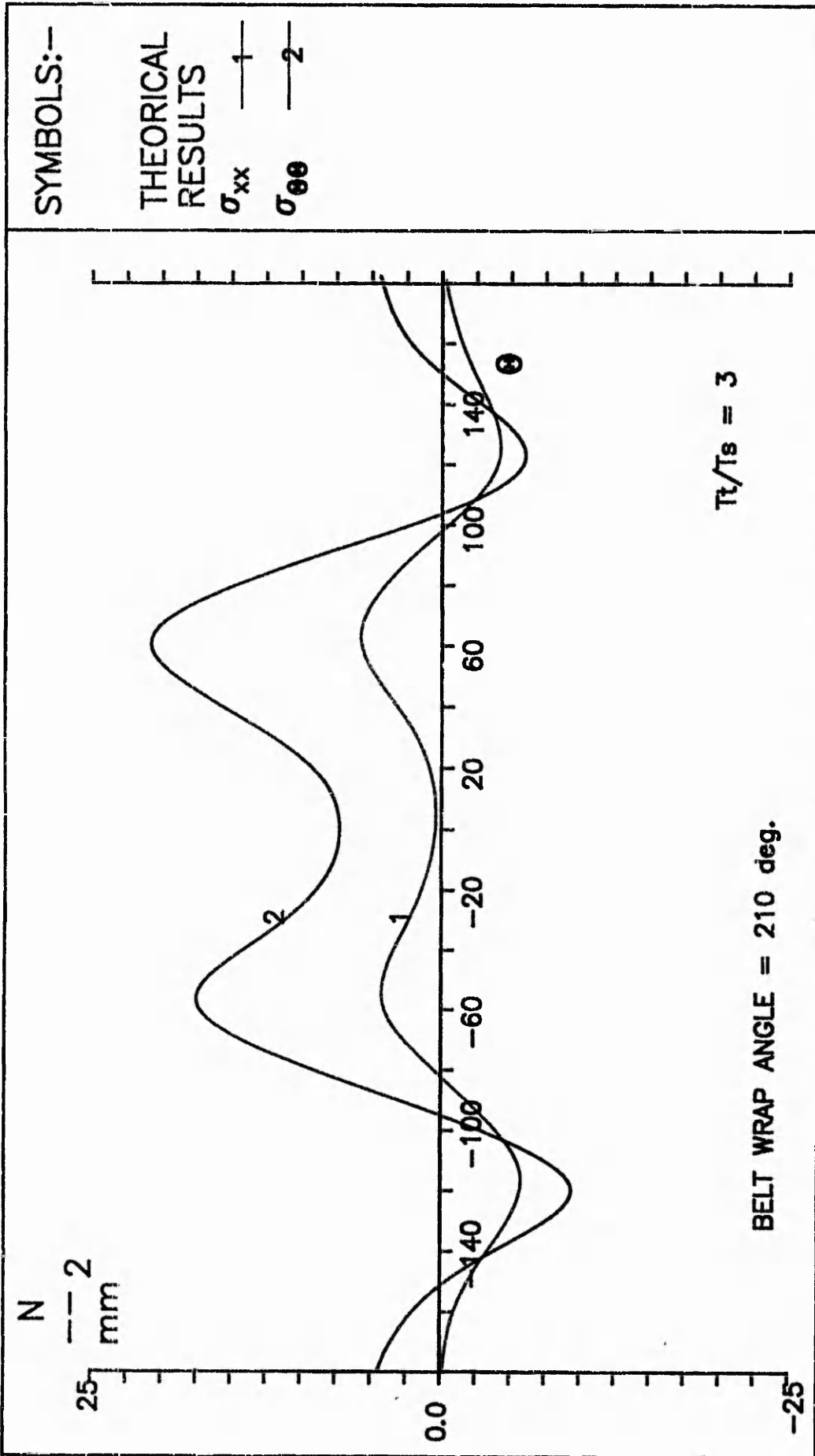
FIGURE: 4.9

TITLE: STRESS COMPARISONS FOR THE SHELL AT $x = W/2$



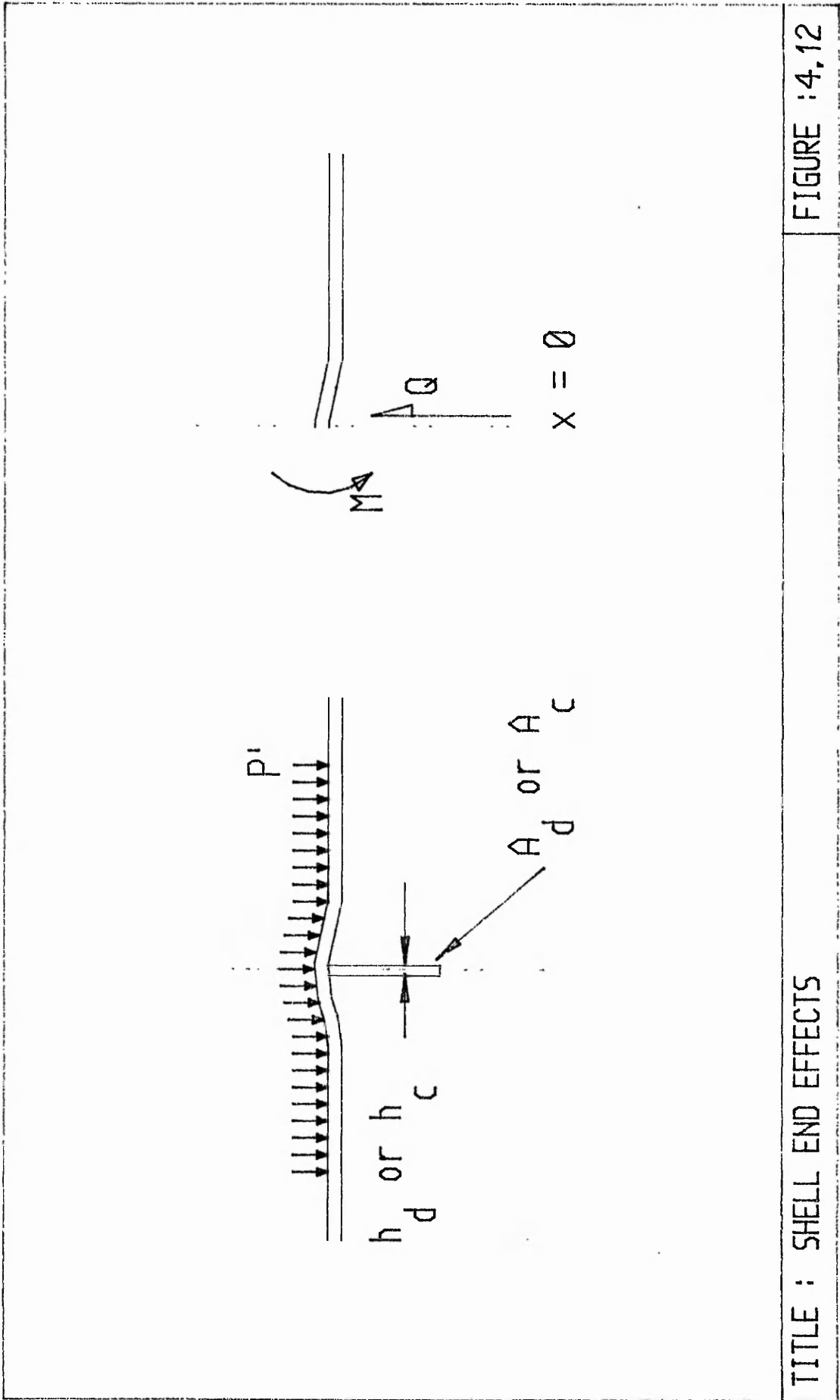
TITLE: STRESS COMPARISONS ALONG THE SHELL AT $\theta = 60, 120$ deg.

FIGURE: 4.10



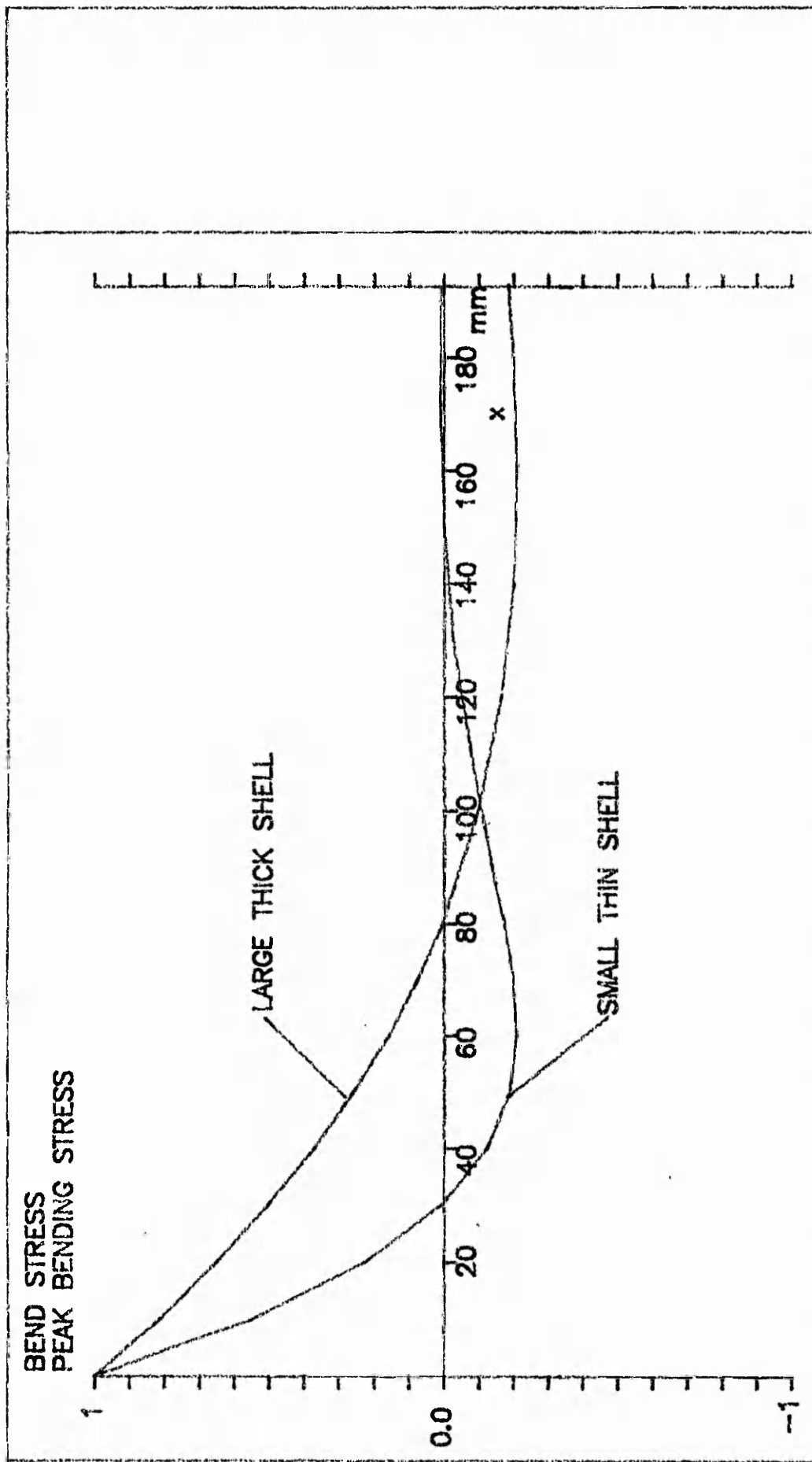
TITLE: STRESS COMPARISONS FOR THE SHELL AT $x = W/2$ (DRIVE PULLEY)

FIGURE: 4.11



TITLE : SHELL END EFFECTS

FIGURE : 4.12



TITLE: VARIATION OF STRESS ALONG THE SHELL DUE TO END EFFECTS FIGURE: 4.13

CHAPTER 5

STATIC BELT PULL SUBJECTED TO A PULLEY ASSEMBLY

Following the preliminary experiment with the model steel discs described in chapter 3, which studied in isolation the bending and in-plane stresses in a disc, a second test rig was constructed to perform a more comprehensive study of the stresses induced in a pulley when loaded by a conveyor belt. This experiment would impose a static loading of the belt on a pulley assembly, to establish the accuracy of the boundary conditions assumed in chapters 3 and 4. Figure 5.2 shows schematically some of the equipment details shown in figure 5.1.

5.1 PULLEY ASSEMBLY

A conveyor pulley with a diameter of 455mm, length of 600mm and end disc centres of 484mm was constructed, with two 70mm diameter shafts machined, one for a bearing centre of 750mm and the other for a bearing centre of 1200mm. Following the preliminary experiments described in chapter 3, which clearly demonstrated that for both constant and variable thickness discs, theoretical and experimental stresses compared very closely. This study therefore, was confined to determining the stress variations in a single conveyor pulley constructed with 'constant' 8mm thick discs and a 6mm thick shell. This was regarded as cost effective, as any variation in the predicted stress behaviour could be accounted for by the boundary conditions not being exactly modelled. All components selected were typical for the size of pulley used.

5.2 EXPERIMENTAL FRAME

The apparatus consisted of two heavy duty frames with a design rating of 12 tonnes, built into an 'Avery' tensile loading frame, which was hydraulically-operated with a maximum loading capacity of 20 tonnes for the pulley shaft arrangement shown. The Avery tensile loading frame was calibrated prior to carrying out these experiments. The first frame (figure 5.2 item A) was used to secure the conveyor belt (figure 5.2 item C) to exert a static belt pull (entry belt tension = exit belt tension) with a fixed 180 degree angle wrap. The second frame (figure 5.2 item B) supported the pulley, shaft and bearings and was designed to enable 750mm and 1200mm bearing centres to be utilised. The pulley was attached to the shaft by means of a single split taper compressive fastener, manufactured by the writer's company.

A 500mm man-made woven carcass conveyor belt (type 315/3) was used, with a minimum rating of 120kN/metre of width. In an attempt to ensure that the belt tension would be constant for the entire wrap angle, P.T.F.E. sheets were laid between the belt and the pulley shell. This would minimise the tangential forces which may be set up between the belt and steel shell due to uncontrolled tightening of the belt. In order to obtain the radial and tangential strains within a disc, five 120 ohm two-element, ninety-degree stacked rosette strain gauges (Welwyn Strain Measurement_CEA-06-125WT-120ohm) were glued equal distances between the centre boss and the shell rim. Five additional gauges of the same type were used

to measure the axial and tangential strains in the shell rim. The gauges attached to the shell were placed in a groove 0.5mm deep to prevent them from coming into contact with the belt, and were spaced at equal distances between one end disc centre line and the shell centre line. Since the loading was symmetrical, only one half of the pulley was strain gauged. All gauges were wired into a strain bridge in a quarter bridge configuration. To eliminate any strains produced during assembly all gauges were set to zero after the shaft had been secured into the pulley and fixed into the testing frame (figure 5.2 item B).

Strain gauges were not attached to the inside surfaces of the end disc and shell because of the limited size of the pulley used. Therefore, the variation of stress across the plate thickness was not measured.

By means of a D.T.I attached to the bearing mounting, the deflection at various angular positions on the disc at the inner boundary and the fastener adjacent to the shaft were measured. The difference between the two results is the actual displacement w . These displacements followed the same cosine variation as illustrated in section 3.6.3.

5.3 RESULTS

Figure 5.3, 5.4, 5.5, 5.6 and 5.7 illustrate the comparison between the experimental and theoretical stresses at various positions on the disc and shell respectively.

To illustrate the theoretical stresses summarised in table 3.4, it was necessary to determine the moment carried by the disc. Equation 2.8 describes the distribution of the bending

moment M_t between the drum assembly and shaft.

$$M_p = \frac{M_t}{\left[k_s \cdot \left(\frac{1}{k_d} + \frac{1}{k_{sh}} \right) + 1 \right]} \quad (5.1)$$

Referring to figure 2.2, the total bending moment just outside the hub is given by

$$(5.2)$$

$$M_t = \frac{P \cdot L}{2} \quad \text{where } L = \frac{X}{2} - \frac{W}{2} = \frac{1200}{2} - \frac{484}{2} = 358 \text{ mm}$$

$$M_t = \frac{25E6 \times 358}{2} = 4.39E6 \text{ Nmm}$$

k_s , k_{sh} ; k_d are determined using equations 2.10, 4.37, table 3.3 respectively. Therefore, the moment carried by the disc which has the same value as the moment carried by the drum assembly, may be calculated by

$$(5.3)$$

$$k_s = 1.024E12 \text{ Nmm}, \quad k_d = 4.62E11 \text{ Nmm}; \quad k_{sh} = 1.83E15 \text{ Nmm}$$

$$M_d = \frac{4.39E6}{\left[1.024E12 \times \left(\frac{1}{4.62E11} + \frac{1}{1.83E15} \right) + 1 \right]} = 1.36E6 \text{ Nmm}$$

Figure 5.3 illustrate the variation of stress with respect to ρ on the disc's surface at $\theta = 0$. The theoretical and experimental stresses compare favourably, with a difference of 6% to 12% between the two sets of results. The theoretical stresses were greater (ie. safer) than the experimental at all points measured on the disc's surface. Figure 5.3, curve 2 illustrates the theory (section 3.1.2, case 3) developed to

take into account any local rotation in the shell at the outer boundary of the disc. It can be seen that there were some small discrepancies in the levels of stress at the inner and outer boundaries of the disc. It may be concluded that the discrepancy at the outer boundary is due to the disc-to-shell joint not being as rigid as prescribed in the theory. The discrepancy at the inner boundary of the disc is special to the components used in the experimental pulley. The theory assumes that the components between the shaft and disc (ie. fastener and hub) are perfectly rigid. By measuring the actual displacements of both the compressive fastener and the attached hub at various radii this assumption was found to be inaccurate. A very small amount of rotation was present in the fastener and hub assembly, resulting in the differences between experimental and theoretical stresses at the inner boundary of the disc. The magnitude of the rotation was small and it was impossible to detect whether this was due to the compressive joint relaxing and allowing movement or the rigidities of fastener and hub were not as stiff as assumed.

Figure 5.4 and 5.5 illustrates the variation of stress with respect to θ on the disc's surface at various radii. It clearly confirms that the angular variation of stress closely follows a simple cosine function irrespective of radial position.

Therefore, it can be concluded from the results obtained above and the results obtained in chapter 3, that the theory developed in chapter 3 accurately describes the behaviour of an end disc within a pulley.

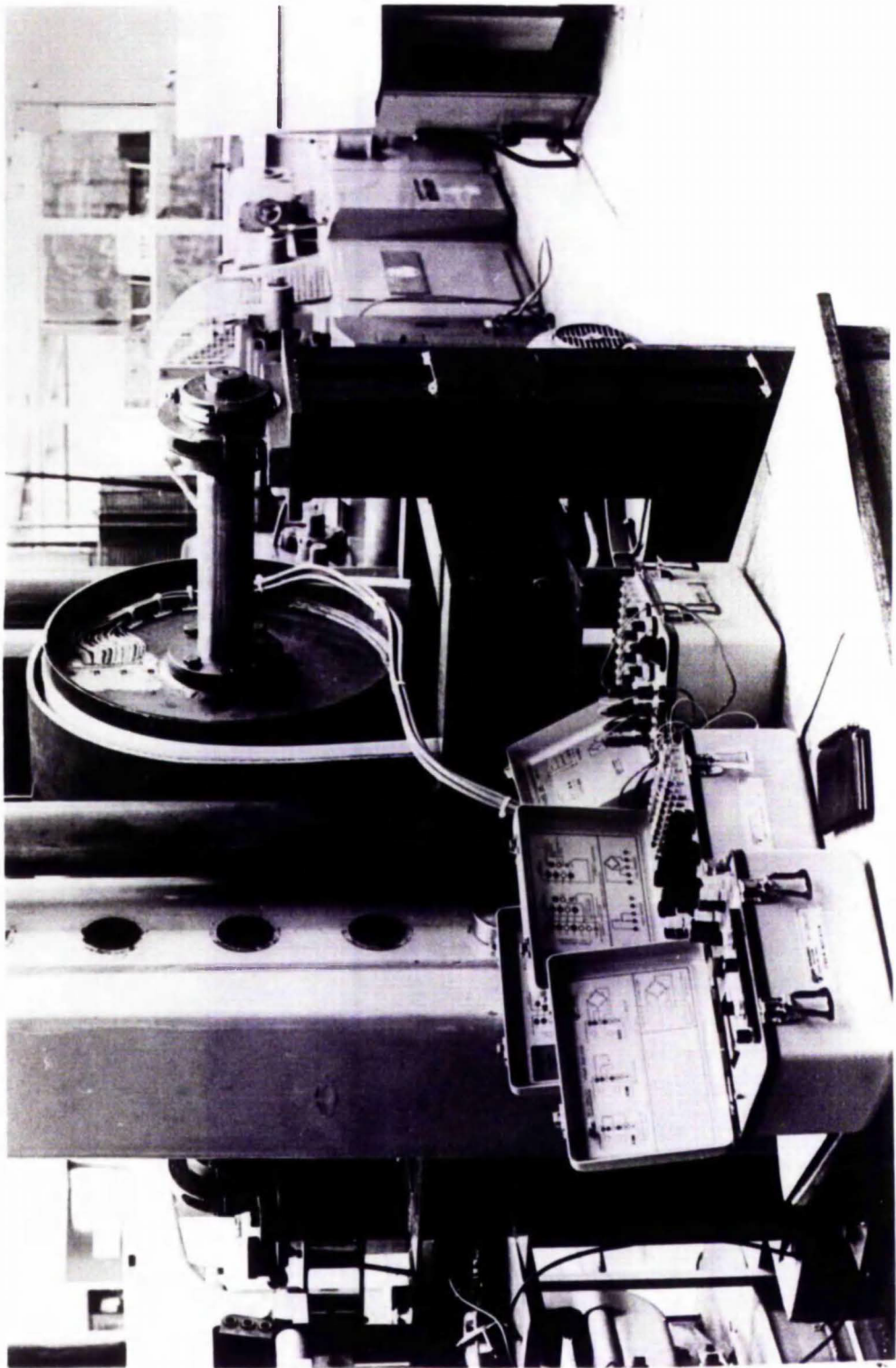
Figure 5.6 and 5.7 illustrates the variation of stress with respect to θ on the shell's surface midway between the end discs.

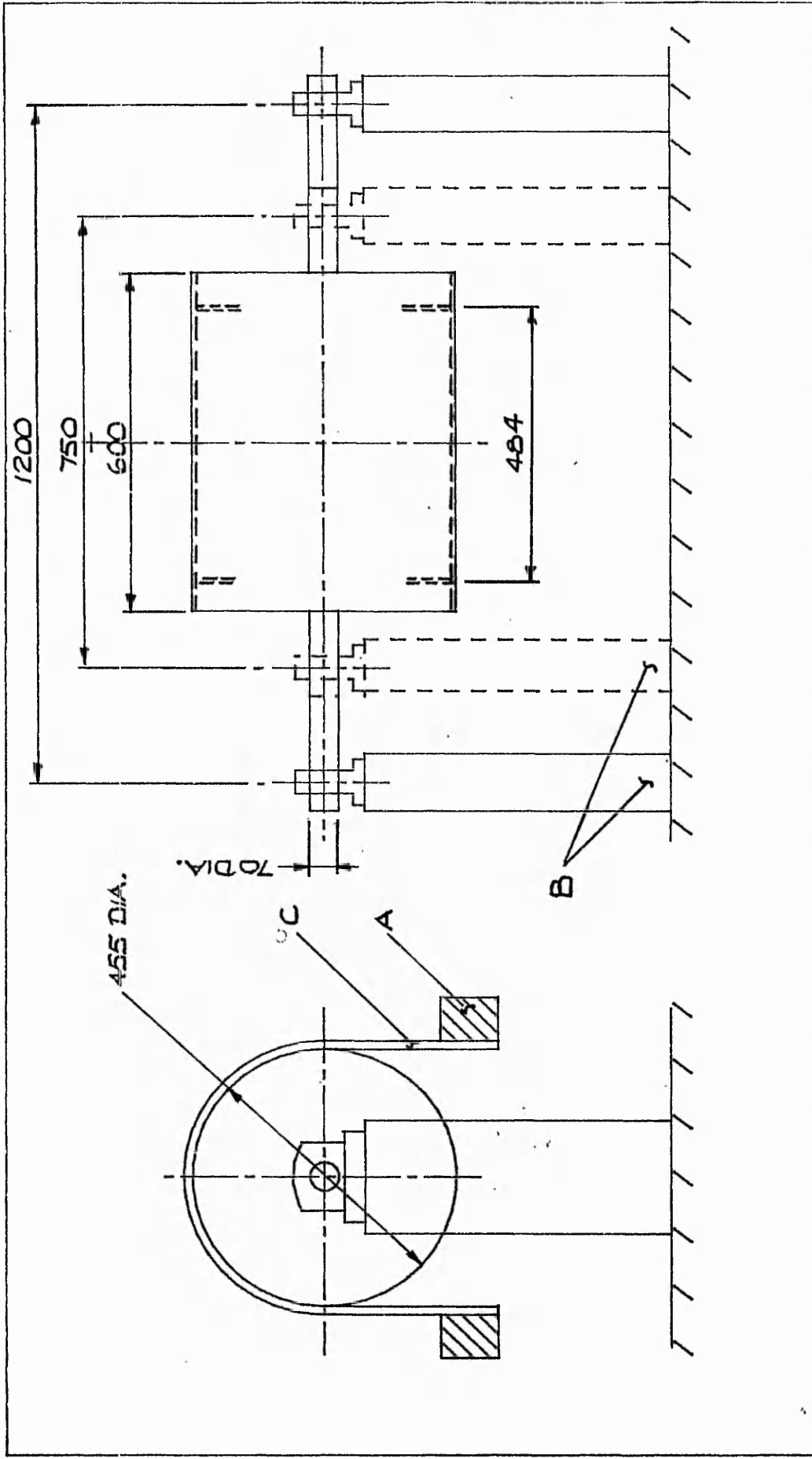
As described in section 5.2, it was necessary to machine out a 0.5mm deep channel on the outer surface of the shell for placement of the strain gauges. This was unavoidable, but immediately imposed an error in the comparison of the theoretical and experimental results, because it is impossible to account for the stress concentration caused by the channel.

The variation of stress of the theoretical curves display good comparison with the experimental results. The theoretical and experimental tangential stresses compared well, with a 10% difference between the two for the maximum stress at $\theta = 70\text{deg}$. However, the axial stresses do not compare as well, with the experimental results 16% higher than the maximum theoretical stress at $\theta = 70\text{deg}$. Making allowances for the machined channel described above, the theory gives a close approximation of the behaviour a shell within a pulley

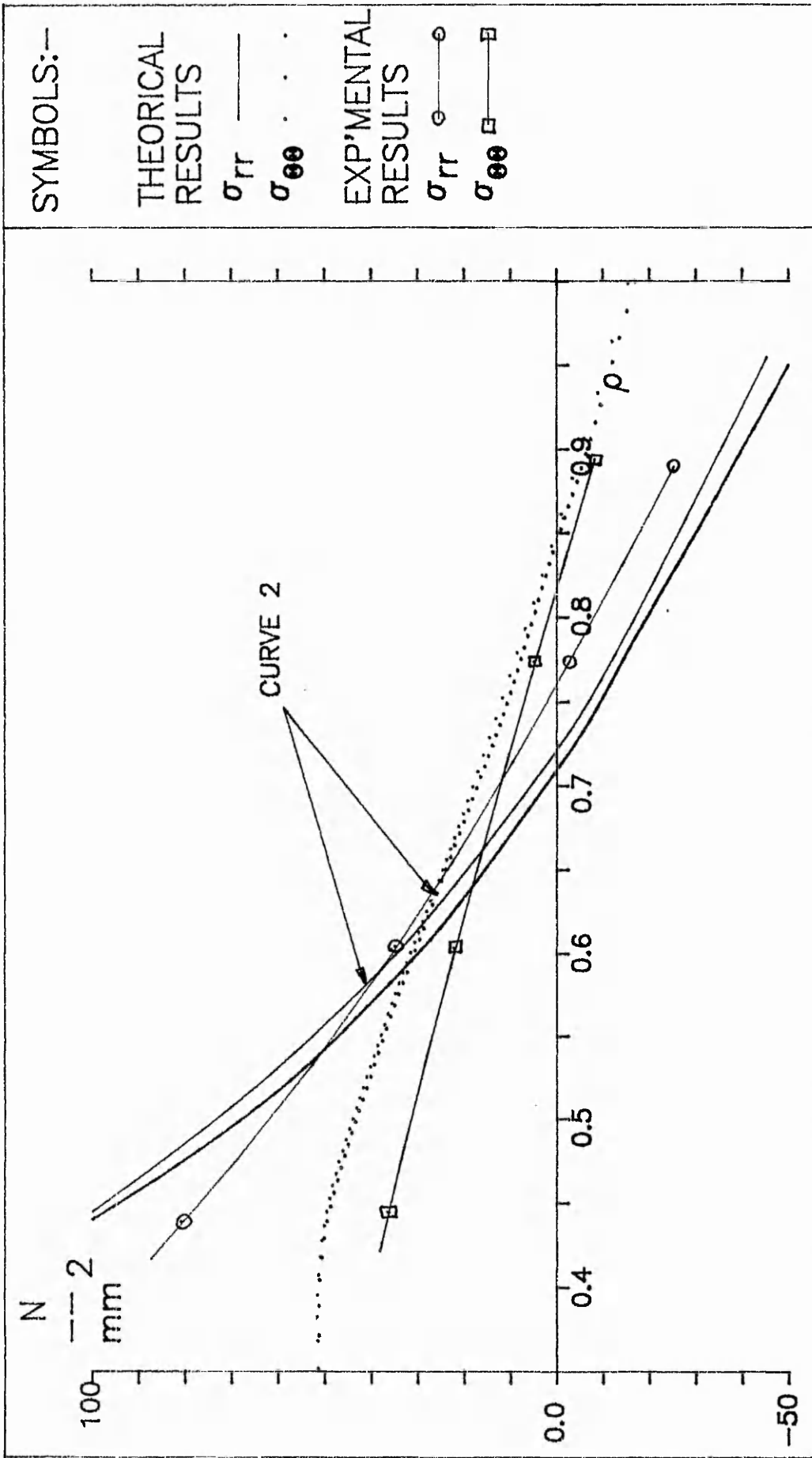
Figure 5.8 and 5.9 illustrates the variation of stress with respect to x on the shell's surface at $\theta = 60\text{ deg}$. The experimental curve shows clearly a peak stress close to $x = 0$, which is produced by end effects between the end disc and shell as described in chapter 4. Theoretical curve 1 gives a good account of the localised stress near $x = 0$ (also $x = W$ due to symmetry). Curve 1 is the summation of the stresses established for belt pressure only (curve 1A) and end effects as described in sections 4.1 and 4.2 respectively.

The results discussed in this section are only related to the bearing centres set at 1200mm. The results obtained when the bearing centres were set at 750mm followed very closely the comparisons with theory shown above and are thus not illustrated.



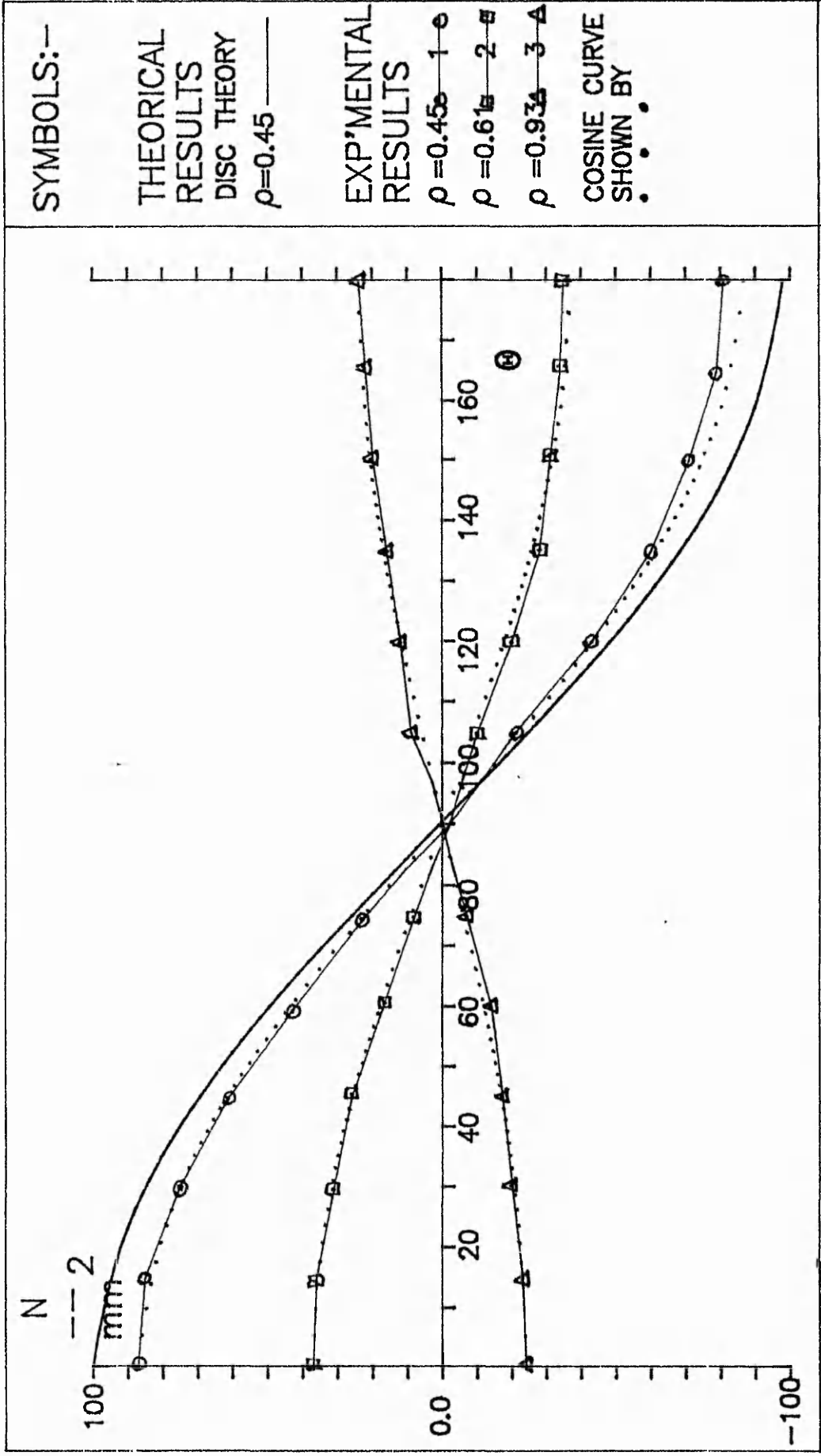


TITLE : SCHEMATIC DIAGRAM OF EXPERIMENT FRAME (STATIC BELT PULL) FIGURE : 5.2



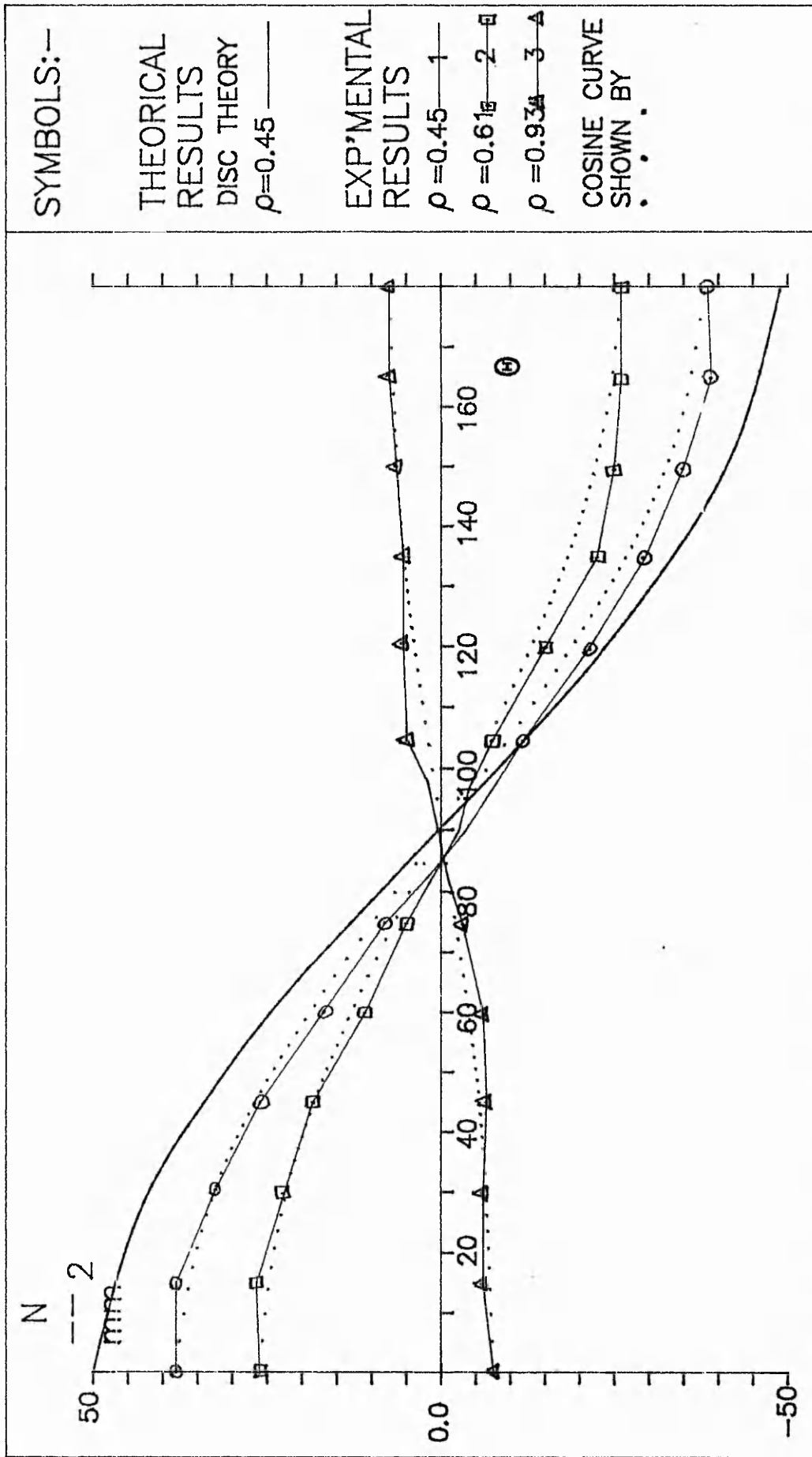
TITLE: STRESS COMPARISONS AT VARIOUS RADII ON THE DISC ($\beta = 0.35$)

FIGURE: 5.3

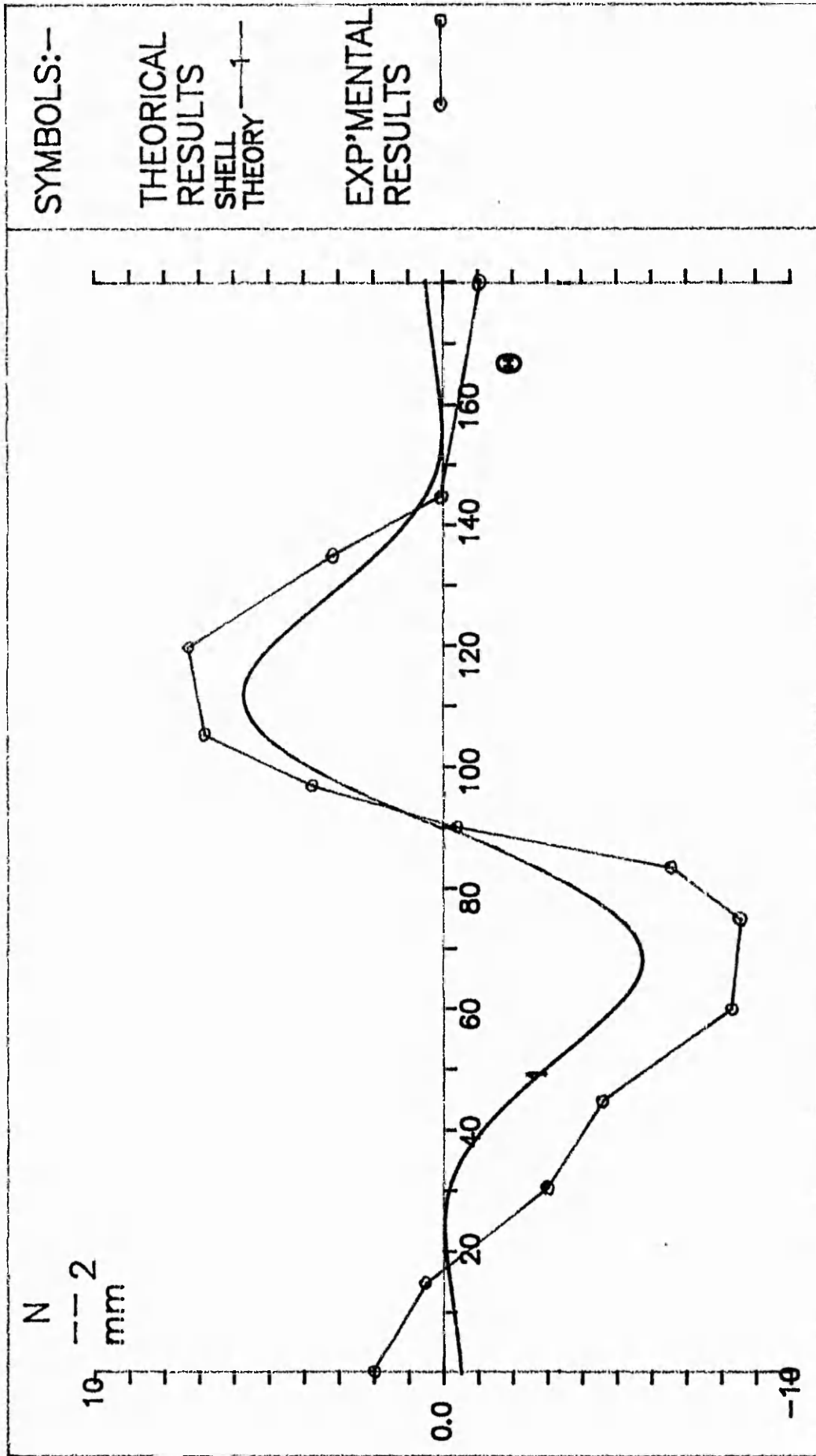


TITLE: VARIATION IN STRESS σ_{rr} AT VARIOUS POSITIONS ON THE DISC ($\beta = 0.35$)

FIGURE: 5.4



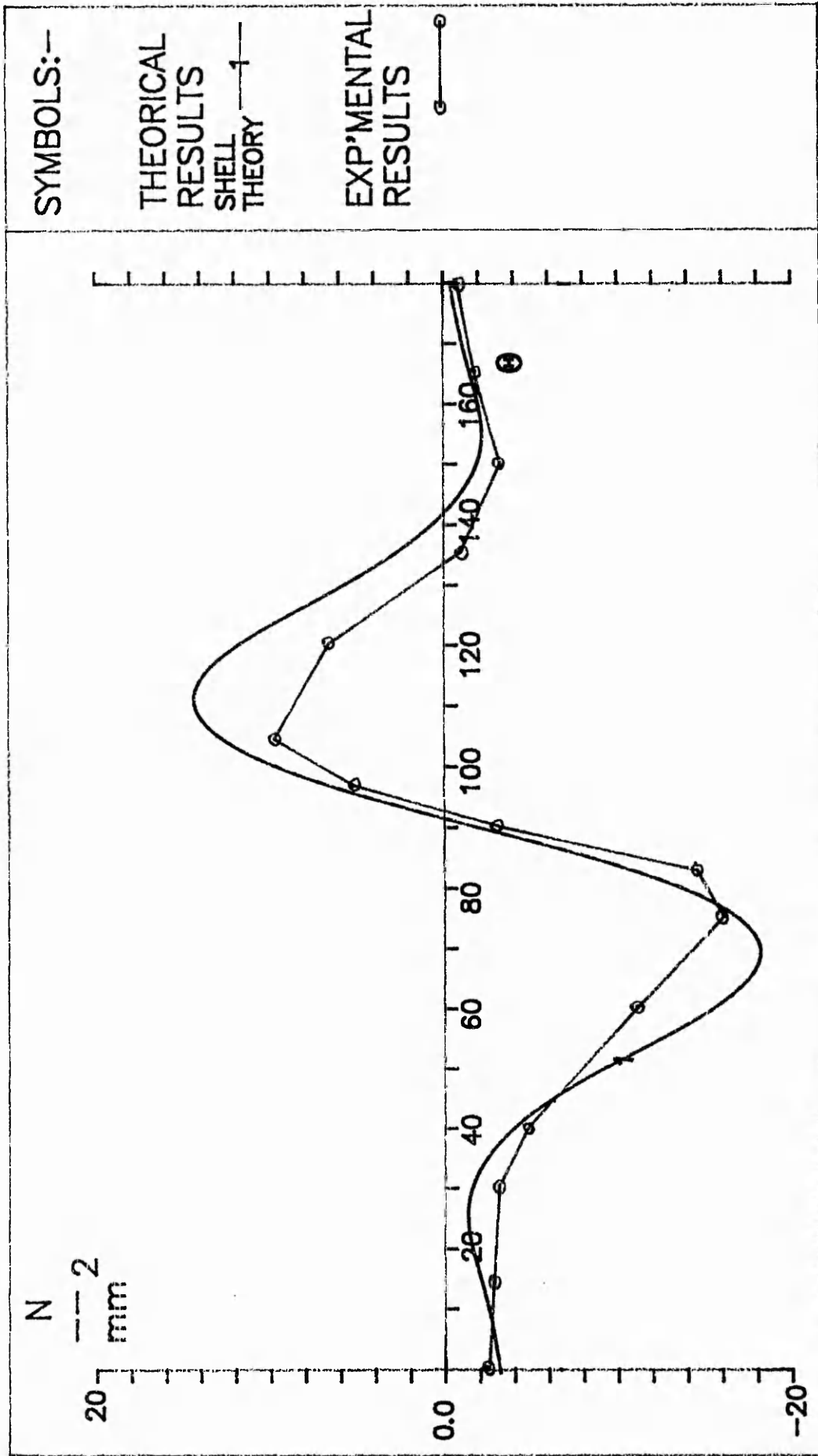
TITLE: VARIATION IN STRESS $\sigma_{\theta\theta}$ AT VARIOUS POSITIONS ON THE DISC ($\beta = 0.35$) FIGURE: 5.5



TITLE: STRESS σ_{xx} COMPARISONS FOR THE SHELL AT $x = w/2$

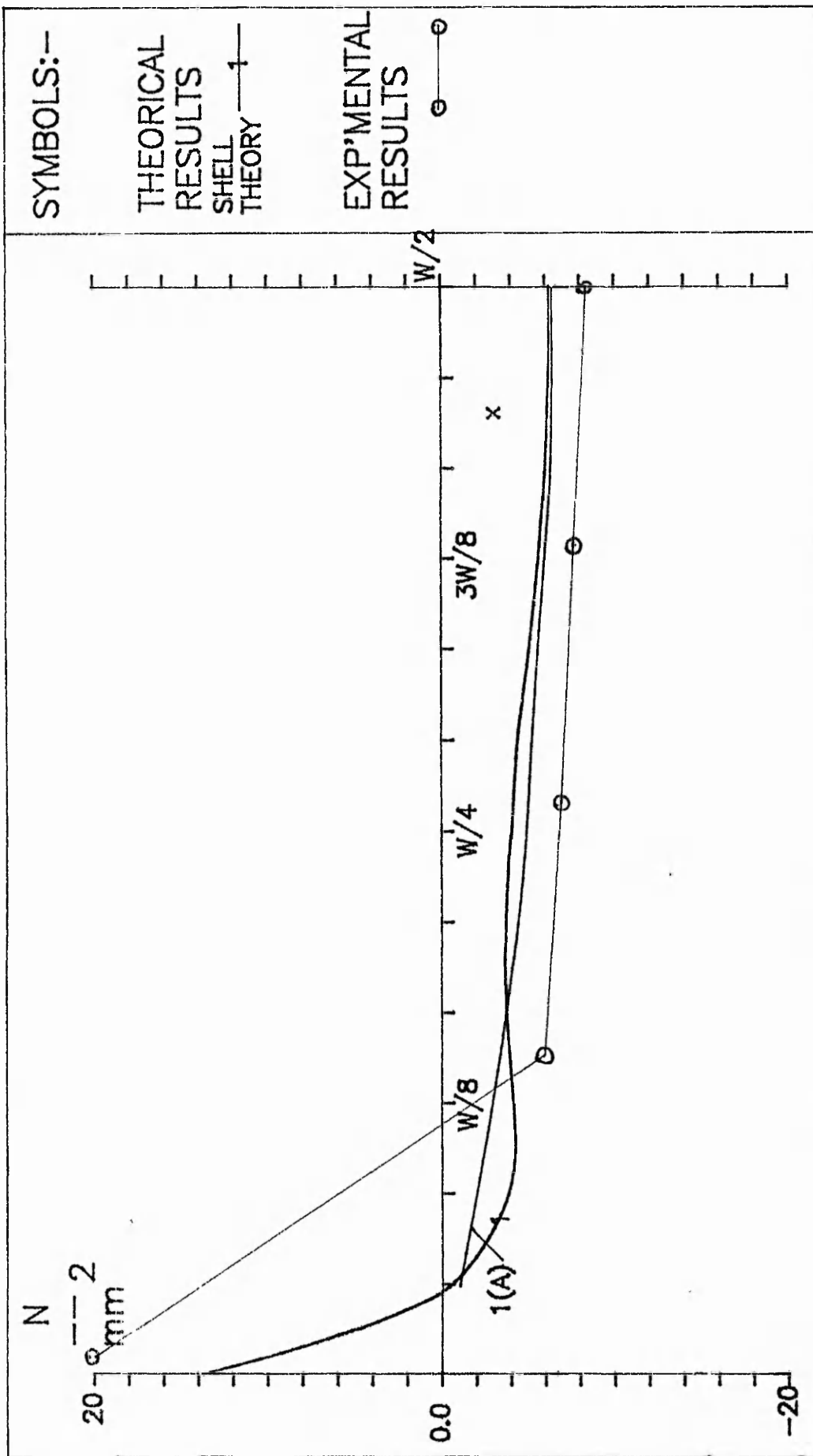
FIGURE: 5.6

EX-5071(2) (REV. 6/67)



TITLE: STRESS σ_{00} COMPARISONS FOR THE SHELL AT $x = W/2$

FIGURE: 5.7

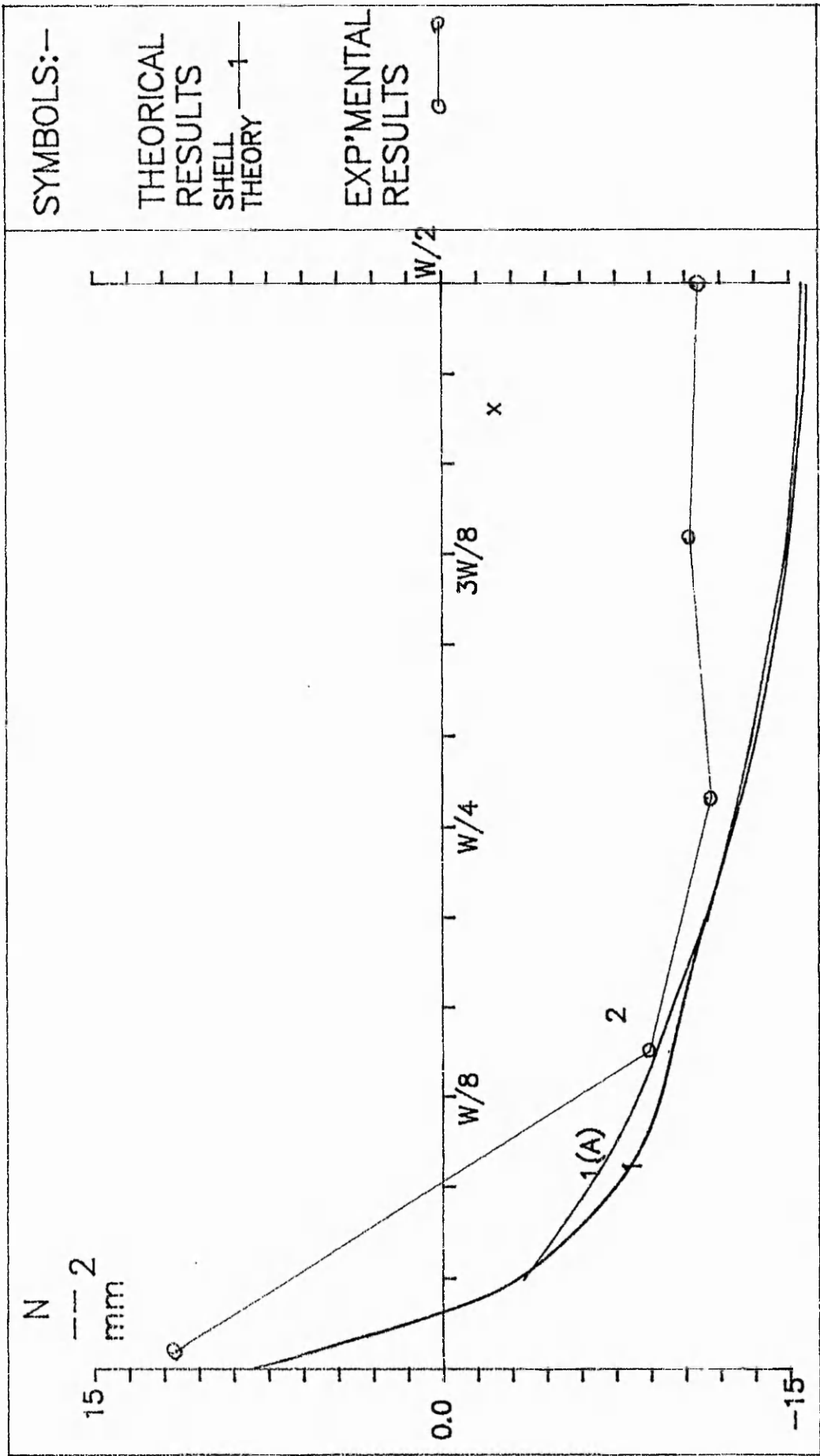


SYMBOLS:—
 THEORETICAL RESULTS SHELL THEORY ——— 1

EXP'IMENTAL RESULTS ○

FIGURE: 5.8

TITLE: STRESS σ_{xx} COMPARISONS FOR THE SHELL AT $\theta = 60$



TITLE: STRESS σ_{xx} COMPARISONS FOR THE SHELL AT $\theta = 60$

FIGURE: 5.9

CHAPTER 6

FINITE ELEMENT ANALYSIS (FEA) OF A PULLEY ASSEMBLY

For further comparison between the theory developed in chapters 3 and 4 and the experimental data obtained in chapter 5, a finite element study was carried out. To analyse a complete pulley assembly using finite elements is a very expensive and time consuming exercise. Therefore, the model was kept as simple as possible, without jeopardising too much the accuracy of the analysis.

6.1 METHOD OF ANALYSIS

The pulley assembly was modelled using the ANSYS Finite Element package installed onto a VAX 785 mainframe operating at Nottingham Polytechnic Computer Centre. The model was developed in ANSYS PREP7 preprocessing module. The analysis phase for the shaft, end disc and shell elements were carried out in ANSYS POST1 postprocessing module.

6.1.1 MESH GENERATION

The conveyor pulley described in section 5.1 was modelled using two types of elements:

- (i). Three dimensional elastic beam element (ANSYS STIF4) was used to represent the shaft. This element is a uniaxial type with tension, compression, torsion, and bending capabilities.
- (ii). Quadrilateral shell element (ANSYS STIF63) was used to represent the bush, hub, end disc and shell. This element has both bending and membrane capabilities.

The disc was constructed with nine radially spaced, 15 degree pitched elements. Similarly, the shell was constructed with nine axially spaced, 15 degree pitched elements.

Both types of elements have six degrees of freedom at each node: translations in the nodal x, y, and z directions and rotations about the nodal x, y, and z axes.

To simplify the model, full use of symmetry was made, enabling only one quarter of the pulley to be modelled (figure 6.1).

6.1.2 LOADING OF THE FINITE ELEMENT MODEL

A pulley belt wrap of 180 degrees on the experimental pulley was simulated by applying an uniformly distributed pressure load acting radially inwards over a arc of 90 degrees between $z = 34\text{mm}$ to $z = 280\text{mm}$. The pressure load of 0.11N/mm^2 produced a total load of 25kN acting on the actual pulley resulting in a reaction of 12.5kN at each of the bearings.

6.1.3 MODEL RESTRAINTS

The conveyor pulley used in the static loading experiment (section 5.1) was modelled, with bearing centres of 1200mm. The weld between the hub/disc and the disc/shell were ignored as their effects on the overall stress distribution would be negligible.

The finite element model was restrained at both symmetrical boundaries (figure 6.1):-

- (i). Symmetrical boundary midway between the bearings.
Restrained in the Z direction (axial direction) and rotation about the Y axis.
- (ii). Symmetrical boundary along the length of the pulley.
Restrained in the Y direction (hoop direction) and rotation about the Z axis.

To restrain the model in the X direction, a restraint was applied to the bottom surface of the shaft, at a position corresponding to the bearing in the actual experimental pulley.

6.2 RESULTS

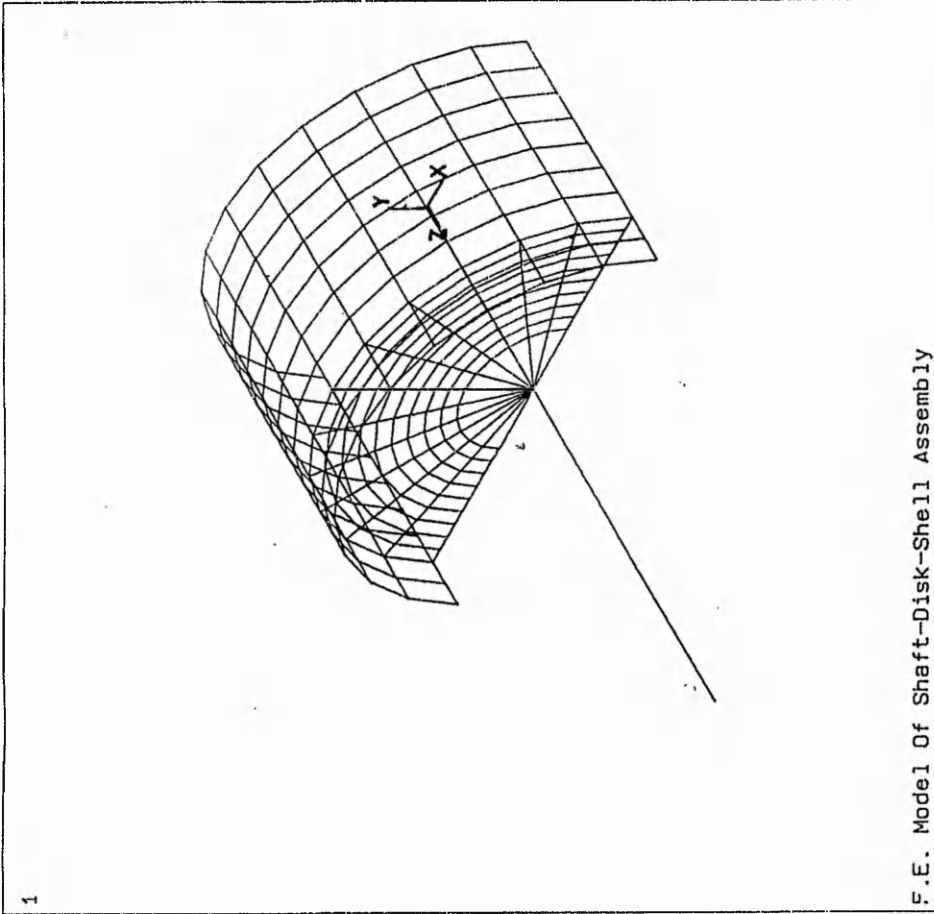
Figure 6.2 illustrates the comparisons between experimental and theoretical stresses at various radii on the disc at $\theta=30\text{deg}$. Clearly, the statements in section 5.3 concerning the discrepancies at the inner and outer boundaries are further reinforced. The FEA will account for a less than rigid fastener and hub components resulting in a closer comparison with the experimental results as shown. However, due to the simplicity of the FEA model, there was no account taken of the mating surfaces within the compressive fastener. This, in theory, was a reasonable assumption. However, this cannot be ruled out as a reason for the discrepancy found between the experimental and FEA results at the inner boundary. Figures 6.3 and 6.4 illustrate the variation of stress with respect to θ on the discs surface at the position of the first strain gauge, (nearest to the hub), on the test pulley ($\rho = 0.45$). All the experimental results confirm that the deflections and stresses induced in a disc, closely follow a

cosine function. The dotted line on curve 2 illustrates that the FEA stress results local to the axis of symmetry ($\theta = 0, 180_{\text{degree}}$) do not. It was discovered that the rotation restraint at the axis of symmetry (section 6.1.3) was not acting perpendicular to the axis. The actual mis-alignment will correspond to the angular pitch of the first two elements. ANSYS states that a 15 degree increment for the elements is satisfactory for the type of model considered. Thus, increasing the number of elements close to the axis of symmetry will minimise the influence of these effects. However, as the effects were localised, no improvements were made due to the expense of further re-runs. It is clear that FEA results further endorse previous claims in section 5.3, that the theory developed in chapter 3 accurately prescribes the behaviour of an end disc within a pulley.

Figures 6.5 and 6.6 illustrate comparisons between experimental and theoretical stresses on the shell's surface at various angular positions midway between the end discs. The FEA curves demonstrate that the theoretical results give a good account of the stresses in the shell. Figures 6.7 and 6.8 illustrate comparisons between experimental and theoretical stresses along the shell. The theoretical and FEA curves give a good account of the localised stresses produced by end effects between the shell and end disc as discussed in section 4.2. In conclusion, the FEA results confirm that the behaviour of the shell is well prescribed by the theory developed in chapter 4.

ANSYS 4.4
UNIV VERSION
JUN 19 1990
13: 16: 09
PLOT NO. 1
PREP7 ELEMENTS
TYPE NUM

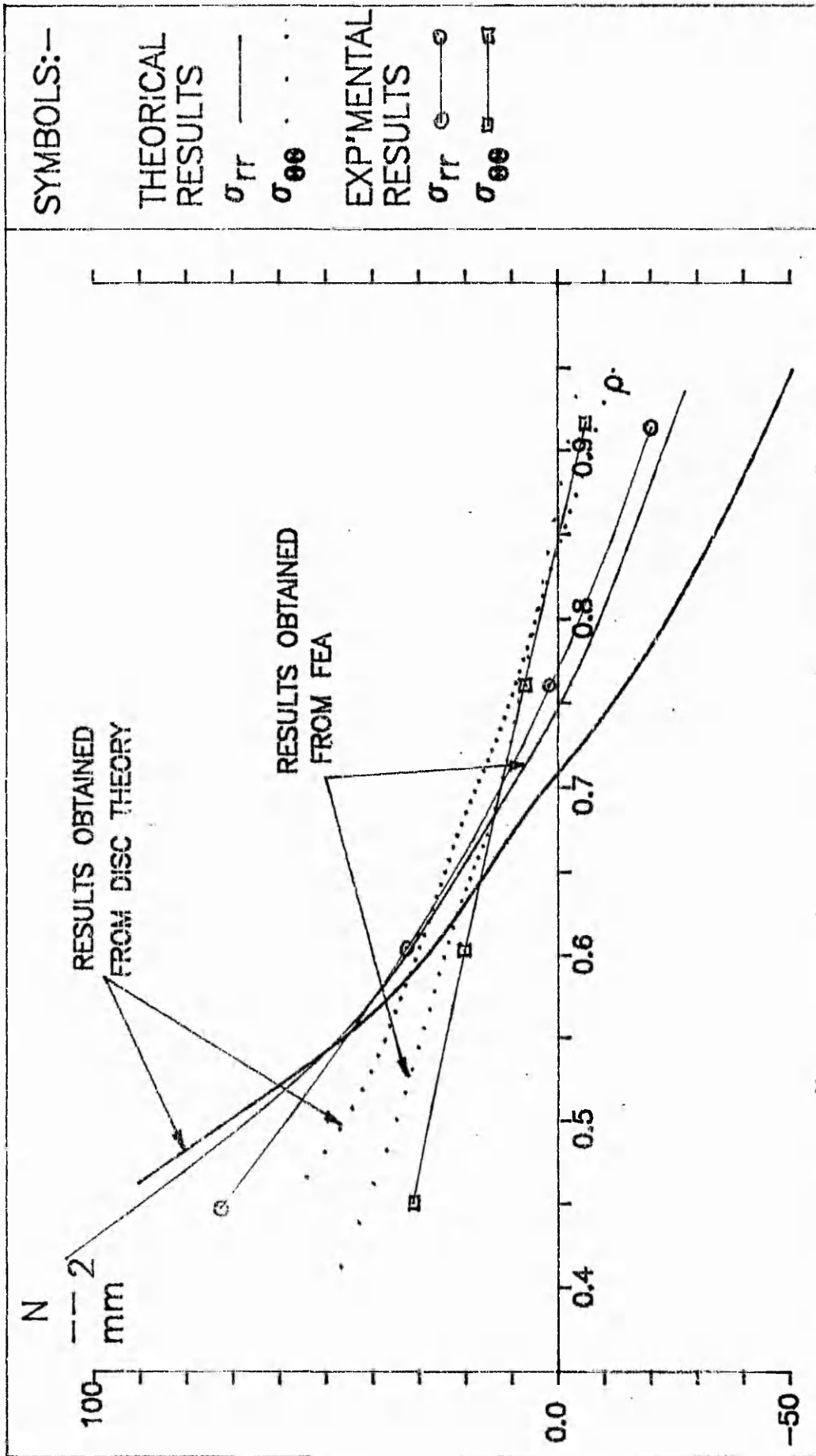
XV =1
YV =1
ZV =1
DIST=433.632
YF =113.75
ZF =330



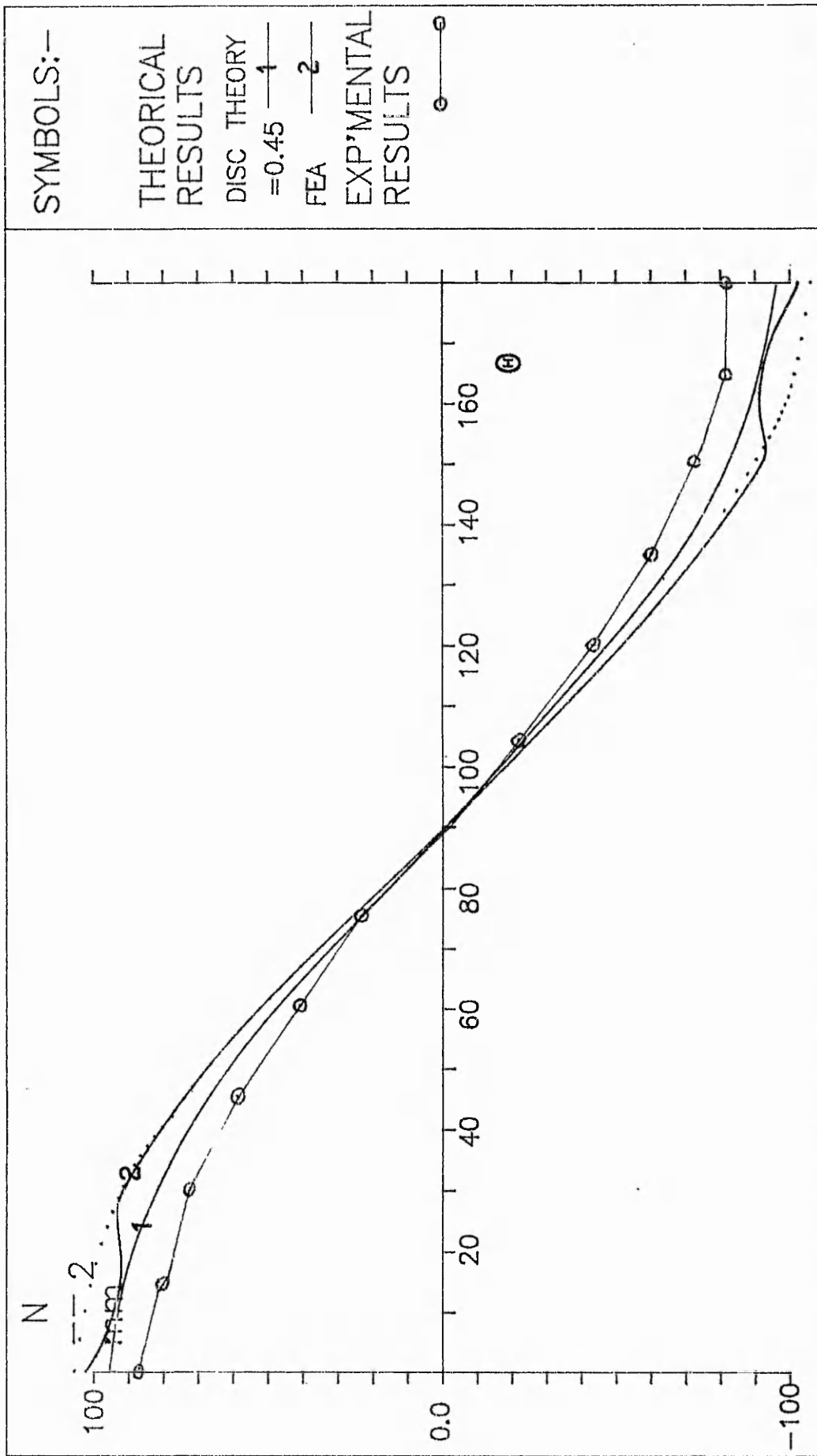
F.E. Model Of Shaft-Disk-Shell Assembly

TITLE: FINITE ELEMENT MODEL

FIGURE: 6.1

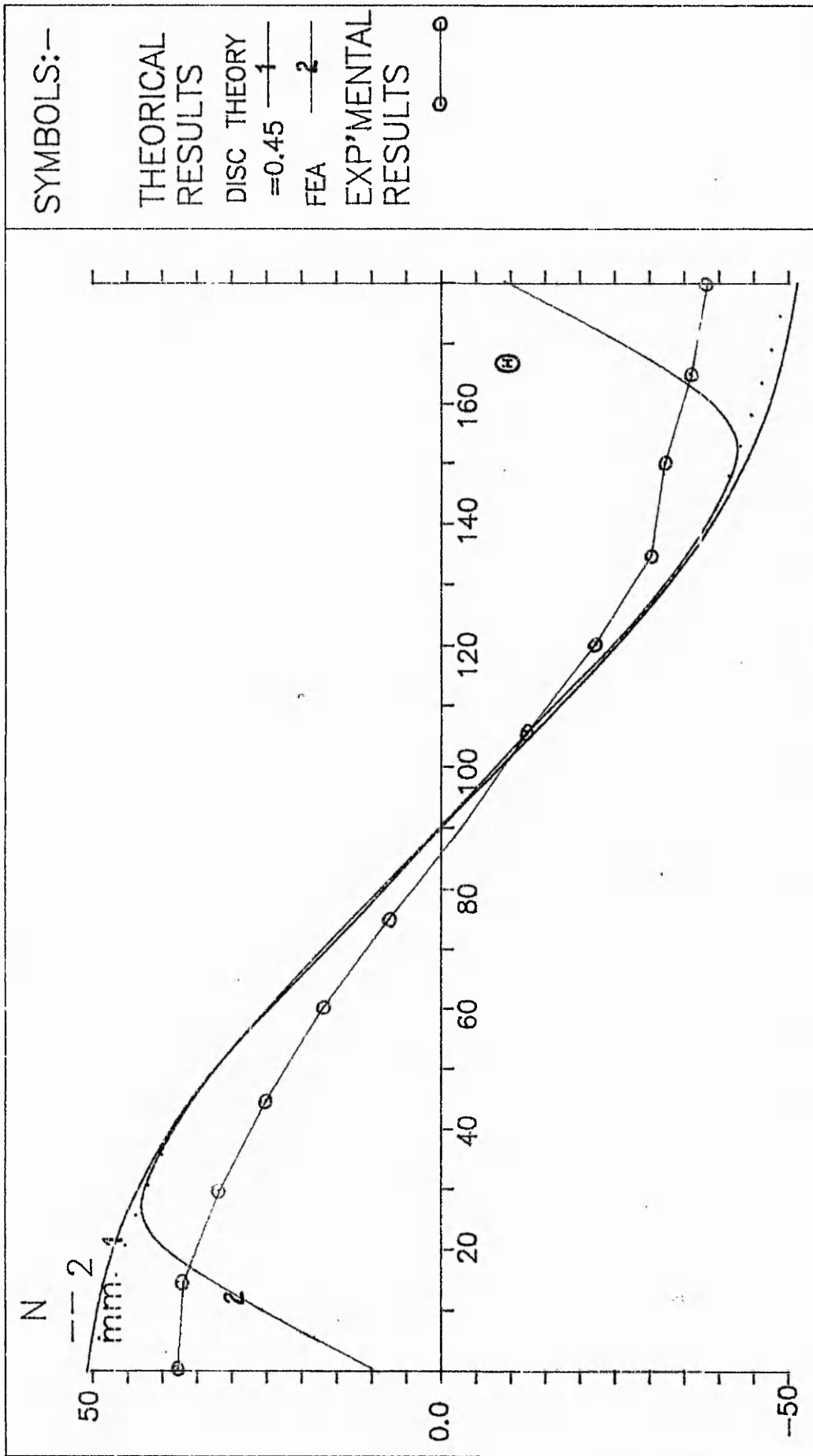


TITLE: STRESS COMPARISONS AT VARIOUS RADII ON THE DISC AT $\theta=30$ ($\beta = 0.35$) FIGURE: 6.2

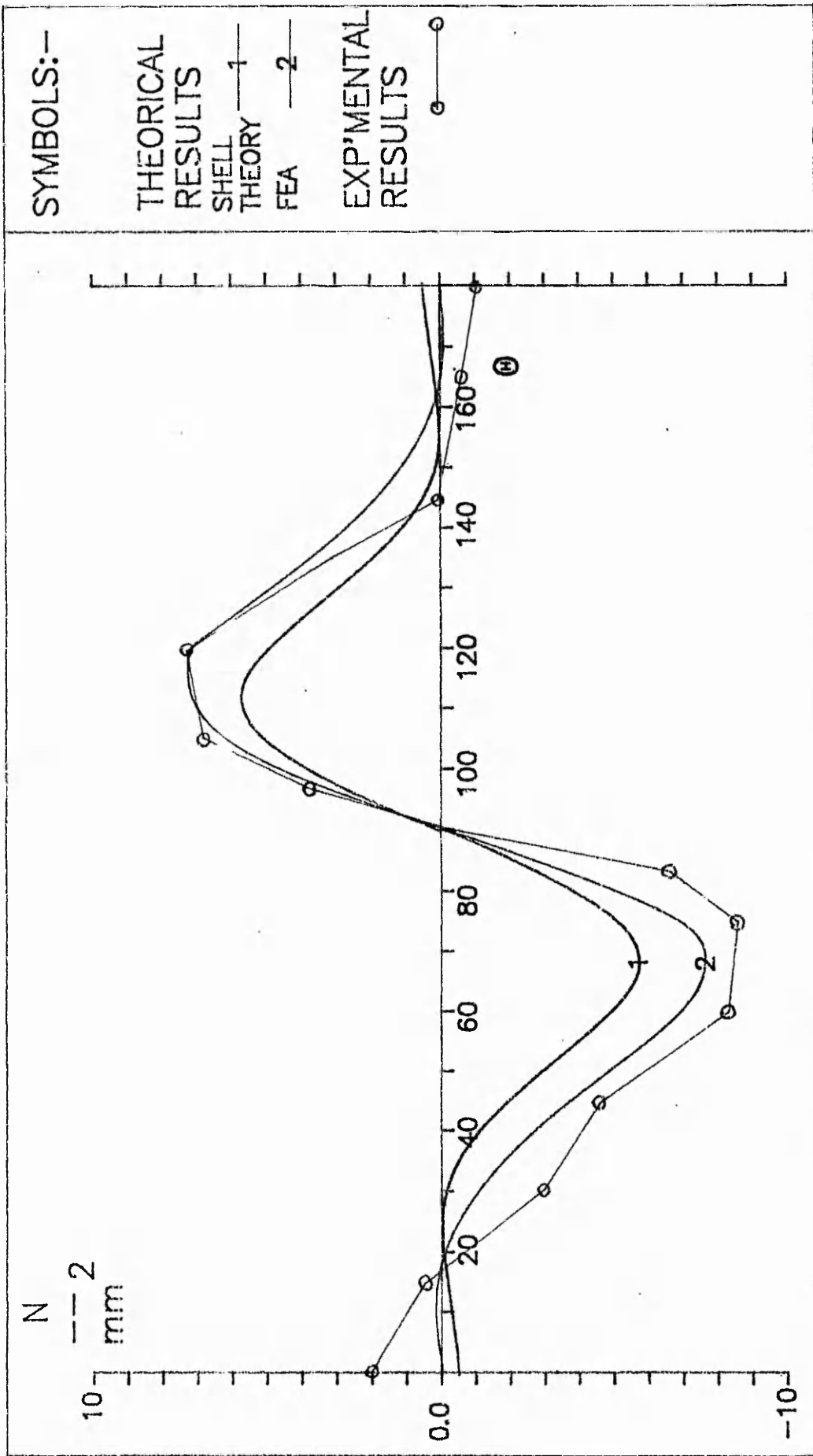


SYMBOLS:—
 THEORETICAL RESULTS
 DISC THEORY =0.45 — 1 —
 FEA — 2 —
 EXP'MENTAL RESULTS

TITLE: VARIATION IN STRESS σ_r AT VARIOUS POSITIONS ON THE DISC ($\beta = 0.35$) FIGURE: 6.3

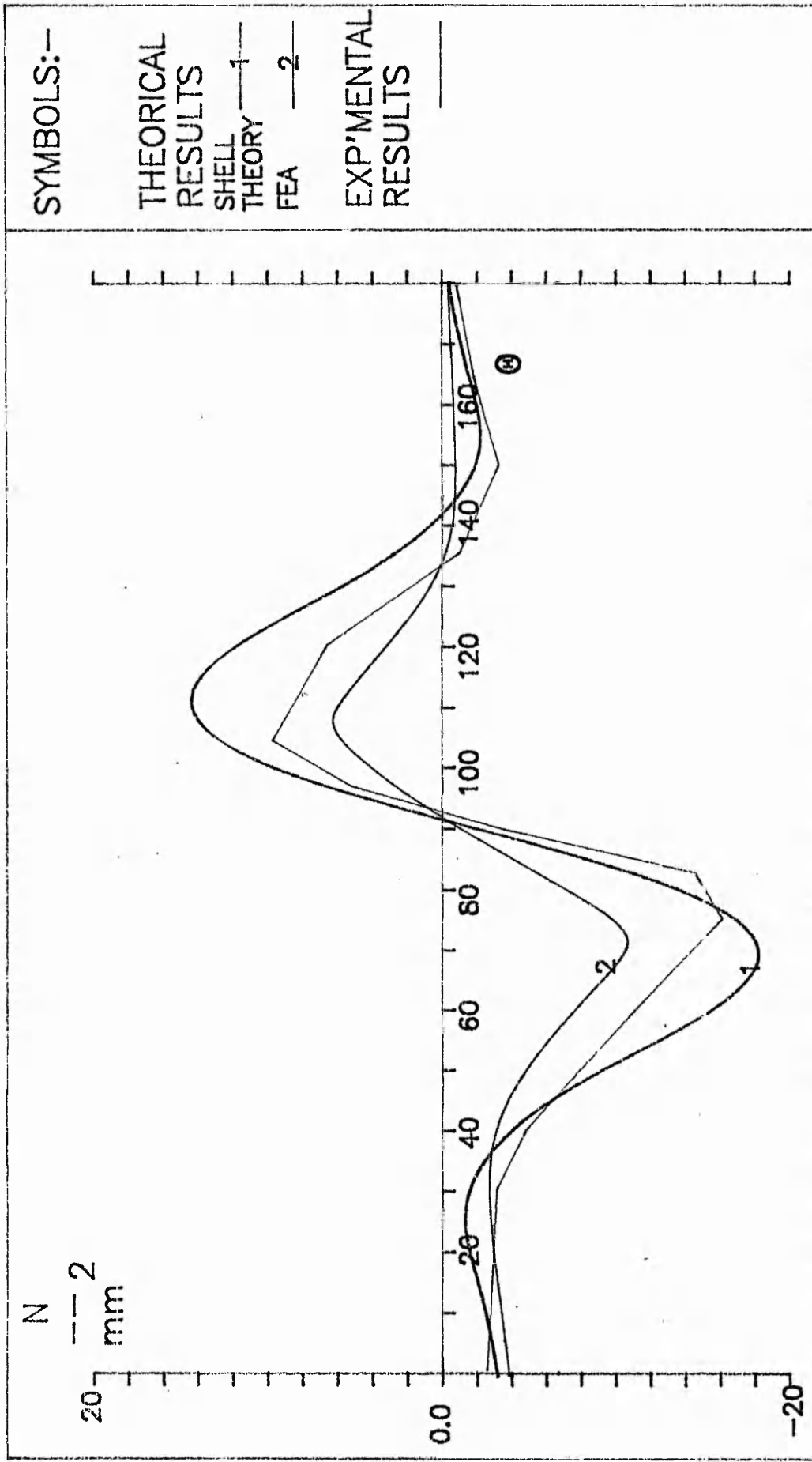


TITLE: VARIATION IN STRESS $\sigma_{\theta\theta}$ AT VARIOUS POSITIONS ON THE DISC ($\beta = 0.35$) FIGURE:6.4



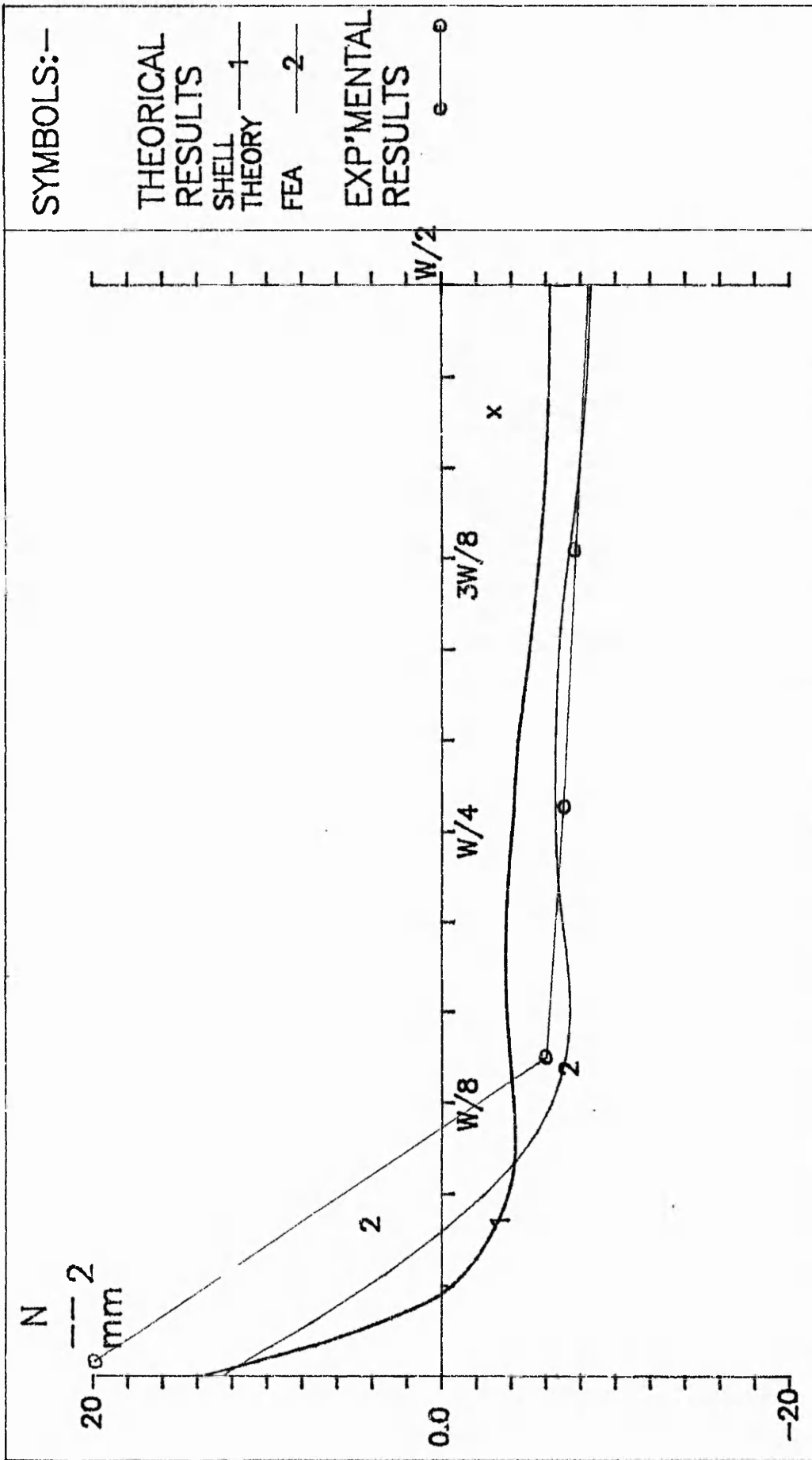
TITLE: STRESS σ_{xx} COMPARISONS FOR THE SHELL AT $x = w/2$

FIGURE: 6.5



TITLE: STRESS σ_{xx} COMPARISONS FOR THE SHELL AT $x = w/2$

FIGURE: 6.6



SYMBOLS:—
 THEORETICAL RESULTS
 SHELL THEORY — 1 —
 FEA — 2 —
 EXP'IMENTAL RESULTS
 e — o

TITLE: STRESS σ_{xx} COMPARISONS FOR THE SHELL AT $\theta = 60$

FIGURE: 6.7

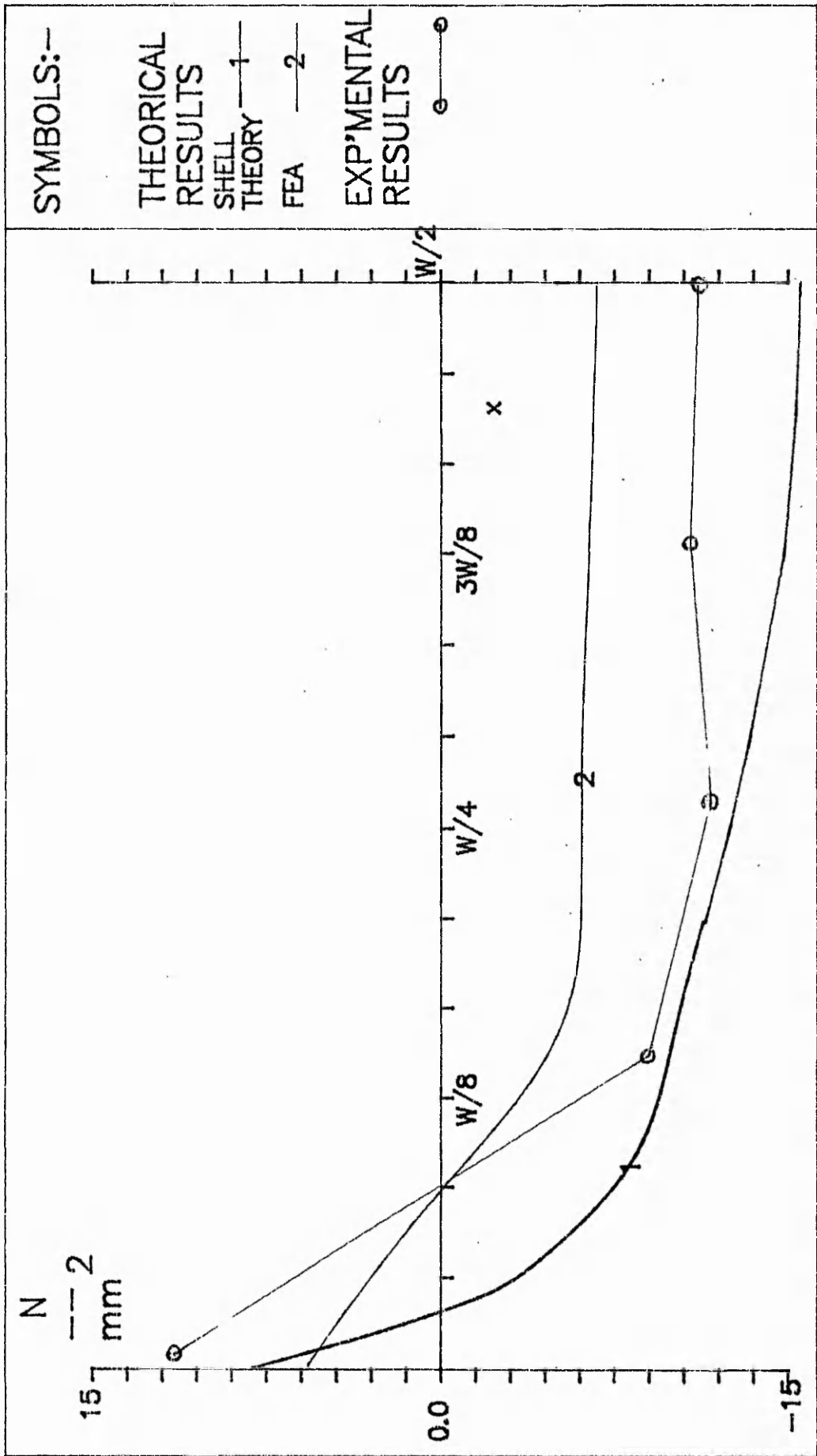


FIGURE: 6.8

TITLE: STRESS σ_{xx} COMPARISONS FOR THE SHELL AT $\theta = 60$

DESIGN PROCEDURE

The methods used to design the components of a conveyor pulley were presented in chapters 2, 3 and 4 with experimental verification carried out in chapter 3 and 5. It is clear from section 3.1 that changes to one component of the pulley assembly have a strong influence on the rest of the construction. A generalised design procedure is presented below to highlight the importance of accurate design of each of these components.

7.1 DESIGN PROCEDURE

To carry out Finite Element Analysis on a day-to-day basis as required by the pulley designer, it needs the software to be quick and available. Although, micro/mini computers are becoming a more practical machine for carrying out Finite Element Analysis of a pulley, it still requires a high level of technical skill and capital investment. The time to input construction data, processing the model and post-processing assessment does not allow Finite Element Analysis to be regarded as sufficiently quick in obtaining a final solution. A typical pulley engineer in the UK may be required to design upto 20 or 30 different pulley constructions per day because of the various industry standards (ie. British Coal, C.E.G.B, British Steel, etc, etc). Thus, Finite Element Analysis can only be considered for refinement of standard pulley constructions. Therefore, it would be useful if the engineer had available to him, a simple and quick method of designing

conveyor pulleys with the same order of accuracy as Finite Element Analysis. The flowchart (figure 7.1) illustrates the calculations and decision making process required to design any conveyor pulley using the methods described in this work. The flowchart is the basis of a computer program installed onto a micro computer in the writer's company, which allows a full design analysis of any pulley shape within seconds. There are three phases to designing a conveyor pulley are shown in figure 7.1 .

7.1.1 Receive load and dimensional data from client

This is an important stage which dictates the level of specification the pulley engineer will work to. All external loads are established by the belt conveyor designer, who also determines the overall dimensions of the pulley which will fit into his structure or drive frame. He will also specify the operational requirements of his conveyor system, with the pulley being one of several components which must comply.

7.1.2 Design evaluation

The design procedure (figure 7.1) for conveyor pulleys is best served by a worked example which has been manufactured by the writer's company. There is over 100 of this predictual pulley operating in a number of large underground conveyors (750kW drive) initially installed during 1987 at British Coal's largest mine. A careful design study was carried out as these conveyors operate for 20 hours per day which equates to over 25 million revolutions per year. The design of the belt conveyor was determined by specialist conveyor system

designers. The basic design data provided by the system designer is summarised in table 7.1.

The first consideration in the design stage is to determine the minimum shaft diameter based on the calculations listed in table 2.1. These are elementary equations with only fastener selection requiring comment. The fastener size cannot be selected independently of the pulley stiffness, because its size is a function of the bending moment required to be transferred through it. However, the initial choice may be made by estimating this moment as a proportion (say 90%) of the total bending moment.

Unless the pulley designer is using his own fastener or a shrink fit method of attaching the pulley to the shaft, he can use standard design data published by specialist fastener manufacturers. This data provides him with information to select a fastener to absorb the driving torque and the bending moment transferred through the device.

Recommendations on hub diameter are also provided. Thick cylinder theory and the analysis of frictional fasteners are the basis of their designs, which have been further verified by extensive field trials. The merit of their designs are not a subject of this work.

The hub should be sufficiently large to absorb the stresses induced by the shaft connection, whether shrink-mounting, press-mounting or compression type fastener mounting.

The shaft, end disc and shell stiffnesses are now calculated to establish the bending moment carried by the drum assembly. The initial choice of fastener is now checked and modified, requiring the moment M_p to be re-calculated. Similarly, the

end disc shape is initially estimated and then modified to suit the re-calculated moment M_p . Obviously, as the shaft, end disc and shell stiffnesses change, a constant reassessment of moment M_p is required. This iterative process can only be effectively carried out on a computer. The results obtained for this example using the above procedure are summarised in Table 7.1.

Figure 7.2 illustrates the final design along with the stresses for the shell using the theory developed in chapter 4. The weld connection between the cast end disc and shell as shown in figure 7.2 is positioned to correspond with zero shell stress. It is important that the position of this joint does not coincide with the high local stresses induced by the shell end effects as described in chapter 4 (figure 4.12 illustrates) and further experimentally verified in chapters 5 and 6 (figures 6.7 and 6.8 illustrate).

Chapter 3 discussed the problems in designing a profiled disc in practice. The size of the blending curve, the minimum cross-section and the complexity of the profile are all constraints of manufacture which require careful consideration when designing the end disc. Each affects the disc stiffness and therefore moment M_p . Thus, standardisation can only be carried out on a pulley assembly basis. Figure 7.3 illustrates the disc profile created for this example and the problem areas which needed to be overcome to enable the shape to be manufactured. Figure 7.3 also illustrates the maximum stress profiles (i.e. $\theta = 0$ deg.) for the profile shown using the theory developed in chapter 3.

The above illustrates the simplicity of the design procedure

developed. Once it has been computerised it will allow the engineer to design any pulley shape within minutes which, as previously stated is impossible with Finite Element Analysis. Furthermore, he is allowed to do this without sacrificing accuracy.

7.1.3 Examination of the proposed design

This phase is rather simple and often requires no design work, but is essential in assessing that the design can be manufactured and complies with customer specification.

TABLE 7.1

INPUT DATA (read in conjunction with figure 2.1 and 2.2)

$$T_t = 342.5\text{kN}, T_s = T_t, \theta_s = \theta_t = 0\text{deg.}, 2.\theta_v = 180\text{deg.},$$

$$2.b = 800\text{mm}$$

$$\text{Face width} = 1500\text{mm}, X = 1974\text{mm}, B = 1400\text{mm}, W = 1360\text{mm},$$

$$\text{Shaft Length} = 2208\text{mm}, d_b(\text{specified}) = 240\text{mm}.$$

CALCULATION

$$P = 685\text{kN}, \theta_p = 0\text{deg.}$$

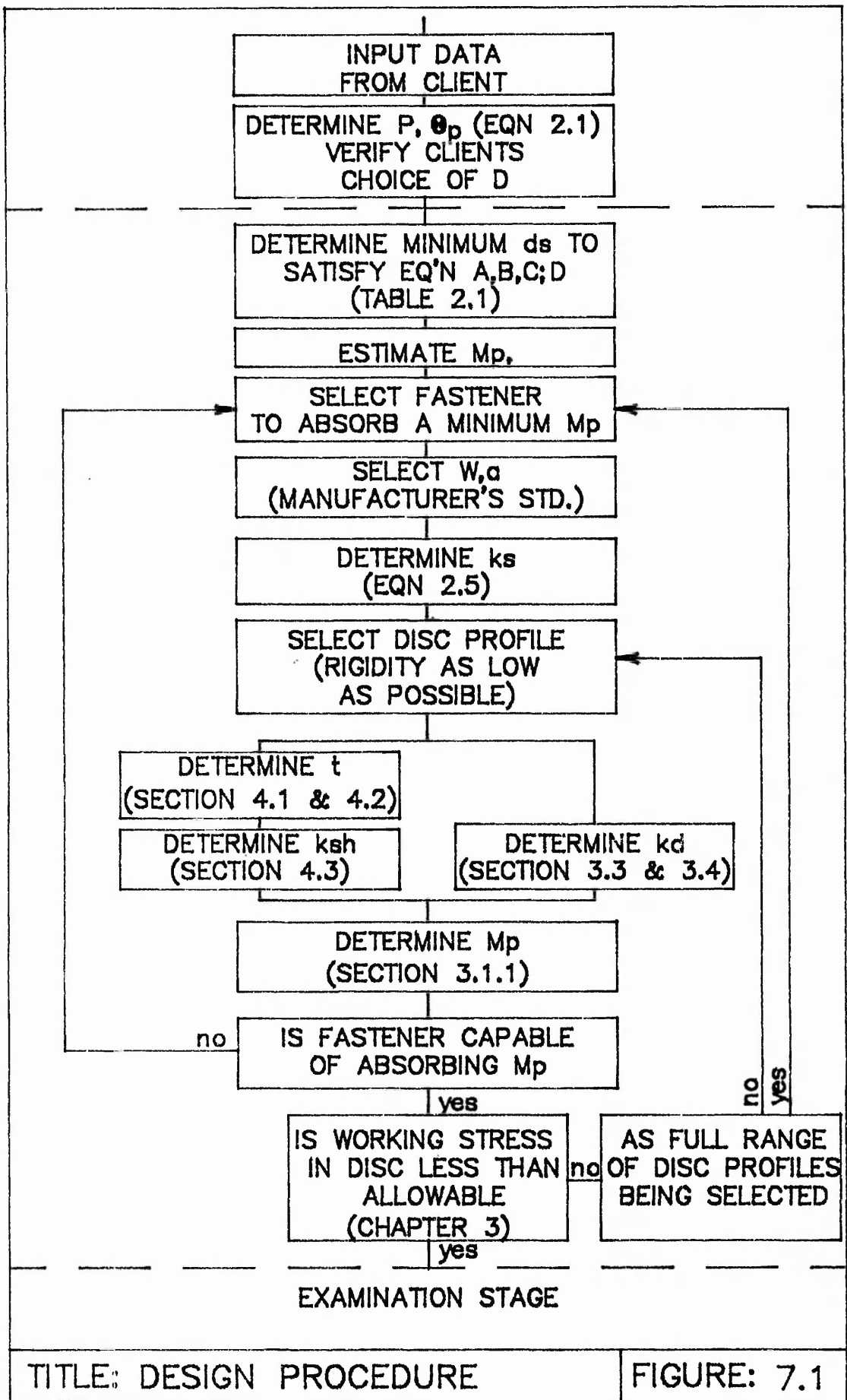
$$d_s = 264\text{mm} \text{ _ Table 2.1 Reference B (slope)}$$

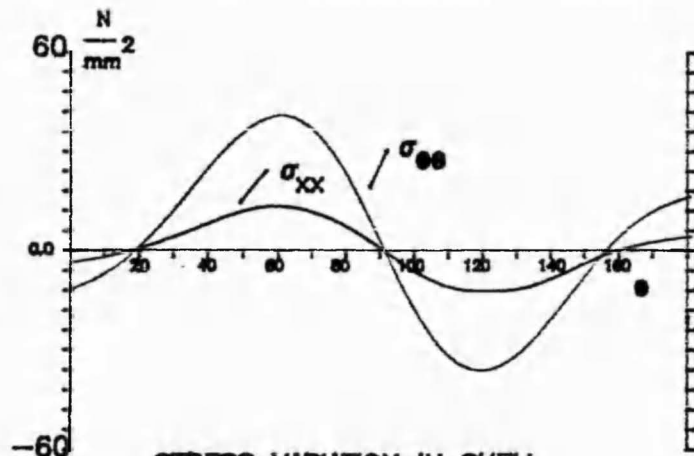
$$d_s = 251\text{mm} \text{ _ Table 2.1 Reference D (bending only)}$$

$d_s(\text{actual}) = 280\text{mm}$, standard compressive type fastener with centering web (illustrated in figure 1.7) were used. Using hub size recommended by fastener supplier (ie. $2.a = 510\text{mm}$).

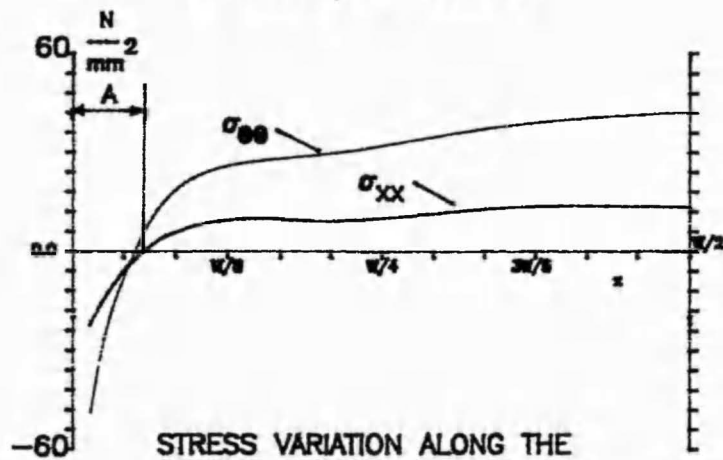
Using chapter 4, shell thickness $t = 20\text{mm}$.

Disc profile was developed using design procedure (figure 7.1) and figure 7.3 illustrates.



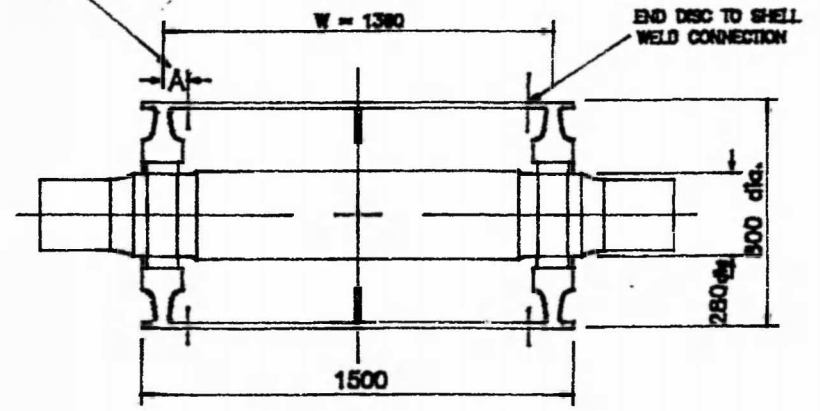


STRESS VARIATION IN SHELL
AT $x = W/2 = 680\text{mm}$



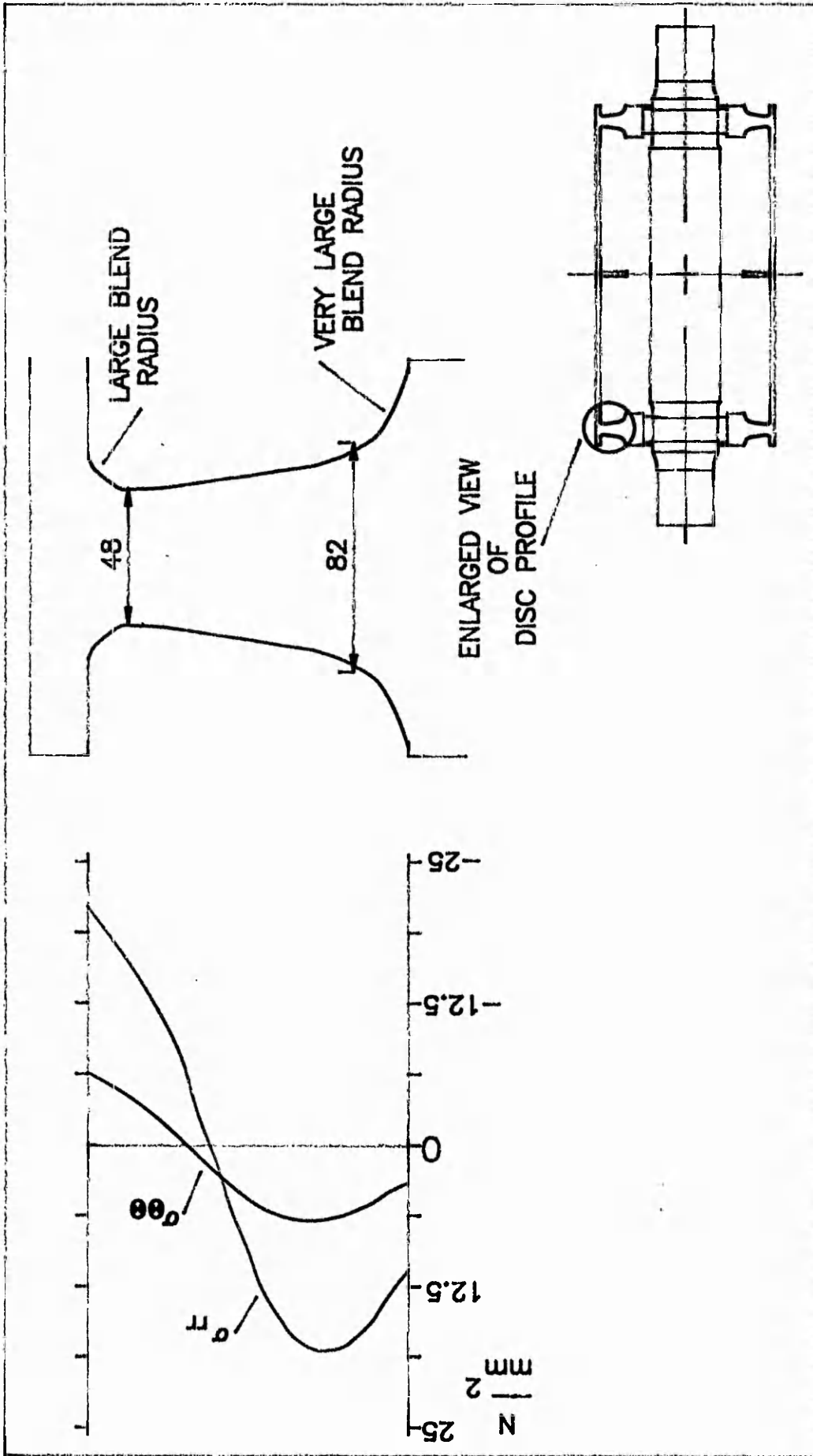
STRESS VARIATION ALONG THE
SHELL'S LENGTH, $\theta = 60 \text{ deg.}$

DISTANCE BETWEEN CENTRE LINE OF
END DISC AND
WELD CONNECTION



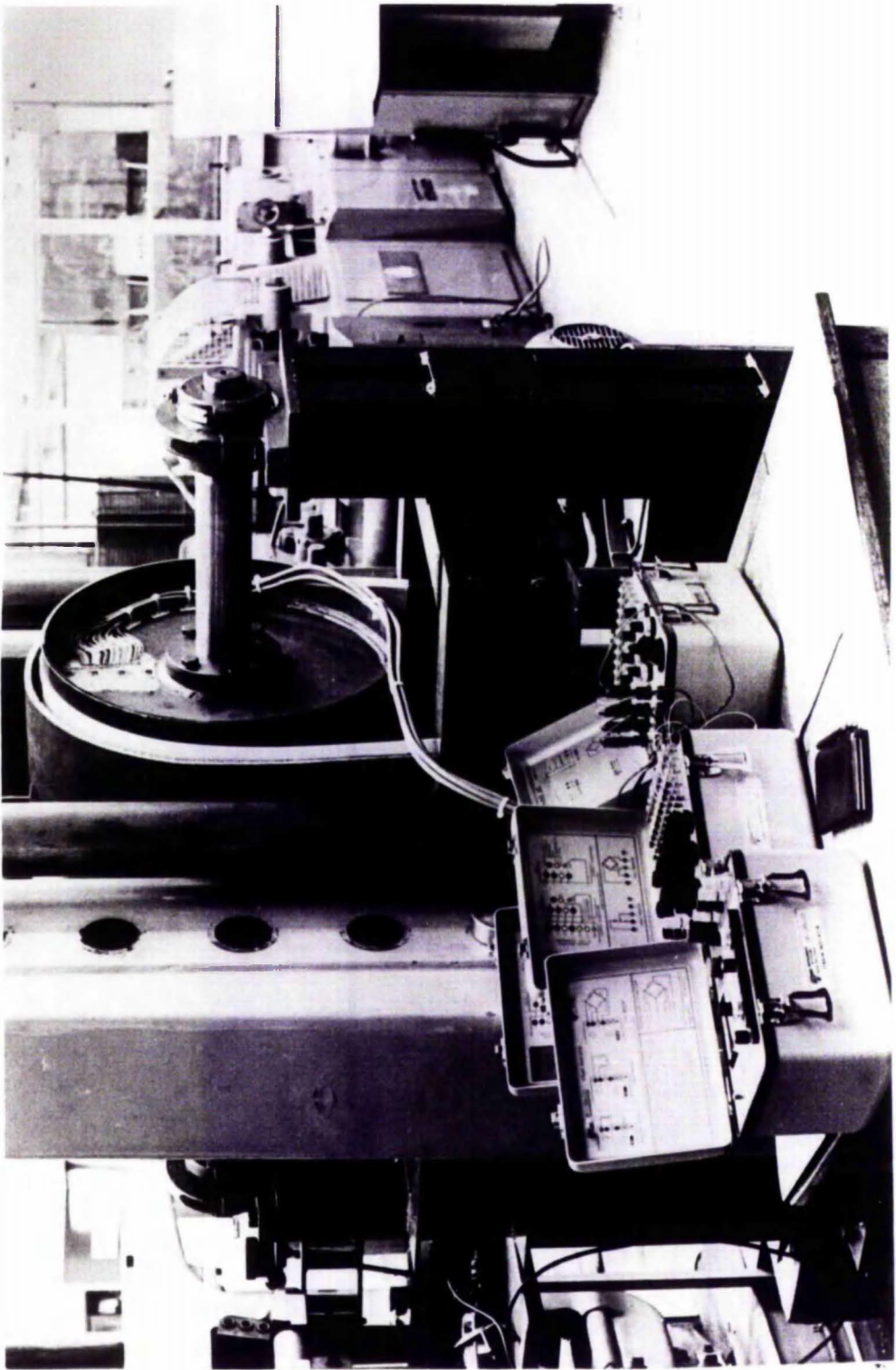
TITLE: STRESS VARIATION WITHIN THE SHELL

FIGURE: 7.2



TITLE: VARIATIONS IN STRESS FOR A PROFILED DISC

FIGURE: 7.3



CONCLUSION

8.1 SUMMARY OF WORK

This study has developed a series of theoretical techniques to examine the stress behaviour within the conveyor pulley. We proceeded in chapter 1 with a description of the environment which the conveyor pulley operates in. The development of the conveyor pulley over the last 30 years was then reviewed, with a summary of the limited literature directly and indirectly related to this work.

In chapter 2, we considered the selection process for the shaft and pulley diameter and presented the formulae for determining the resultant belt pull.

In chapter 3, we first considered the distribution of the bending moments within pulley assembly and various boundary conditions which an end disc of a pulley is subjected to. To achieve our ultimate aim of developing a technique to analyse variable-thickness (i.e. minimum weight) discs, two analytical techniques were presented. The first well-proven technique was limited to the analysis of a constant-thickness disc, but did provide a benchmark to assess the accuracy of an adapted Ragleigh-Ritz energy method. The rate of convergence of the Ragleigh-Ritz energy method was rapid and compared favourably with the "known" results. As a further enhancement to the energy method, cubic spline functions were formulated to enable any disc shape and thickness to be considered. The choice of Ragleigh-Ritz energy method to analyse constant and variable-thickness discs was

further ratified by extensive experimental studies. To isolate any boundary conditions which may emanate from surrounding pulley components (ie shaft, shell), various discs were subjected in isolation to bending and in-plane loadings. Both theoretical stress and deflection results show sufficient correlation with the experimental results to conclude that the disc behaviour is adequately prescribed and the Ragleigh-Ritz technique is sound.

The belt traction distribution between the belt and pulley was presented in chapter 4. The analysis of the shell was developed for both symmetrical and anti-symmetrical loading conditions produced by the belt traction for drive and idler pulleys respectively. The stress distribution for drive and idler pulley belt tractions were illustrated, along with the effects produced by different belt wrap angles on the shell. An introduction to the analysis of shell end effects was also included.

In chapter 5, we described a test rig which was constructed to perform a more comprehensive study of the stresses induced in a pulley when loaded by a conveyor belt. The experiment imposed a static loading of the belt on a pulley assembly to establish the accuracy of the boundary conditions assumed and theories developed for the end disc and shell. The correlation between the theoretical and experimental results were good. The test pulley was then re-examined in chapter 6 by a Finite Element Analysis to futher compare the theoretical and experimental results obtained in chapters 3, 4, and 5. Again, the results obtained show sufficient correlation to conclude that the techniques developed in this

work, adequately prescribe the behaviour of all components considered.

Finally, in chapter 7 the theoretical techniques were brought together in a design procedure, with an illustrated example. Further discussions concluded, that the use of Finite Element Analysis was limited to the design of standard pulley constructions and not as a day-to-day design tool. Once the design procedure was computerised it would allow the engineer to design any pulley shape within minutes with comparable accuracy with Finite Element Analysis.

8.2 FUTURE WORK

The main topic for future work would be to evolve a greater understanding of the dynamic effects on a conveyor pulley. This is especially important with the use of steel cord and newly developed Kevlon reinforced belts which allow the belt to be wrapped around comparatively small diameter pulley. A number of studies have been instigated in Australia and Japan to investigate the various stress fronts recently being discovered in steelcord belt. British Coal are currently investigating this phenomenon on a five mile long conveyor, where a number of large stress fronts occur every time the conveyor starts and stops. These fronts travel at very high speeds and are causing many problems with bearings, pulleys and take-up mechanisms. Kevlon, as mentioned, is a new type of belt and presently no dynamic effects have been recorded. To establish more accurate belt traction model to comply with static and dynamic characteristics for the following:-

- a). Belt constructions.
- b). Pulley positions within a conveyor system.
- c). Belt wrap angles.

Any of the belt traction models can be inserted into the shell analysis presented. This work can only be explored by large experimental rigs and on-site field trials.

Finally, establish all possible dynamic variations in belt loading to determine a load history for various pulleys types. This would enable a comprehensive fatigue analysis to be undertaken. Again this would involve extensive on-site field trials.

8.3 ACKNOWLEDGEMENTS

The author is grateful for the support and efforts of the following people and organisations:-

Jenkins of Retford Limited, Nottinghamshire, England, for sponsoring the programme of research into the design of heavy duty conveyor pulleys at Nottingham Polytechnic, Nottingham. Nottingham Polytechnic for the provision of computing and experimental facilities. A special thank you to Alan Crisp, Head Technician in the Mechanical Engineering Department at Nottingham Polytechnic for his efforts in the smooth running of all the experiments.

A special thank you to Dr. D. A. Hills and Dr. M. Lacey for their guidance and perseverance in their supervision of this project.

Finally, a very special thank you to my wife Alex, who has supported me throughout the project.

REFERENCES

- [1] NOT USED
- [2] CHENEY, W and KINCAID. D.,
"Numerical Mathematics and Computing", 1979, (Brooks/Cole)
- [3] CONWAY, H.D.,
"The bending of Symmetrically Loaded Circular Plates of Variable Thickness.", J.Applied Mech., March 1948, pp1-6.
- [4] CONWAY, H.D.,
"Axially Symmetrical Plates with Linearly varying Thickness.", J.Applied Mech., June 1951, pp140-142.
- [5] CONWAY, H.D.,
"Closed-form solutions for Plates of Variable Thickness.", J.Applied Mech., Dec. 1953, pp564-568.
- [6] DENNEHY, J.T.J.,
"Belt Conveyor Transport Systems.", The Australian I.M.M Conference, 1976, pp281-291.
- [7] DIETER, G.E.,
"Mechanical Metallurgy.", 1976, (McGraw-Hill, London).
- [8] FIRBANK, T.C.,
"A Laboratory study of the Dual-drum Multimotor Conveyor Drive.", The Mining Engineer, May 1972, pp385-393.
- [9] FIRBANK, T.C.,
"On the Forces between the Belt and Driving Pulley of a Flat Belt Drive.", ASME, 1977.
- [10] FLUGGE, W.,
"Stresses in Shell.", 1960, (Springer-Verlag).

- [11] GRAHAM, J.,
"Investigation of Conveyor Pulleys at N.C.B (now British Coal) Selby (Gascoigne Wood Colliery).", unpublished work for Babcock Jenkins Ltd., England, 1986.
- [12] HARTENBURG, R.S.,
"The strength and stiffness of thin cylinder shells on saddle supports.", University of Wisconsin (USA), 1941.
- [13] HILLS, H.A and BAUGH, S.,
"A Review of the Design Procedures for Fabricated Conveyor Pulleys.", Int.J.Storing and Handling Bulk Material, 1983, Vol.3, No.3, pp469-474.
- [14] JACKSON, R.H.,
"Special Conveyor Pulleys.", Machine Design, Sept. 1955, pp159-161.
- [15] JOHNSON, K.L.,
"Contact Mechanics", 1984.
- [16] KOSTER, K.H., (part translated, German origin)
"Design of Multi-pulley Drives for Belt Conveyors.", Formern Und Heben (Germany), 1972, Vol.21, Pt.14, pp832-837.
- [17] LANGE, H., (part translated, German origin)
"Investigation of Stresses in Belt Conveyor Pulleys.", Technical University, Hannover, Germany, 1963.
- [18] LINDNER, L., (untranslated, German origin)
"Construction of a Conveyor Belt Pulley with the Aid of the TPS-10 Finite Element Program.", Braunkohle 3 (Germany), March 1975, pp81-97.
- [19] MANSFIELD, E.H.,
"On the analysis of elastic plates of variable thickness.", Quart.J.Mech. & Applied Maths., 1962, pp167-192.

- [20] OLSSON, R.G.,
"Nonsymmetrical bending of circular plates of variable thickness.", Ingr-Arch, 1939, Vol.10, pp14-24.
- [21] PARLANE, A and MARTIN, B.A.,
"Strain Gauge Stress Analysis of Dick Conveyor Pulleys.", unpublished work for Babcock Jenkins Ltd., England, 1977.
- [22] RICHARDS, T.H.,
"Energy Methods in Stress Analysis.", 1977, (Ellis Horwood).
- [23] ROARK, R.J. and YOUNG, W.C.,
"Formulas for Stress and Strain.", 1975, (McGraw-Hill).
- [24] ROUTLEY, K.F.,
"Pulleys Developments.", J.Mining Conveyors (Australia), 1978.
- [25] SCHMOLTZI, W., (part translated, German origin)
"Design of Conveyor Belt Pulleys with Continuous Shafts.", Technial Universit, Hannover, Germany, 1974.
- [26] SCHORER, H.,
"Design of Large Pipe Lines.", Proc. ASCE, Sept. 1935, pp101-119.
- [27] SWIFT, H.W.,
"Power Transmission by Belts: An Investigation of Fundamentals.", Proc.I.Mech.E., Nov. 1928, pp659-699.
- [28] TIMOSHENKO, S.P. and WOINOWSKY-KRIEGER, S.,
"Theory of Plates and Shells.", 1984, (McGraw-Hill).
- [29] WILLIAMS, W.,
"Design and Construction of Wide Face Steel Pulleys.", Product Engineering, Aug. 1950.

[30] WOSTASZAK, I.A.,

"Deformation of Thin Cylindrical Shells subjected to Internal Loading.", Phil. Mag., 1934, Vol.18, Ser.7, pp1099-1116.